Ministry of Higher Education and Scientific Research

University of Baghdad

Institute of Laser for Postgraduate Studies

Pulse Compression Using Polarization Maintaining Fiber Mach-Zehnder Interferometer

A Thesis Submitted to the Institute of Laser for Postgraduate Studies, University of Baghdad in Partial Fulfillment of the Requirements for the Degree of Master of Science in Laser / Electronic and Communication Engineering

By

Baraa Hassan Mutar

B.Sc. Laser and Electro-Optic Engineering
2016

Supervisor
Asst. Prof. Dr. Tahreer Safa'a Mansour

2021 AD **1442 AH**

بِسْمِ اللَّهِ الرَّحْمَٰنِ الرَّحِيمِ

(وَأَنْ لَيْسَ لِلْإِنْسَانِ إِلَّا مَا سَعَىٰ ﴿٣٩﴾ وَأَنَّ سَعْيَهُ سَوْفَ
يُرَىٰ ﴿٤٠﴾)

صدق الله العظيم

سورة النجم.

Dedication

To my family

Acknowledgement

First of all, I am grateful to the creator "**ALLAH**" for giving me the strength, enablement, knowledge and understanding required to complete this work .

I would like sincerely thank my supervisor, **Asst. Prof. Dr. Tahreer Safa'a**, for her great contribution, scientific generosity, continuous support and encouragement during the research period .

I would like grateful thanks go to **Prof. Dr. Hussein Ali Jawad**, Dean of the Institute of Laser for Postgraduate Studies, for his unlimited encouragement, and support during the period of my study and research work .

Special thanks are to **Dr. Mahmoud Shaker Mahmoud** Asst. Dean of the Institute of Laser for Postgraduate Studies.

I would also express my great gratitude to **Asst. Prof. Mohammed K. Dhahir,** head of the Engineering and Industrial Applications Department, to his encouragement, constant and great support.

Many thanks go to all the faculty members and staff of Institute of Laser for Postgraduate Studies, University of Baghdad, especially to **Dr. Jawad A. Hasan**, for his encouragement, help, and support during my study.

Abstract

Laser pulse compress is an important technique in high data rate communication system especially in the application of optical fiber network sensing. Single Polarization Maintaining Fiber-Mach Zehnder interferometer pulse compressor was designed using Comsol multi-physics version 5.5, with 8,16 and 24 cm Polarization maintaining fiber spliced between two segments of SMF with lengths of 23 and13 cm. Single and cascaded polarization maintaining fiber-Mach Zehnder interferometer were implemented using 1546.7nm and 286 pm full width at half maximum with 9 ns. Maximum Excitation to the higher-order modes in the cladding region were visualized by Comsol which indicated to optimum values of compression factors that are 1.1103 in the case of 5 g is applied on 8 cm on the cross-sectional area of the Polarization Maintaining Fiber. Practically two compression factors were obtained one with single polarization-maintaining Fiber-Mach Zehnder interferometer , 5 g force that applied on the micro cavity splicing region that is 1.13 and second with cascaded polarization-maintaining Fiber-Mach Zehnder interferometer with two Polarization Maintaining Fiber each with 8 cm length and 10 g weight applied on the second PMF cross-sectional area which is 1.10. Cascaded Polarization-Maintaining Fiber-Mach Zehnder interferometer has minimum compression factor due to the fact of many splicing regions act as double convex lens that cause excitation to the higher order modes propagated in the fiber Interfromter and then causes broadening FWHM spatially and compressed pulse temporally.

List of Contents				Page No.

List of Abbreviations

Abbreviation	**meaning**
ER	Extinction Ratio.
EFFPI	Extrinsic fiber Fabry-Perot interferometer.
Fc	Compression Factor.
FPI	Fabry-Perot Interferometer.
GVD	Group Velocity Dispersion.
IFFPI	Intrinsic fiber Fabry-Perot interferometer.
L_c	Cavity Length.
MZI	Mach Zehnder Interferometer.
PMF-MZI	Polarization Maintaining Fiber- Mach Zehnder Interferometer.
MFD	Mode-Field Diameter.
MCSRs	Micro Cavity Splicing Regions.
OSA	Optical Spectrum Analyzer.
OFI	Optical Fiber Interferometer.

OC	Optical Coupler.
PMF	Polarization Maintaining Fiber.
PMD	Polarization Mode Dispersion.
SMF	Single Mode Fiber.

List of Symbols

Symbols	**meaning**	**units**
α	Attenuation coefficient.	cm−1
λc	central wavelength.	nm
ΔL	The change in length.	m
A	The cross sectional area.	m^2
c	speed of light in vacuum.	m/s
d	Diameters.	µm
F	Applied force.	N
FWHM	Full Width Half Maximum.	pm
L	The original length.	m
m	Value of the standard weight mass.	g
n_{eff}	effective refractive index.	-
n_{co}	Refractive index of core.	-
n_{cl}	Refractive index of cladding.	-
Pi	Input power.	W
Po	Output power.	W
P_B	Power budget.	dB
P_{TX}	transmitter power.	dBm
P_{RX}	receiver power.	dBm
r	Radius.	µm

List of Tables

List of Figures

Chapter One

Introduction and Basic Concept

1.1 Thesis layout

This thesis contains three chapters and is organize as follows:

Chapter One: Gives a general introduction about, all-fiber pulse compression and the optical interferometers that are based on polarization maintaining fiber. Then a brief literature survey related to optical pulse compression introduced.

Chapter Two: Presents the simulation and experimental setups and explained the entire component and the equipment are used in experimental work. Then explained how to design and construct inline interferometers, and using them for all- fiber pulse compression.

Chapter Three: Illustrates and discuss the simulation and experimental results. Next, summarizes the main conclusions drawn from this study followed by suggests some points which need further investigation as a future work.

CHAPTER ONE

1.2 General Introduction and Motivation

The Compressed laser source is an essential part for high data rate communication system in the applications of network fiber sensing and wavelength division multiplexing[1-3]. The interest of the scientific community has been focused on the development of new technologies of light sources and applications based on special kind of fibers like high birefringent polarization-maintaining fiber PMF which is a type of specialty fiber that can retain linear polarized states of light propagation over a long distance on a single-mode waveguide[4-8]. Polarization-Maintaining Fiber have a wide range of applications in the telecommunications and sensor fields[9]. Panda-type PMF have dominated on most of applications because of its flexible and compatible with regular telecommunication optical fibers[10].

There are many advantages of using different arrangements of in-line fiber interferometers in communications, optical modulation, pulse compression, and sensing applications due to their ability to measure different parameters such as pressure, force, strain, temperature, etc. along with having high sensitivity immunity to electromagnetic interference and simple structure[11-14]. The most significant types were those of cascaded in-line fiber interferometers for example the in-line Mach-Zehnder interferometer can be used for this purpose due their easy implementation. [15-18]. This work introduced a tunable narrow pulsed laser source by using polarization-maintaining fiber to build an In-line Mach-Zehnder fiber interferometer PM-MZI practically and theoretically with three variable-lengths of single-mode PM fiber spliced between two segments of SMF. A tunable interferometer was implemented by applying mechanical forces on the cross-sectional area of the PM fiber and the micro cavity splicing regions to change the interference cavity length.

1.3 Aim of the work

Design and construct in line cascaded PM-Mach zehnder interferometer pulse compressor using spatial type of optical fiber that has zero polarization mode dispersion.

1.4 Polarization Maintaining Fiber (PMF)

Polarization Maintaining Fiber (PMF) is a special type of single mode fiber, designed to transmit only one polarization of the input light. It has a high birefringence with predetermined slow and fast axes while conventional single mode fibers are design to carry randomly polarized light [5,19].

It is a great interest for many applications in fiber lasers, non-linear optics, coherent optical communication systems fiber-optic sensing systems and telecommunications[20].

Polarization Maintaining Fibers (PMFs) have subdivision as shown below:

1.4.1 Panda Polarization Maintaining Fiber

This type of polarization maintaining fiber using round and symmetrical stress rods on either side of the core[21]. In which design two stress applying part to create symmetric birefringence to maintain the polarization of lunched light as shown in figure (1.1a). Typical Panda fiber has the polarization maintain performance of 23 dB extinction ratio (ER) and beat length is 6 mm. Extinction ratio and beat length are parameters that used to evaluate polarization-maintaining property of conventional single mode fiber-polarization maintaining fiber, SM-PMFs [10,22]. Originally developed for the telecommunication industry , PMFs including Panda types filled the need for low cost , high volume , high reproducibility of fiber[23].

1.4.2 Elliptical-clad Polarization Maintaining Fiber

In which born glass silica in elliptical shape around the fiber core to create asymmetric stress, these stress on the core leads to create birefringence as shown in figure (1.1b) , from this type ER is 30 dB and beat length is 2 mm [24]. Compared to panda and bow-tie types , elliptical-clad has higher polarization maintaining property [19].

1.4.3 Bow-tie Polarization Maintaining Fiber

In which two opposing wings designed to create more birefringence than any other stressed design. ER of 25 dB and beat length of 6.3mm is reported from this type[25,26]. Those properties are said to be similar to the panda type [19]. As shown in figure (1.1,c).

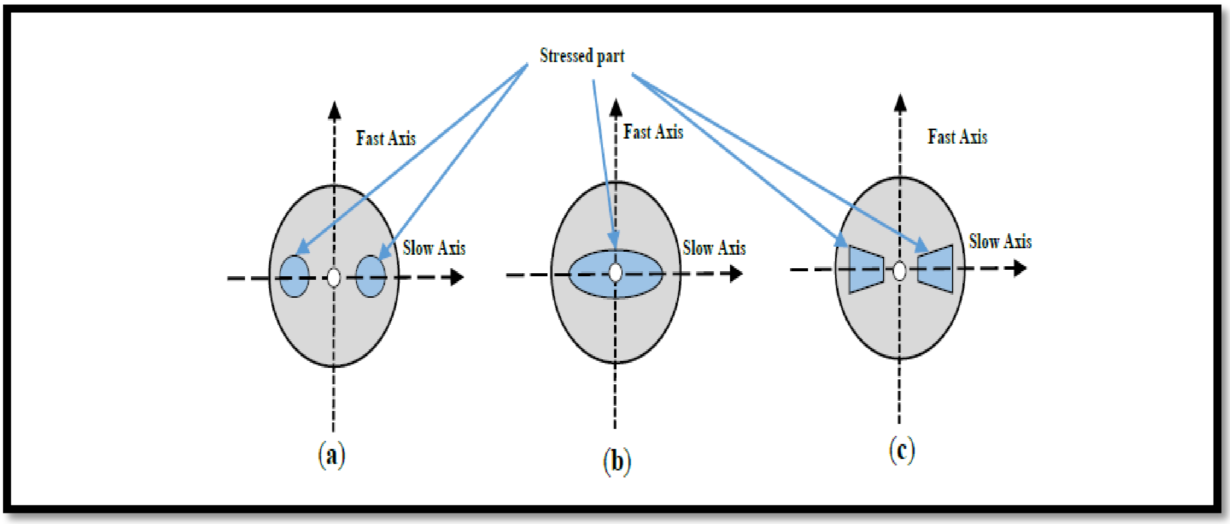

Figure (1.1): (a) Schematic of PM Panda fiber, (b) Schematic of PM Elliptical-clad fiber, (c) Schematic of PM Bow-tie fiber [19].

1.5 Application of Polarization Maintaining Fiber

Polarization maintaining fibers are used for special applications such as in interferometry, fiber optic sensing and quantum key distribution[27]. There are also commonly used in telecommunications for the connection between a laser source and a modulator , since the modulator requires polarized light as input.

They are rarely used for long-distance transmission, because PMF is expensive and has higher attenuation than single mode fiber[28].

1.6 The Degradation of Signals in Optical Fiber

The main reason for degradation of optical signals after propagated are described in the block diagram which is shown in figure (1.2)[29].

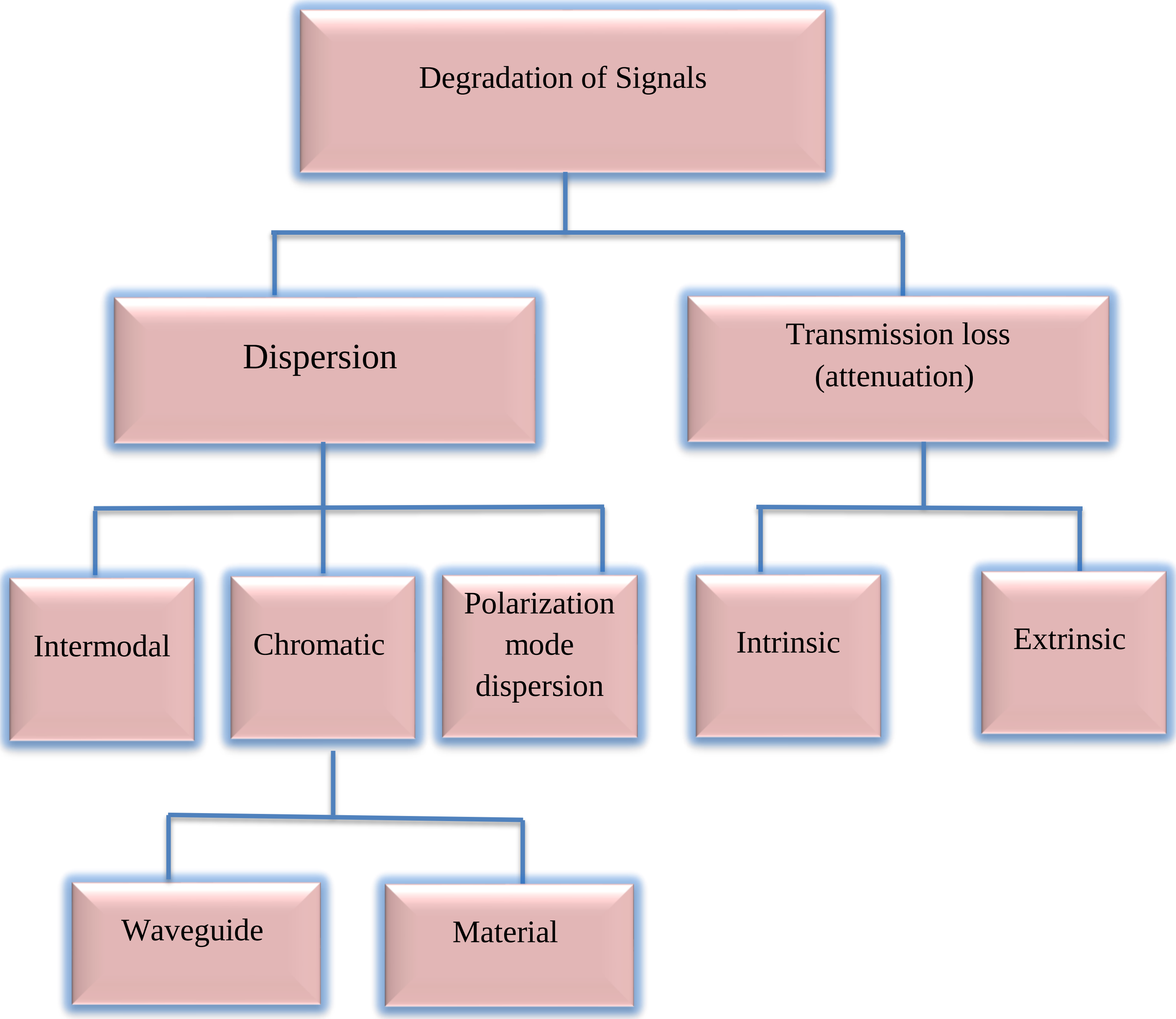

Figure (1.2): The block diagram shows the reason of degradation of optical signals.

1.6.1 Transmission loss (attenuation)

For any communication system, the most important factor is the losses of the optical signals that are transmitted through the optical fiber. For fused silica, which it is wavelength is around 1550 nm, the minimum loss is slightly less than 0.2 dB/km[30,31]. as it is shown in figure (1.3). This limit is important, since it sets the spacing of amplifier in communications systems, and thus is a major cost of a transmission system[32].

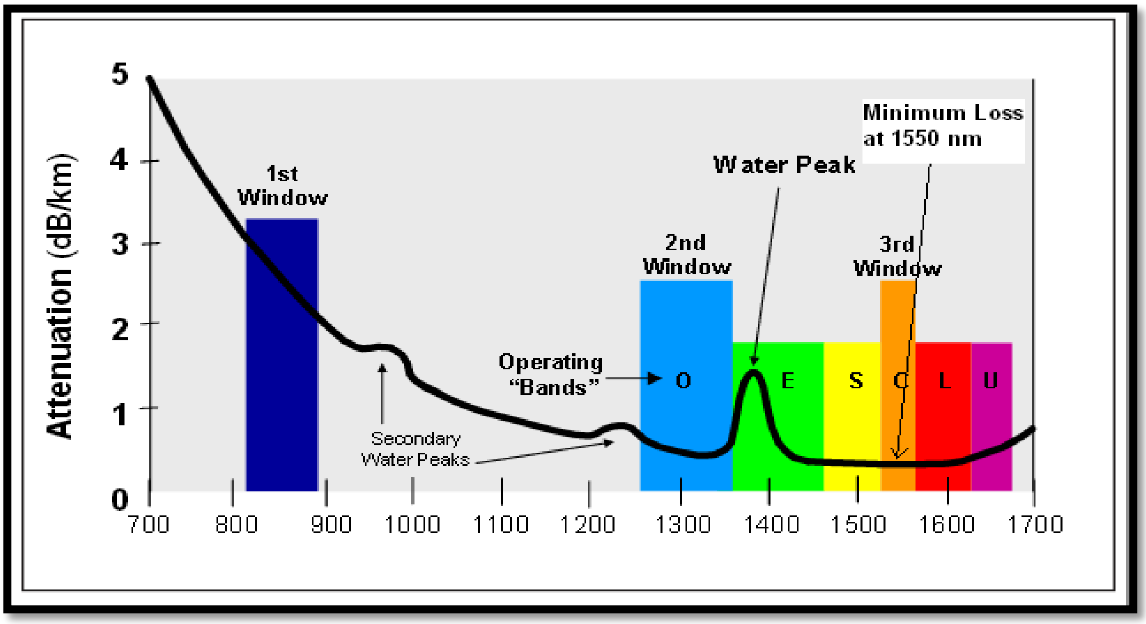

Figure (1.3): Attenuation spectrum of optical fiber [33].

So that the attenuation or the loss (α) represent energy loss during the transmission of the data in the fiber and it can be defined as below [33]:

$$\text{Loss}\ (\alpha) = -10 \log \frac{p_o}{p_i} \qquad (1.1)$$

Where:

p_i is the input power.

p_o is the transmitted (output) power.

Attenuation may be divided into two kinds: Intrinsic and Extrinsic losses [34,35] ,as which are presented in the block diagram as shown in figure (1.4).

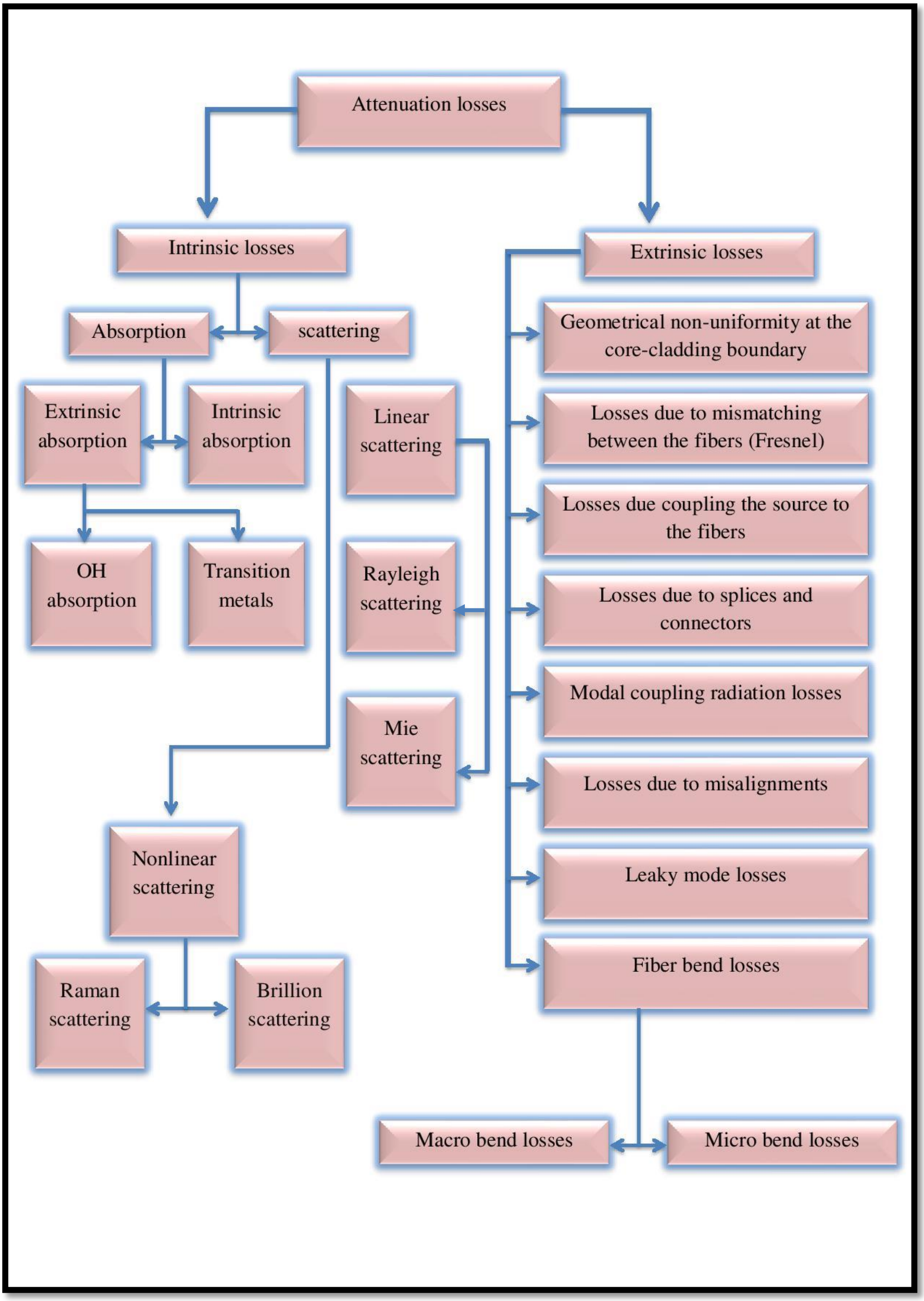

Figure (1.4): The block diagram of the attenuation losses.

1.6.2 Dispersion

In the field of optical waveguides, dispersion is a general term referring to all phenomena causing these pulses to spread while propagating, and they ultimately overlap and light pulses could not be distinguished by the receiver [36]. There are essentially three causes of dispersion.

1.6.2.1 Chromatic Dispersion

Chromatic dispersion is an important phenomenon in the propagation of short pulses in optical fibers[36]. It is caused by delay differences among the group velocities of the different wavelengths composing the source spectrum[37]. The consequence of the chromatic dispersion is a broadening in the transmission of the impulses.

Chromatic dispersion is essentially due to two contributions. material dispersion and waveguide dispersion[38]. Material dispersion (D_M) occurs as the refractive index changes the optical frequency, as shown in figure (1.5)[37]. Generally the dominant contribution, except for the wavelength region in which it vanishes (for silica based material this happens around 1300nm).The waveguide dispersion(D_W) depends on the dispersive properties of the waveguide itself [38]. From a practical point of view, it is significant property that the dispersion of waveguide has opposite signs with respect to the material dispersion in the wavelength range over 1300 nm[37,39].

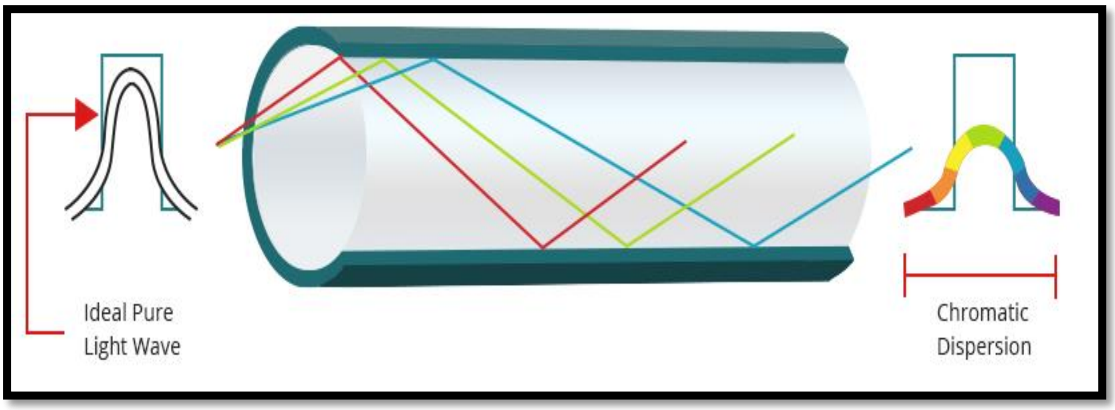

Figure(1.5): Chromatic dispersion[37].

1.6.2.2 Intermodal Dispersion

Intermodal dispersion is spreading of light, intermodal dispersion is that type of dispersion that results from the varying modal path lengths in the fiber[39]. It is occur in multimode fiber as a results from the propagation delay differences between modes, this occurs because rays follow various paths through the fiber and Consequently, at different times, reach the other end of the fiber[40]. Thus different rays take a shorter or longer time to travel the length of the fiber. The ray that goes straight down the center of the core without reflecting, arrives at the other end first, other rays arrive later. Thus light entering the fiber at the same time exit the other end at different times. The light has spread out in time[39,41].

1.6.2.3 Polarization Mode Dispersion

Polarization refers to the electric-field orientation of a light signal, which can vary significantly along the fiber's length[42]. Signal energy at a given wavelength occupies two orthogonal polarization modes, as shown in figure (1.6)[43]. A varying birefringence along its length will cause each polarization mode to travel at a slightly different velocity and the polarization orientation will rotate with distance. The resulting different in propagation modes will result in pulse spreading that called Polarization Mode Dispersion (PMD)[42].

Polarization mode dispersion is related to the differential group delay, the time difference in the group delays between two orthogonal polarized modes, which causes pulse spreading in digital systems and distortions in analogue systems. The polarization mode dispersion value is the average of the differential group delay values. While the individual values can shift from one time to another the overall distribution, hence the average is assumed to be fixed[44,45].

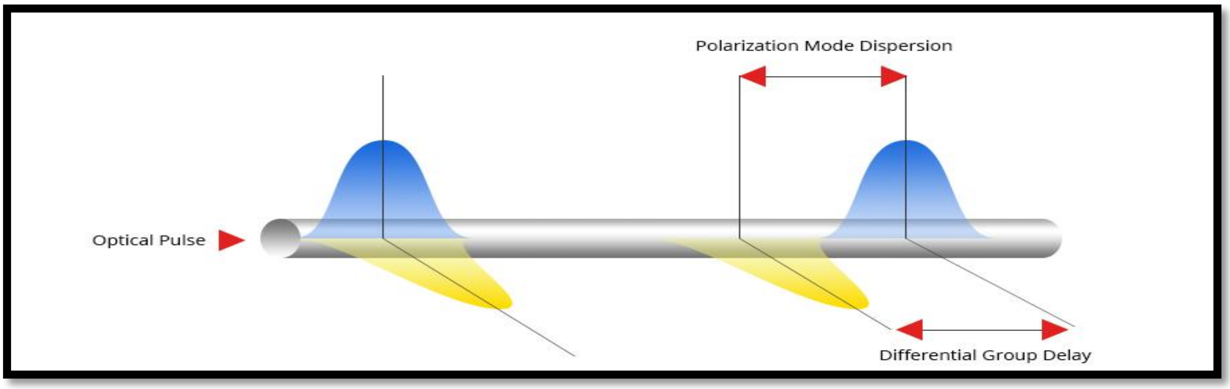

Figure (1.6): Variation in polarization states of an optical pulse at it passes through a fiber [43].

1.7 In Line Fiber Interferometers

Interferometry is based on two or more light beams superimposed to measure the phase difference between them. Interferometer uses two light beams with the same frequency[46].

Typically an incident light beam of interferometer is divided into two or more parts and then recombined together to create an interference pattern[47]. For the optical path difference between the two paths, the integer number of wavelength corresponds to constructive points and odd number of half wavelengths corresponds to destructive points of the interference pattern[46,47]. So in the output optical spectrum of the optical fiber interferometer, the position of minimum can be shifted to maximum position if the optical path difference varies by odd number of half wavelengths. At least two optical paths are necessary for an interfererometery experiment[48]. These optical paths can be in one optical fiber with two or more different optical fiber modes. Each of modes defines one optical path for the interferometer such as the Sagnac interferometer where the optical paths are defined by the clockwise and counter clockwise modes. There are many types of interferometers configurations , to see the principle of their operation, the detail of some interferometers such as Fabry-perot, Sagnac, Michelson and Mach-zehnder interferometers[49,50].

1.7.1 In Line Fabry-Perot Interferometer

A Fabry-Perot interferometer (FPI) consists of two optically parallel reflectors with reflectance R1and R2 separated by a cavity of length L[51]. Reflectors can be interface of two dielectrics mirrors, or two fiber Bragg coating cleaved end of the optical fiber [46,52]. Figure (1.7) shows the schematic of Fabry-Perot interferometer.

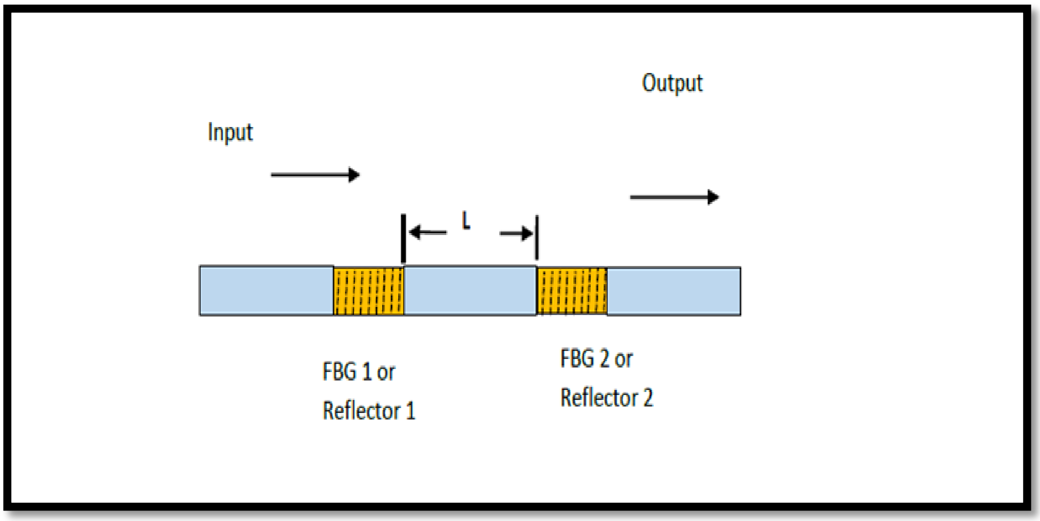

Figure(1.7): Fabry-Perot interferometer[52].

Fabry-Perot interferometer can be largely classified into two categories: one is extrinsic and the other is intrinsic

- The extrinsic fabry-perot interferometer (EFPI) uses the reflections from an external cavity formed out of the interesting fiber [53]. Figure (1.8a) shows an extrinsic FPI sensor, in which the air cavity is formed by a supporting structure. Since it can utilize high reflecting mirrors, the extrinsic structure is useful to obtain a high finesse interference signal[54]. Furthermore, the fabrication is relatively simple and does not need any high cost equipment. However, extrinsic FPI have disadvantages of careful alignment, low coupling efficiency, and packaging problem[55].

- The intrinsic fabry-perot interferometer (IFPI) fiber sensors have reflecting components within the fiber itself. For example, when the reflectors are formed within a fiber by any means, as in figure (1.8b), it can have the intrinsic FP interference[56,57]. The local cavity of the intrinsic FPI can be formed by a lot of methods such as micro machining ,fiber Bragg gratings (FBGs), chemical etching, and thin film deposition [58].

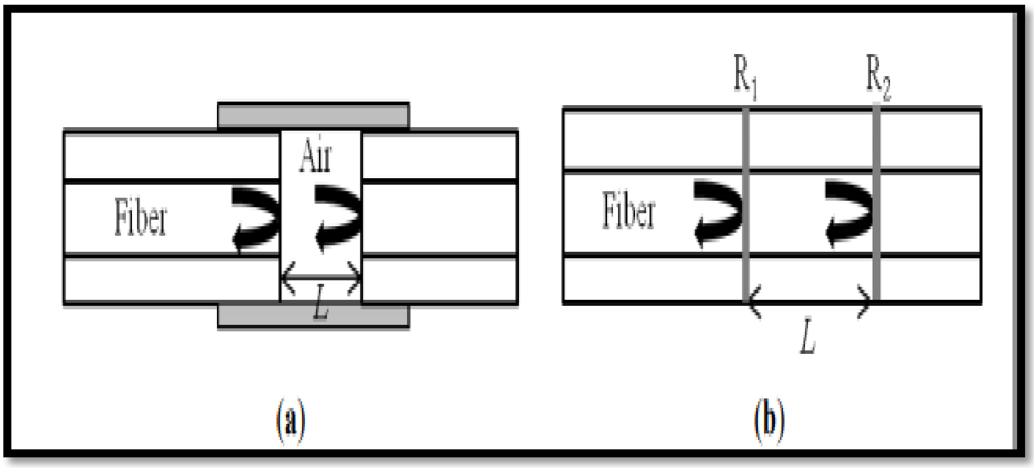

Figure (1.8): FPI (a) extrinsic (b) intrinsic [53].

1.7.2 In Line Sagnac Interferometer

The configuration of a Sagnac optical fiber interferometer is illustrated by figure(1.9). The optical source is a single mode stabilized coherent semi - conductor or erbium doped optical fiber laser[51,46]. The laser output beam is assumed to be well collimated with uniform phase[59,60]. The laser beam enters the lossless 3dB fiber coupler (FC). At the FC the injected light splits into two parts with equal intensity that each of them travels around single mode optical fiber coil in opposite directions. The output of Sagnac coil is guided toward a single detector[61].

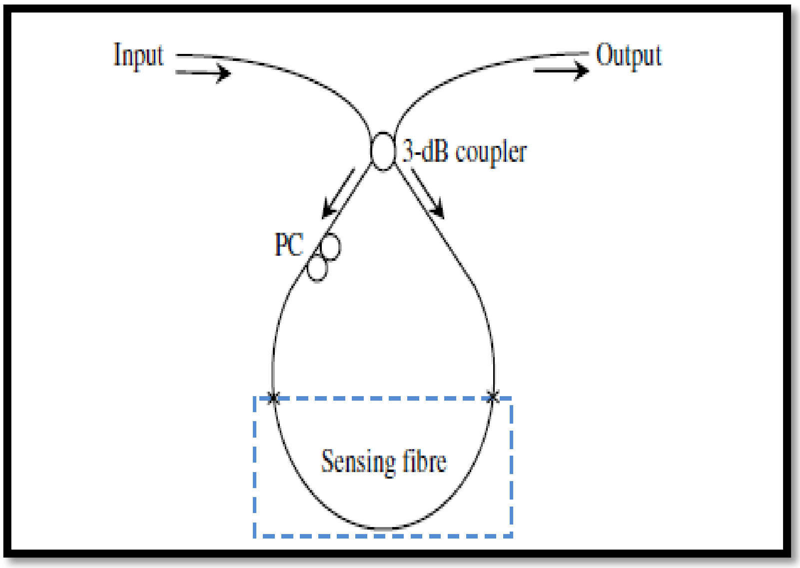

Figure(1.9): A schematic diagram of Sagnac fiber interferometer[61].

1.7.3 In Line Michelson interferometer

A schematic of conventional Michelson optical fiber interferometer is depicted in figure (1.10)[62]. The high coherent light beam is split into two different optical paths in the upper and lower single mode optical fibers by the 2 × 2 optical coupler (OC). The light reflected back by mirrors M1 and M2 are recombined by the OC to produce interference pattern at the receiver[63].

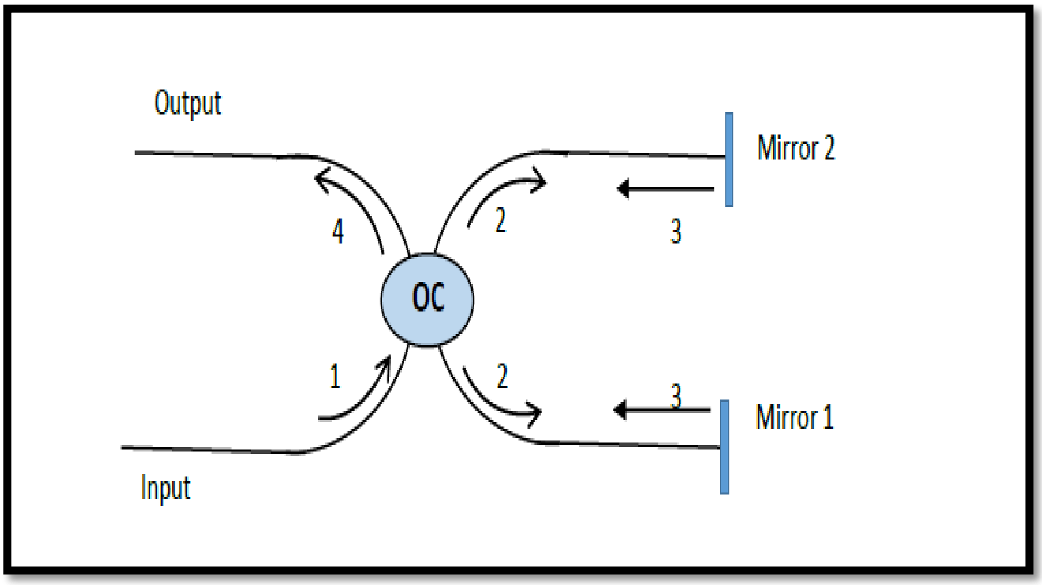

Figure (1.10): A schematic configuration of Michelson interferometer[62].

1.7.4 In Line Mach-Zehnder Interferometer (MZI)

Mach-Zehnder interferometers have been commonly used in diverse sensing applications because of their flexible configurations[64]. Early MZIs had two independent arms, which are the reference arm and the sensing arm, as illustrated in figure (1.11).

An incident light is split into two arms by a fiber coupler and then recombined by another fiber coupler[65]. The recombined light has the interference component according to the optical path difference between the two arms. For sensing applications, the reference arm is kept isolated from external variation and only the sensing arm is exposed to the variation. Then, the variation in the sensing arm induced by such as temperature, strain, force and RI changes the optical path difference of the MZI, which can be easily detected by analyzing the variation in the interference signal [66,67]. In this experimental Mach-Zehnder interferometer was formed.

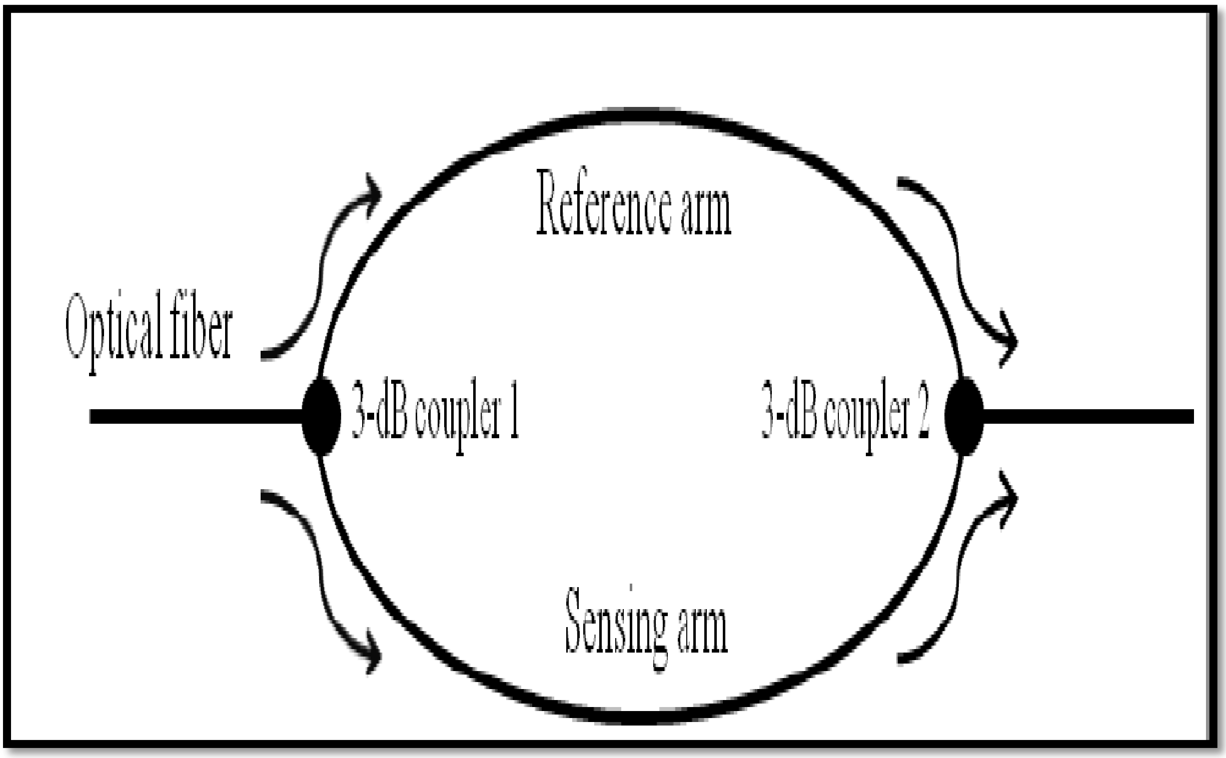

Figure (1.11): A Schematic of optical fiber Mach-Zehnder interferometer[66].

1.8 Fabrication Micro-cavity Interferometers

The micro-cavities implanted within the core can take either spherical or ellipsoidal shape. Figure (1.12) shows an example of a micro-cavity formed at splice joint with different shapes[68]. In this experiment, ellipsoidal shape is formed, according to this shape, it has a size of (2d×2r) with a rotation around the major axis of the coordinate system. Where the 2d and r are the polar diameters and radius, respectively[69].

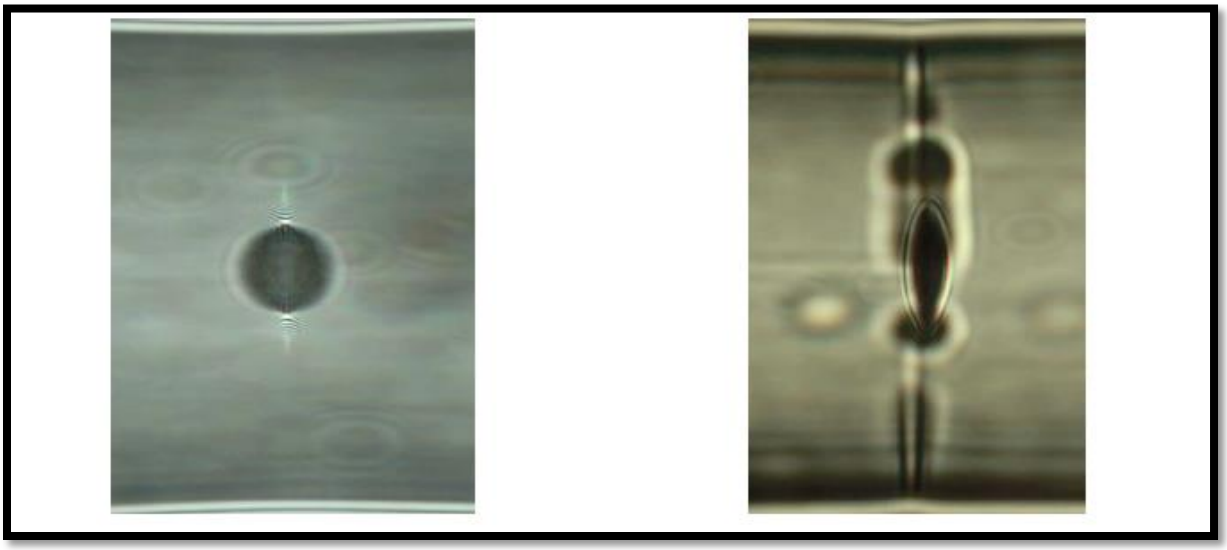

Figure (1.12): Micro -cavities produced by control a fusion splicer parameters [68].

A Mach-Zehnder micro-cavity was fabricated by using a Fujikura (FSM-60S) fusion splicer. Figure (1.13) shows the micro cavity that formed by splicing the single mode fiber on the left with Polarization maintaining fiber on the right[70].The micro-cavity forms an ellipsoid at the splice joint, with the longest axis perpendicular to the axis of the fiber. The PMF air moved to the splice joint because of collapsing which have more force to displace silica of the fibers at the interface between the SMF and PMF[71]. The silica resists displacement, with the resistance weaker along the interface of the splice joint. The excess air moves along this interface, producing an ellipsoidal micro-cavity[72].

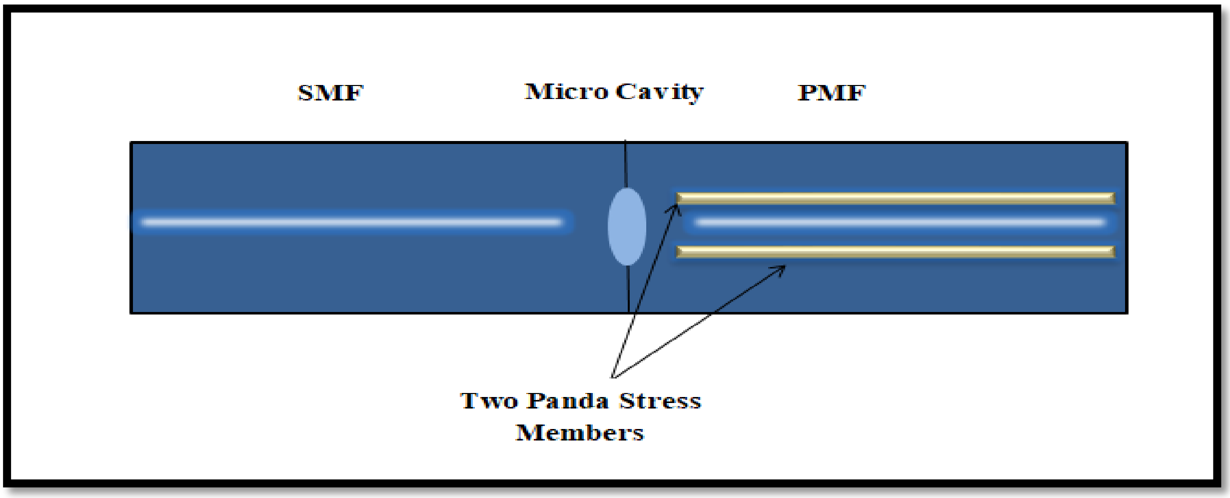

Figure (1.13): Schematic diagram of a PMF to SMF splice to construct the micro- cavity.

The splicing parameters were used to produce ellipsoidal micro-cavity was [68,69]:

- **Perfusion arc power**

The perfusion arc power is used to clean the fiber ends of dirt during splicing. It's a value required to vaporize any dirt residing on the optical fiber end faces.

- **Perfusion time**

The perfusion time refers to the time of the perfusion arc power which needs to be short to avoid unduly heating the optical fiber ends.

- **Arc power**

Arc power is used to heat the fiber ends so they can be melted together. The arc power reduces the viscosity of the silica during splice formation which affected on the shape of the micro-cavity.

- **Overlap**

The overlap refers to the length of the region of the fibers forced to overlap each other. It's used 5µm overlap during the construction of the micro-cavity and this is much shorter than the normal 15µm. Using a shorter overlap weakens the interface of the PMF to SMF which reduces the resistance against air displacing the silica along the interface and resulting in more ellipsoid micro-cavities [70,72].

These parameters affected on the shape and size of the micro-cavity. The arc power was found to change the shape of the micro-cavity, and increasing the arc power during the splice, produced more spherical micro-cavities [73].The main arc power heats the fiber to allow the two cleaved fiber ends to adhere to each other. Heating silica reduces its viscosity, and reduces the resistance against air escaping the hole collapse displacing the silica[74]. The silica was hotter due to the greater arc power, and was more easily displaced by air to form a more spherical micro-cavity.

1.9 Fiber Pulse Compression

It is a process that used the optical fiber for reducing the durations of optical pulses by linear or nonlinear techniques[75]. Pulse compression is used in various applications such as for high resolution in spectroscopy applications, high data rate for communication applications and more effective pulses in medical application[76]. In general, pulse compression in optical media is classified into two types: linear pulse compression and nonlinear pulse compression as shown in subsections below :

1.9.1 Fiber linear Pulse Compression

The techniques of linear pulse compression are purely based on the chromatic dispersion of fibers[77]. They are applied to pulses that are initially chirped, not bandwidth limited. A reduction of pulse duration results from the removal of the chirp, whereas the pulse bandwidth remains more or less unchanged. Normal chromatic dispersion can compensate a down-chirp, whereas anomalous dispersion may remove an up-chirp, but note that higher-order dispersion may also have to be considered [78].

1.9.2 Fiber Nonlinear Pulse Compression

Nonlinear pulse compression techniques are often used , where typically the Kerr nonlinearity is used for increasing the spectral width, and a suitable amount of chromatic dispersion (inside or outside the nonlinear device) removes the pulse chirp, minimizing the pulse duration[79].

1.10 Optical Fiber Communication Budgets

In the optical communication system, fiber patch cables and optical transceivers need to complete the optical signal path, enabling data to be transmitted between devices. In order to ensure that the fiber system has sufficient power for proper operation, it is vital to calculate the power budget of the span[80].

1.10.1 Optical Power Budget

Power budget refers to the amount of loss that can be tolerated by a data link while maintaining proper operation[80]. In other words, the amount of optical power available for a successful signal transmission over an optical fiber distance as shown in figure (1.14). Calculations should always assume the worst-case values in order to ensure that there is sufficient power available for the link, which means that the actual value will always be higher than that. The optical power budget is measured by dB, which can be calculated as shown in equation below[80,81]:

$$P_B\,(\mathrm{dB}) = P_{TX}\,(\mathrm{dBm}) - P_{RX}\,(\mathrm{dBm}) \quad \ldots\ldots\ldots(1.2)$$

where

P_{TX}: the minimum transmitter power.

P_{RX}: the minimum receiver power..

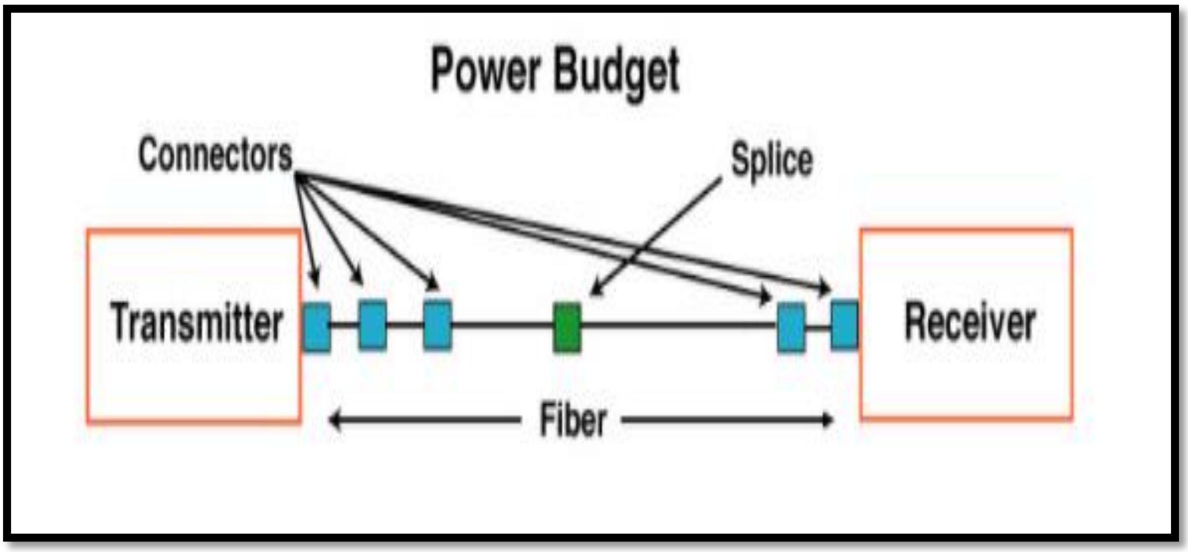

Figure(1.14): Optical power budget graph[81].

When calculating the performing of power budget, there is a long list of items to account for. In this subsection some of basic items that determine the overall performance of the transmission system are listed[80,81].

1.10.1.1 Fiber Loss

Fiber loss has a significant impact on the overall system performance, which is expressed by dB per kilometer. The total fiber loss is calculated based of the distance multiplied by loss factor[82].

1.10.1.2 Connector loss

Loss of a matched pair of connectors. Multimode connectors will typically have losses of 0.2-0.5 dB. Single-mode connectors that are factor made and fused will have losses of 0.1-0.2 dB. Field terminated single-mode connectors may have losses of up to 0.5-1.0 dB[83].

1.10.1.3 Splicing Loss

Splicing Loss is an important factor for optical fiber technology. Mechanical splice loss is generally between 0.7 and 1.5 dB per connector. Fusion splice loss ranges from 0.1 to 0.5 dB per splice. Due to their limited loss factor, fusion splices are preferred[84].

Table(1.1): compares general important factors between the fiber connectors and splices.

Table (1.1): Connectors versus Splices[85].

Connectors	**Splices**
Provide temporary connections	Provide permanent connections
Higher loss	Lower loss
Larger sizes	Smaller sizes
Immune, or not immune, to environmental effects (depends on the connector type)	Immune to environmental effects
It takes a long time to build a connector	It takes a very short time to build a splice
Diverse applications	Connection between a pair of fiber cables
Many types	Few types
New technology reduces installation time	Conventional technology keeps the same installation time
Building reasonable mechanical stability at the connection points	Building better mechanical stability at the connection points

1.10.2 Bandwidth Budget

Bandwidth is measured as the amount of data that can be transferred from one point to another within a network in a specific amount of time. Typically, bandwidth is expressed as a bitrate and measured in bits per second (bps). There are several different ways to measure bandwidth[86]. Some measurements are used to calculate current data flow, while others measure maximum flow, typical flow, or what is considered to be good flow. Bandwidth is also a key concept in several other technological fields. In signal processing, for example, it is used to describe the difference between the upper and lower frequencies in a transmission such as a radio signal and is typically measured in hertz (Hz)[87].

1.11 Compression Factor (Fc)

The narrower pulse in the time domain has the broader spectrum in the spatial domain [1,88]. Therefore the figure of merit of this study is characterized by the compression factor. The compression factor is a good indication for obtaining a narrow laser pulse with different technique of compression. This factor is explained by the relation between input and output pulses for the system of compression as shown in equation bellow [88,89].

$$\text{Fc} = \frac{FWHM_{i/p}}{FWHM_{o/p}} = \frac{\Delta\lambda_{FWHM-i/p-}}{\Delta\lambda_{FWHM-o/p-}} \qquad (1.3)$$

where

FWHM (i/p) is the full width half maximum of input pulse of the system.

FWHM (o/p) is the full width half maximum of output pulse of the system.

Temporal FWHM can be obtained from the spatial FWHM using the equation (1.4). [11,89]:

$$FWHM_{(temporal)} = \frac{(\lambda c)^2}{c \times FWHM\,(spatial)} \qquad (1.4)$$

where:

λ_c central wavelength in nm.

c speed of light in vacuum.

1.12 Literature survey.

1. **P. Colman et al., (2010)[90].**

- Technique used /Decreasing Energy for pulse that inject in solid core PCF.
- Wavelength (1.555) nm.
- Input pulse width 3 ps.
- Output pulse width 580 fs.
- Compression factor 5.17.
- Theoretical work.

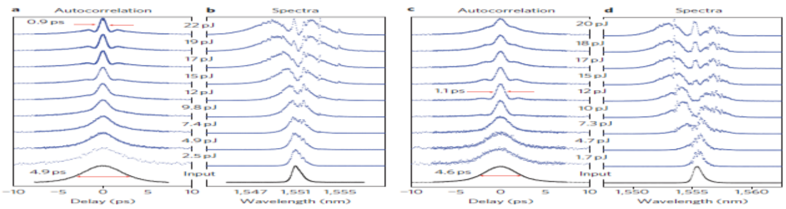

2. **M. Y. Chen et al.,(2011)[91].**

- Technique used:(Compression by using highly anomalous dispersive PCF).
- Wavelength (1554 nm) nm.
- Input pulse width 2898 fs.
- Output pulse width 630 fs.
- Compression factor 4.6.
- Experimental work.

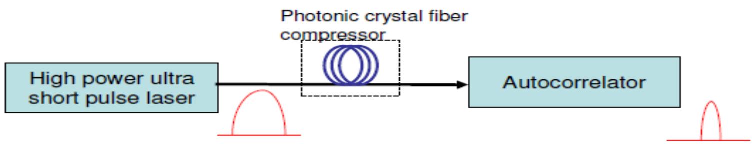

3. N. G. Baquedano et al. , (2012)[92].

- Technique used: (Tunning the cross section of HCPCF).
- Wavelength used 800 nm.
- Input pulse width 5 ps.
- Output pulse width 1.56 ps.
- Compression factor experimentally 3.2.
- Experimental and theoretical works.

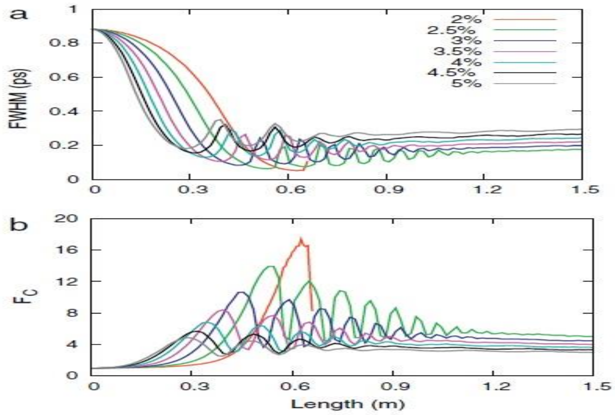

Fig. 5. Full width at half maximum (a), FWHM, and compression factor (b) as a function of the propagation length of a pulse and for different tapering factors.

4. S. Olupitan et al. , (2013)[93].

- Technique used / Robustness of chloroform-filled the solid core PCF.
- Wavelength 850 nm **.**
- Input pulse width 2 ps .
- Output pulse width 0.8 ps.
- Compression factor 2.5.
- Theoretical work.

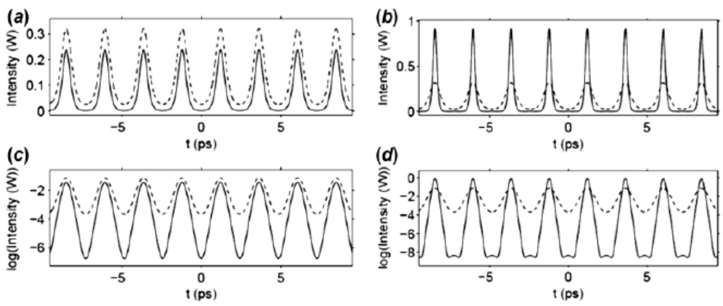

5. L. Cherbia et al. ,(2013)[94].

- Technique used: high level of energy and generating different orders of solitons without resorting tolarge values of fiber'sdispersion.
- Wavelength used 1065 nm.
- Input pulse width 28 fs.
- Output pulse width 1.8 ps.
- Compression factor 15.5**.**
- Theoretical work**.**

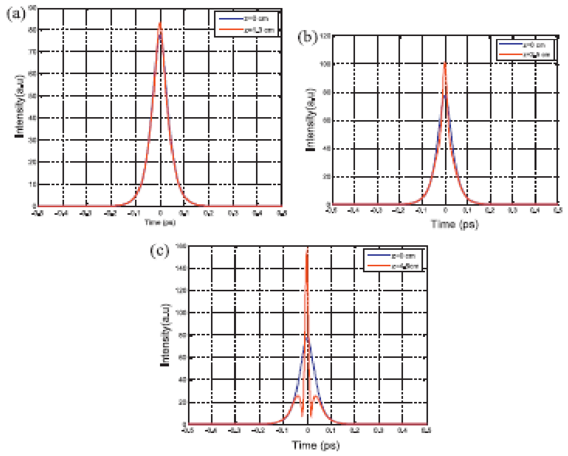

6. S. V. Smirnov et al. (2015)[95].

- Technique used: (Step-Index Large Mode Area Fiber (LMA)).
- Wavelength used 1560 nm.
- Input pulse width 5 ps.
- Output pulse width 3.2 ps.
- Compression factor 1.56.
- Experimental work.

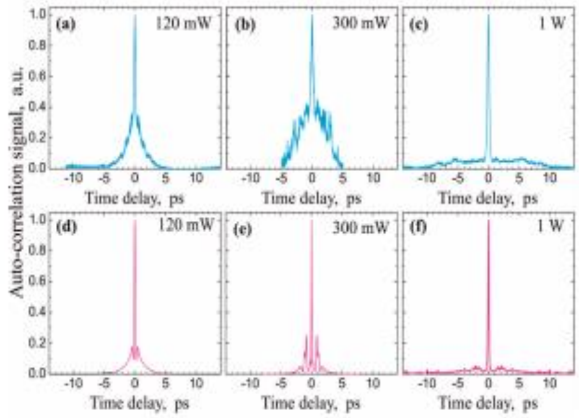

7. S. O. Atuba et al., (2016)[96].

- Technique used: (tapering solid core PCF).
- Wavelength 1550 nm.
- Input pulse width 0.8 ps.
- Output pulse width 0.15 ps.
- Compression factor 5.3.
- Theoretical work.

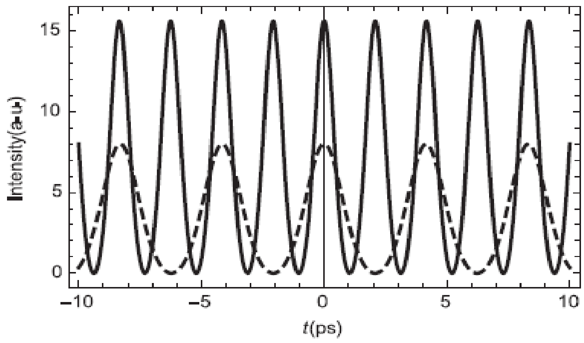

8. X. Feng et al. , (2018)[97].

Technique used: Tapering PCF through self-similar.

- Wavelength used 2.5 μm.
- Input pulse width 1 ps.
- Output pulse width 62.16 fs.
- Compression factor 16.09**.**
- Theoretical work**.**

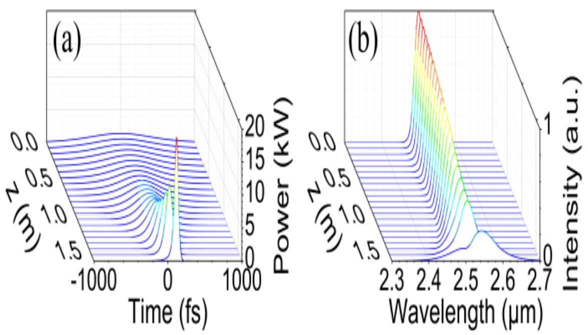

9. Y. G. Jeong et al.,(2019)[98].

Technique used: a single argon-filled HCF and chirped mirrors.

- Wavelength used 1030 nm.
- Input pulse width 170 fs.
- Output pulse width 5.1 fs.
- Compression factor 33**.**
- Experimental work**.**

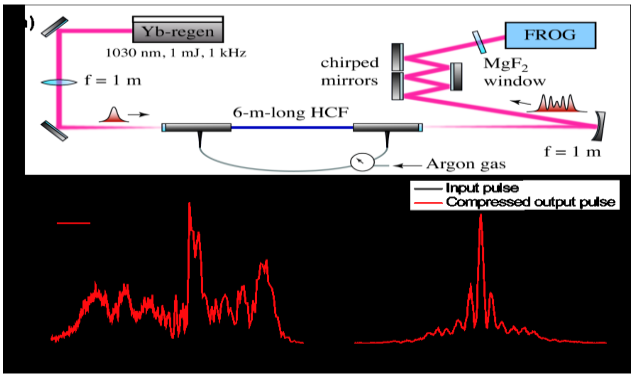

10. M. Rehan et al. ,(2019)[99].

- Technique used: a Large Mode Area Tapered Fiber.
- Wavelength. 1.55 µm
- Input pulse width. 250 *f*s.
- Output pulse width 46 *f*s.
- Compression factor 5.4
- Theoretical work.

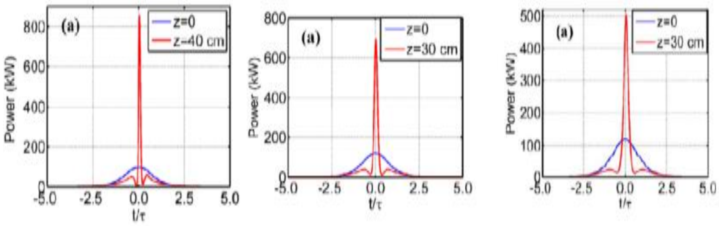

11. A. A. Dawood et al., (2019)[100].

Technique used: (HC-PCF) are used for high power beam delivery and can deliver ultra-short or compressed pulses at 1550 nm.

- Wavelength used 1550 nm.
- Input pulse width 10 ns.
- Output pulse width 6 ns.
- Compression factor 1.36.
- Experimental work.

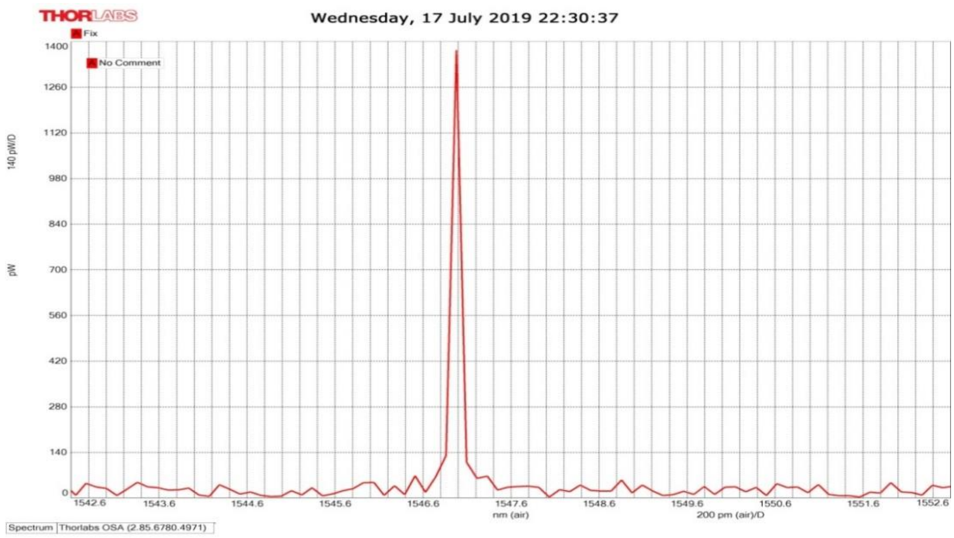

12. E. Vicentini et al. (2020)[101].

- Technique used: nonlinear compression of pulse by using two cascaded all-solid-state multi-pass cells.
- Wavelength used 1.03 μm.
- Input pulse width 460*f*s.
- Output pulse width 22*f*s.
- Compression factor 20.
- Experimental work.

Table (1.2): Compare experimental results of literature survey and this thesis.

Table (3.10): compare experimental results of literature survey and this thesis.

No.	Compression Factor	Year of the work	Notes
1	5.17	2010	Theoretical work
2	4.6	2011	Experimental work
3	5.7	2012	Experimental work
4	2.5	2013	Theoretical work
5	15.5	2013	Theoretical work
6	1.56	2015	Experimental work
7	5.3	2016	Theoretical work
8	1.5	2018	Experimental work
9	33	2019	Theoretical work
10	5.4	2019	Experimental work
11	1.36	2019	Experimental work
12	20	2020	Experimental work
This Thesis	1.10	2021	Experimental work

Chapter Two

Experimental Setup and Procedures of The Works

CHAPTER TWO

Experimental Setups and Procedures of the Works

2.1 Introduction

In this chapter, pulse compression would be constructed using single and cascaded PM-Mach-Zehnder Interferometers. The modal distribution of this Interferomter had been characterized using Comsol multi-physics (version 5.5). In the simulation and the experimental works of modals distribution via this in line interferometer , the tunability was done after applying mechanical forces on the micro splicing region and the PM fibers cross sectional area. The details of the thesis is illustrated in Figure (2.1).

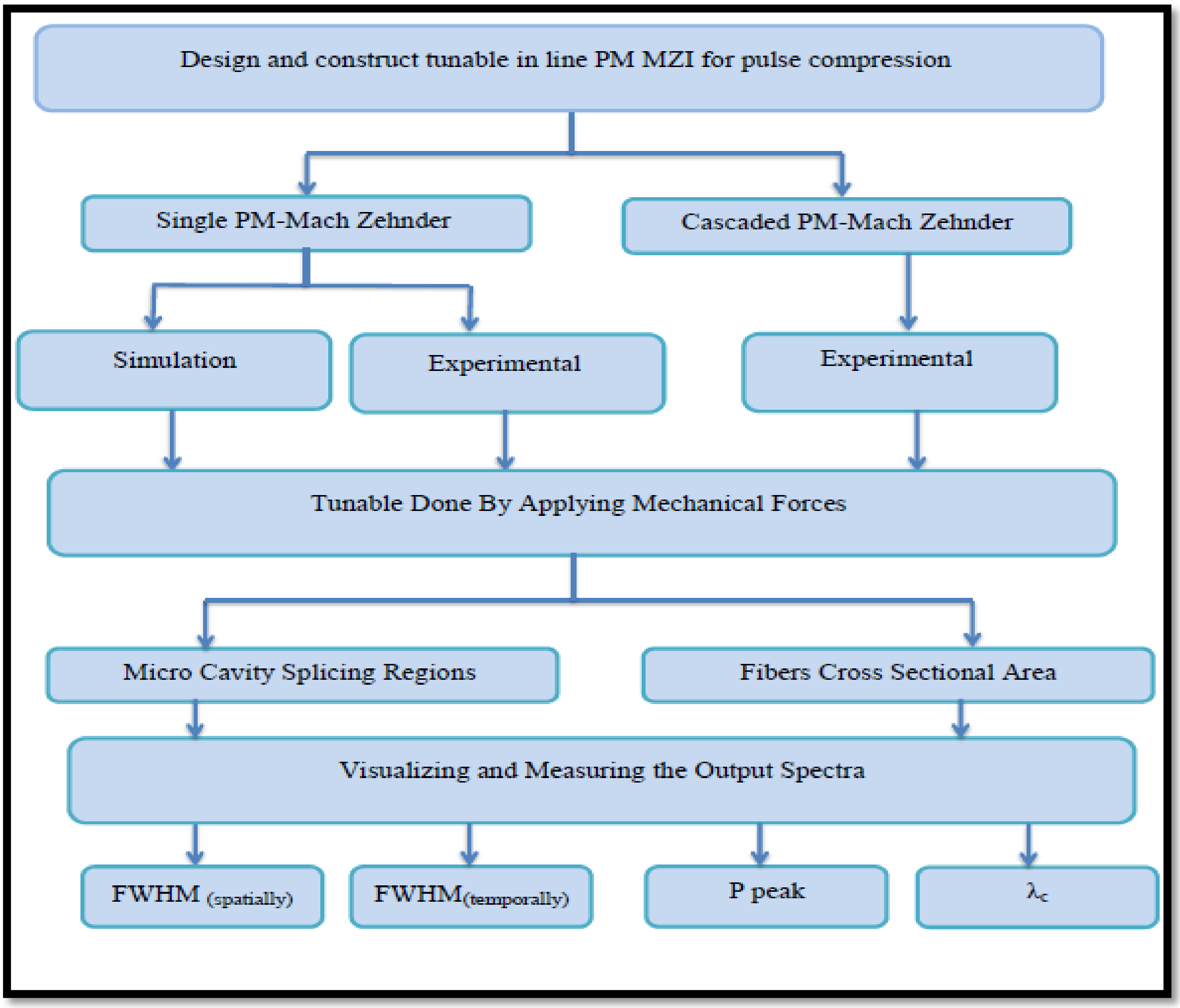

Figure (2.1): Flow chart of the work's steps.

2.2 Simulation Work

2.2.1 Single PM-Mach-Zehnder Interferometer (PM-MZI)

COMSOL multi-physics version 5.5 software was used to provide a clear vision about how optical signals propagate along optical fibers and affected by the outer environment changings, and to simulate the PM-MZI of this experiment , as shown in the following figure(2.2).

The material refractive index of each core and clad of SMF and PMF was selected according to standard fibers data sheet and previous studies [102,103] the effective index resulted by fusion and splicing was calculated using the general form of effective index formula "the n_{eff} is defined as the average of the refractive indices of the constituents" [104-108].

To simulate the effect of external induced force on PMF and splicing region, equations below used to find the elongation of fiber at each force separately. Young's modulus is the modulus of elasticity ranges from 66 Gpa to 74 Gpa for the SiO_2 [109-111].

$$young\ modulus = \frac{stress}{\text{Strain}} \tag{2.1}$$

$$\text{Strain} = \frac{\Delta L}{L} \tag{2.2}$$

$$\text{stress} = F / A \tag{2.3}$$

Where:

L is the original length.

ΔL is the change in length .

F is the applied force in (N).

A is the cross sectional area in (m^2).

The cross sectional area of optical fiber has 125µm cladding is equal to:

$$(62.5e\text{-}6)^2 \times \pi = 1.227e\text{-}8\ m^2$$

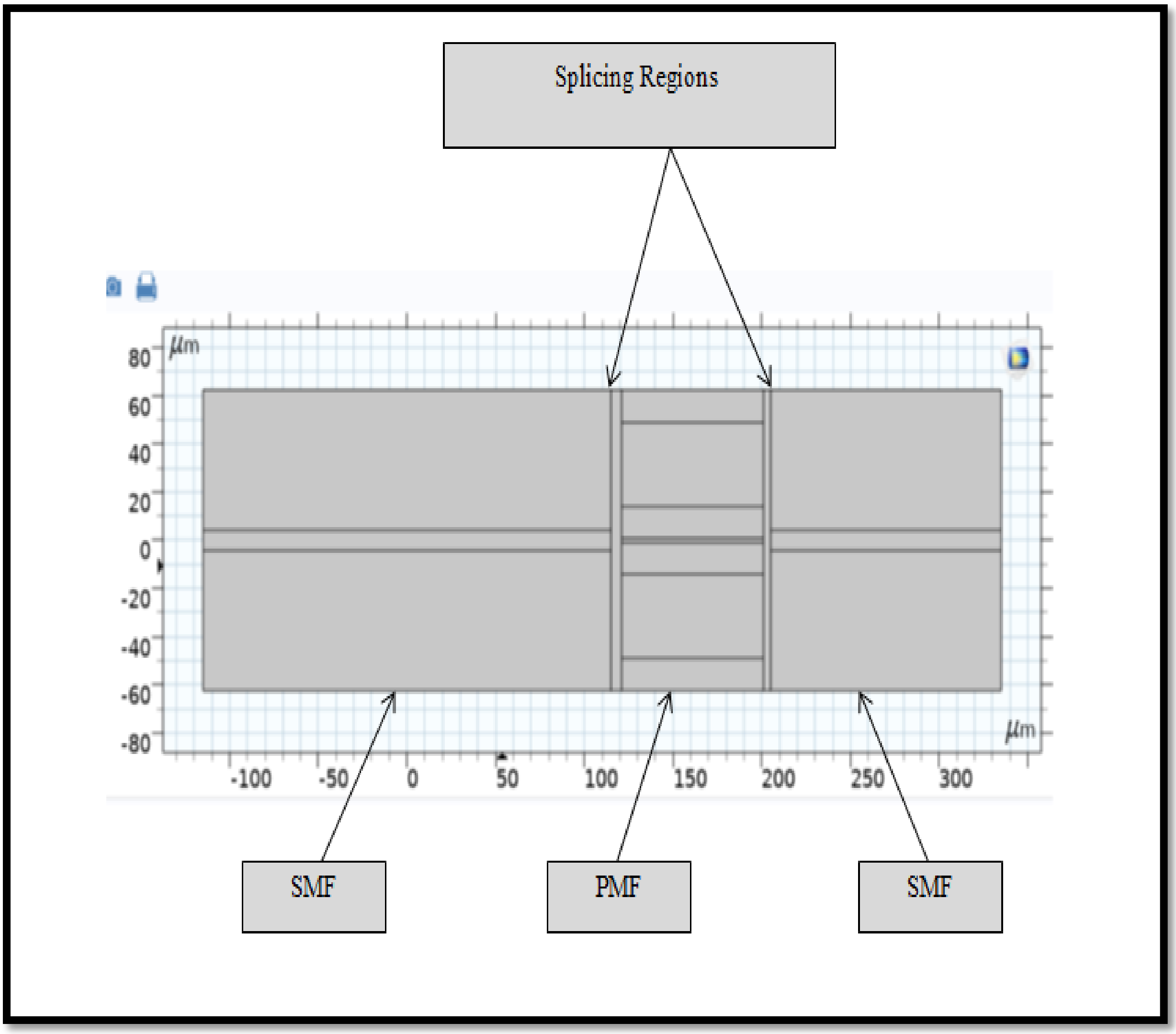

Figure (2.2) Geometrical simulation build-up of PM-MZI using Comsol software.

2.3 The Experimental Work Components and Equipment's

The used components and equipment's in the experimental work will present in the following subsections.

2.3.1 The Optical pulse Laser Source

The spectrum of the pulse Laser source is shown in Figure (2.3).The pulse laser having specific parameters illustrated in Table (2.1) and more detailed in datasheet shown in [appendix A].

Table (2.1): Parameters for pulse laser source.		
Parameter	**Value**	**Unit**
Central wavelength	1546.74	nm
FWHM $_{\text{Temporal}}$	10	ns
FWHM $_{\text{Spatial}}$	286	pm
Pulse repetition rate	30	kHz
Duty-cycle	90%	___
Energy	0.0123	nJ
Power	1.229	mW
Voltage	2	mV

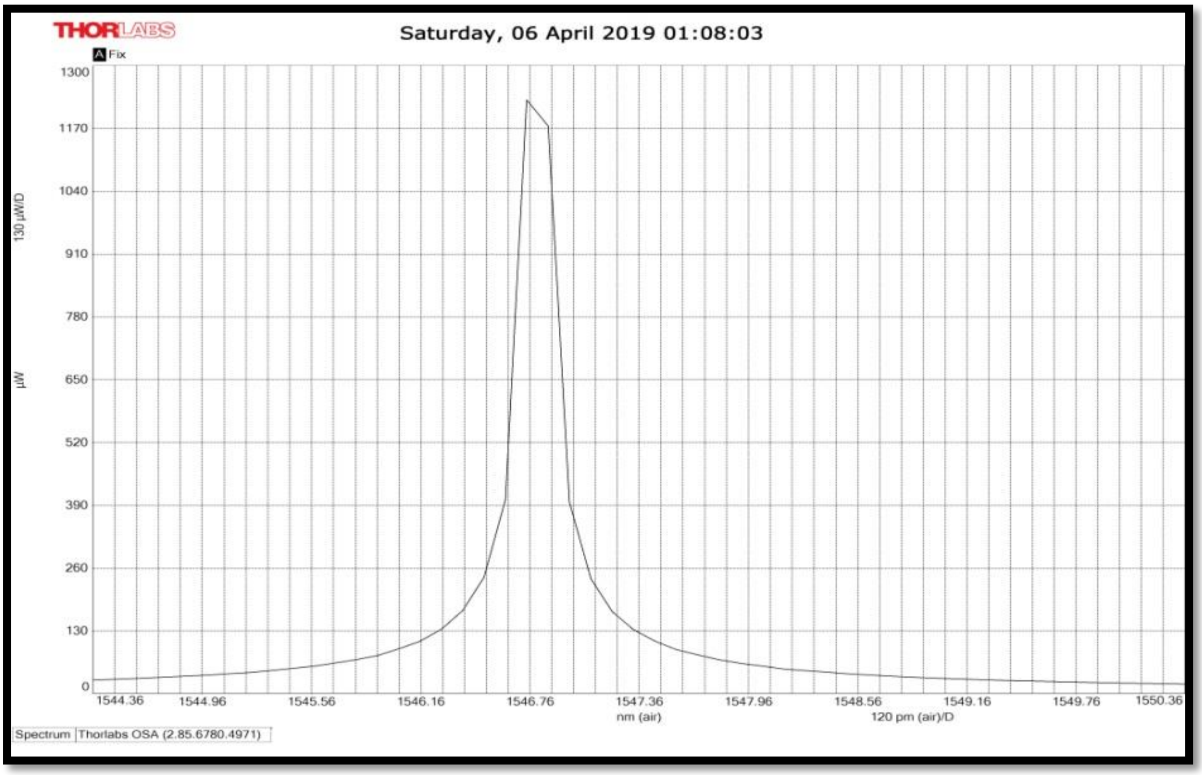

Figure (2.3) :The pulse laser source spectra line.

2.3.2 In-Line PM-MZ Interferometer

This interferometer constructed using two different types of optical fiber in terms of number of the guided mode, which effect on the ratio of core's power to cladding's power, these fibers are demonstrated as follows in term of their cross sectional areas , refractive index and length.

This interferometer was building using two types of fibers, these fibers are explained in subsections below.

2.3.2.1 Single Mode Fiber (SMF)

Single mode optical fiber made from corning company with modal 28 for coupling laser to interferometer and spliced with polarization maintaining fiber to perform fiber interferometer. The optical specifications of SMF are presented in table (2.2), [see appendix B]. Figure (2.4) shows the side view for the SMF fiber under microscope.

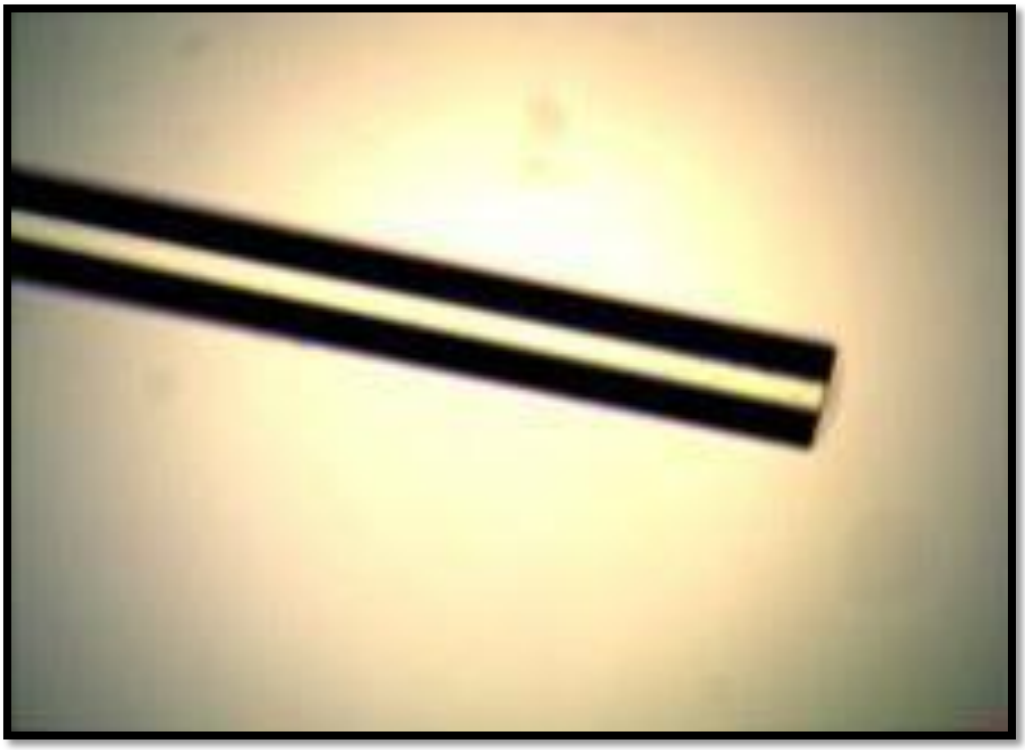

Figure (2.4): Side view for the SMF fiber under microscope.

Table (2.2): Optical specification of SMF.		
Parameters	**Value**	**Unit**
Operating wavelength	1550	nm
Core diameter	8.2-10	µm
Cladding diameter	125 ± 2	µm
Mode-Field Diameter (MFD)	@1310nm 9.2 ± 0.4 @1550 nm 10.4 ± 0.5	µm
Dispersion	@1550nm $\leq$ 18.0 @1625nm $\leq$ 22.0	[(ps/(nm*km)]

2.3.2.2 Polarization Maintaining Fiber

PANDA-PM(P3-1550PM-FC-10, from THORLABS) specialty fibers are designed to maintain properties with the best polarization, the fibers offer low attenuation and outstanding birefringence. Available in a wide range of standard operating wavelengths, with a variety of coating designs and up to 1550 nm. For high performance polarization retaining fiber applications, PANDA PM specialty fibers are optimal. This field-proven fiber supports applications of high growth, and performs well over a broad range of temperatures. The optical specifications of PMF are presented in table (2.3) [Appendix C]. Figure (2.5) shows the Schematic and cross sectional of PM-PANDA.

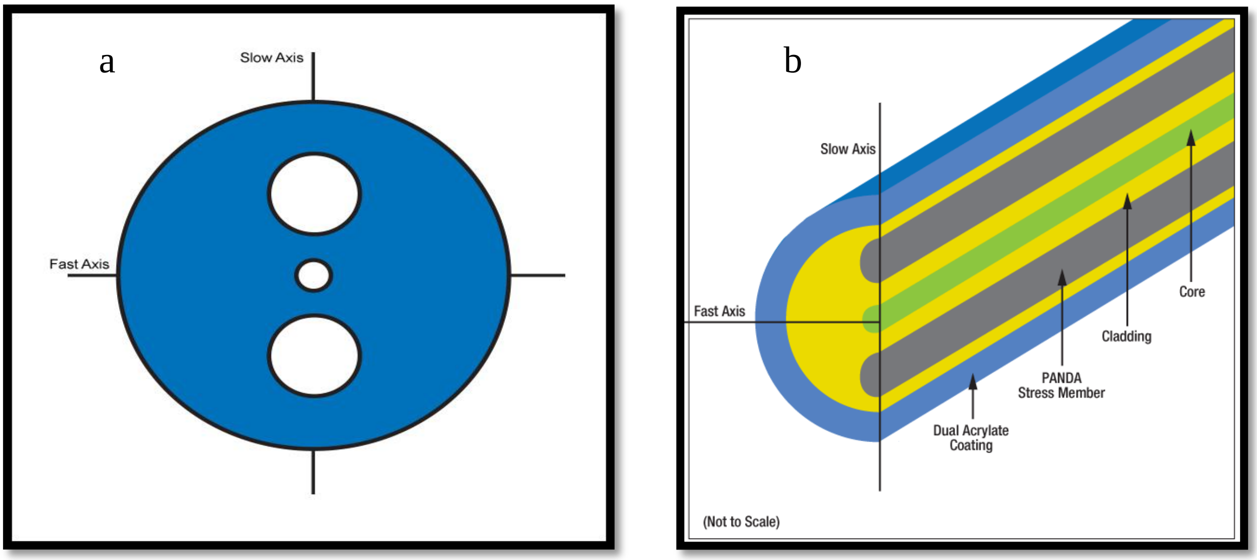

Figure (2.5): (a) Schematic of PANDA-PM Fiber, (b) PANDA-PM Fiber Cross Section.

Table (2.3): Optical Specification (PMF).

Parameters	**Specifications**	**Test data**
Alignment Wavelength	1550nm	
Fiber Operating wavelength Rang	1440-1625nm	
Cutoff Wavelength	1370 ± 70 nm	
Min. Extinction Ratio (Port A/Port B)	23 dB	23dB/23dB

Max. Insertion Loss (Port A /Port B)	0.5 dB	0.11dB/0.24dB
Typical Optical Return Loss (Port A / Port B)	60 dB	
Mode Field Diameter	9.9 ± 0.5 µm @1550nm	
Connector Type	FC/APC	
Key Width	2.0mm(Narrow)	
Key Alignment	Slow Axis	
Fiber Type	PM1550-XP	
Fiber Length	10.0m	
Jacket Type	FT030-BLUE	
Max Power	300mW	
Operating Temperature	0 To 70 °C	
Storage Temperature	-45 To 85 °C	

2.3.3 Mechanical Weights

The Force is physical effect applied on the PMF to insure the compression for the pulse which propagated through the polarization maintaining fiber . The force effect applying vertically on the PMF. It's consists of different dimensions of bases from aluminum. The big ground base dimensions are (27x27x1.5) cm, the pieces over the big ground base are considered as bracketed tool. It consisted of two pieces of polished carbon steel or aluminum with dimensions (5.5x3x1.5) cm. Even is appropriate to dimensions of the used bare the PMF. The purpose of it is to press the bear of the PMF. After pressing, the physical properties of PMF will be changed. The results of press processing indicate the changes the pulse duration of the light that propagate through PMF and knowing the weight amount which has placed on a bare of PMF. The dimensions of upper base of the diagram are (19x19x0.5) cm. It works as a balance where weights placed on it. This design involves reset process for parts of the system over a bracketed tool. The purpose of reset process is to ensure the weights is zero on the PMF without exciting of additional weights. After reset process, when additional weights are applying on the balance it will be calculated precisely.

The weights that used in these experiments are (5,10,20,50,100)g that are applied at the interferometer cavity's regions and fibers cross sectional area to perform the elongation in the interferometer length ,tunability in the fiber interferometer. Figure(2.6) shows the image of forces positioning instrument and different weights.

(a) (b)

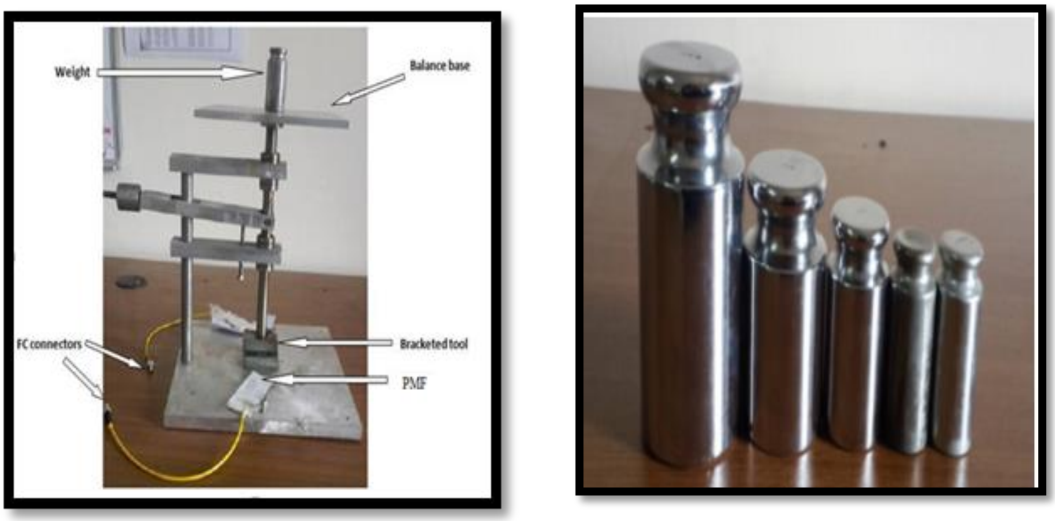

Figure (2.6) : Mechanical forces (a) Image of Forces positioning instrument and (b) Different weights.

2.3.4 Optically Visualizers

The optical signal was visualized by optical spectrum analyzer (OSA202) made by THORLABS. An optical spectrum analyzer is a device was designed to measure and display the power distribution of an optical source over the specified wavelength rang [Appendix D]. The characteristics of this device shown in table below.

Table (2.4): The characteristics of (OSA 202).		
Parameters	**Value**	**Unit**
Wavelength range	600 - 1700	nm
High wavelength accuracy	± 0.01	nm
High wavelength resolution	0.02	nm
Wide level range	+20 to -90	dBm
Fast measurement	0.2 sec.(100nm span).	___

2.4 Procedures of Constructing Interferometers

There are many steps have been achieved for constructing these interferometers as follows:

2.4.1 Optical Fibers Stripping

The first step, stripping define as remove the protective polymer coating using mechanical or thermal effect which allows access to the glass fiber. It is important since it can damage the optical fiber and weaken its long term mechanical reliability. The conventional optical fiber stripping tools (JIC – 375 Tri – Hole), used in this experiments to remove any protective coating.

2.4.2 Optical Fiber Cleaver

The second step is cleaving the optical fibers by the cleaver machine (CT-30) which shown in figure (2.7). The fibers cleaved to produce end faces.
The fiber ends are aligned with each other and the fire tips heated to their softening point, so when they are pressed together they form a joint. The fiber end faces are required for the minimum deformation when the end faces are brought together. Flat in this case means no notches or bumps in the fiber's end face greater than a few percent from the surface. Optical fiber cleaved by placing it under sufficiently high tensile stress, around a sufficiently large surface crack. This crack then propagates across the fiber cross section until the fracture crosses to encompass the whole fiber cross section, and the fiber is detached into two parts. Cleaving may be a violent and difficult to control process, and cleavers will periodically produce defective cleaves. Finally; to ensure the edges of the fiber are well-cleaved, it must be examined under a microscope and in case that the fiber tip is not smoothly cleaved then the fiber must re-cleaved.

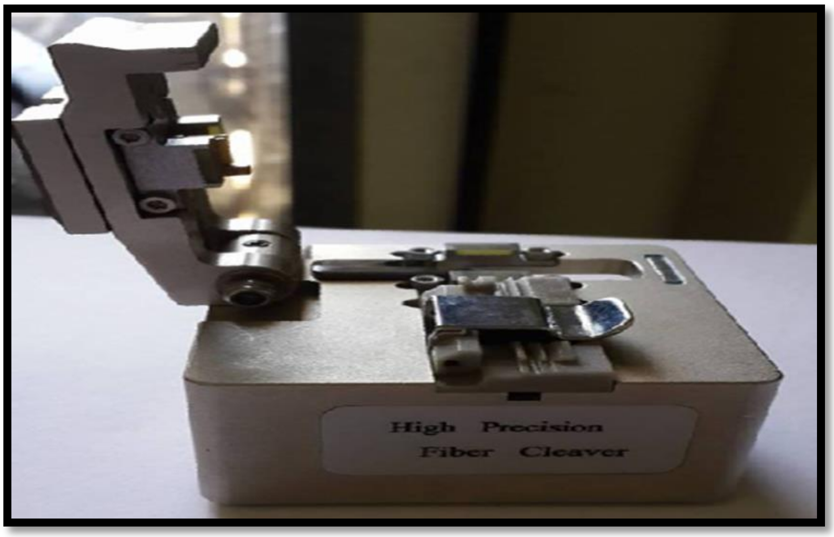

Figure (2.7): Fiber cleaver (CT-30).

2.4.3 PMF and SMF Fusion Splicing

The third step is fusion splicing define as the process by which a permanent low loss, high strength, welded joint formed between two optical fibers. In this work, (DVP-740) splicing machine, shown in figure (2.8) was used to fusion splice PMF and SMF.

Figure (2.8): Optical fiber arc fusion splicer type (DVP-740).

Fusion splicer is the device that splices the fibers, needs to position the end faces closed to each other. The two fibers were held in chucks or v-grooves that could move the fiber ends with four degrees of motion: x, y, z and θ. The splicing region must be strong enough as the original fiber, therefore, when the light passed through fiber, will not be scattered. The source for this process can be getting from electric arc. The softening point for the conventional single mode fiber is different for PMF due to the microstructure of PMF. The surface tension in softening point will overcome the viscosity and make the PMF's collapsing in the air hole. So, the splice process will be done by trial and error by changing arc power and arc time. Figure (2.9) give an example of fibers experiences the arc fusion process:

(a) Fibers have experienced perfusion.

(b) Fibers have been softened and brought together.

(c) The fibers finally formed the splice.

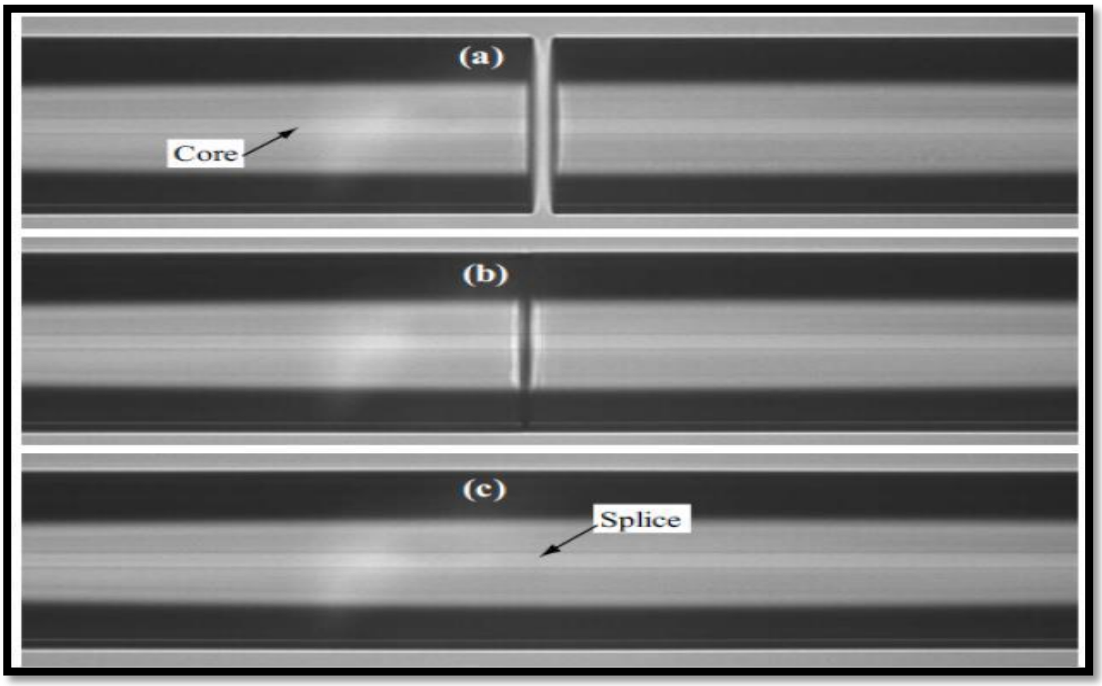

Figure (2.9): Fusion splicer process between two SMF and PMF .

The optimum parameters of the fusion splicing (DVP-740) have been selected to splice PMF to SMF to get accurate measurement of the splice loses was summarized in Table (2.5).

Table (2.5): parameters of fusion splice SMF and PMF.	
Work type	Auto
Arc Time	0.1 Sec
Pre Arc Time	0.20 Sec
Arc Power	0.70
Pre Arc Power	0.78
Cleave Angle	3.0^{o}
Gap Position	Middle

2.5 Experimental Work

As it was listed in figure (2.1), a simulation study for each part in the block diagram was carried out followed by an experiment for that part. In the following sections the details of all the experiments and simulation studies will present.

2.5.1 In-line Mach-Zehnder Interferometers

Two experimental setup were performed using different PMF lengths 8,16 and 24 cm, the first with one Polarization maintaining fiber and two splicing regions , the second setup with two Polarization maintaining fibers and four splicing regions.

Two types of In-line MZI have been used in the simulation and experimental work to design.

2.5.1.1 Single PM-Mach-Zehnder Interferometer (PM-MZI)

The single PM-MZI consists of one PM-MZI which mean two micro cavity splicing regions MCSRs ,one cavity length Lc ,the mechanical force in g was varied from (5-100)g applied on the interferometer splicing regions and also will be applied on the PM fiber cross sectional areas.

Figure (2.10) shows the schematic diagram for experimental setup for the tunable singe PM-Mach Zehnder interferometer.

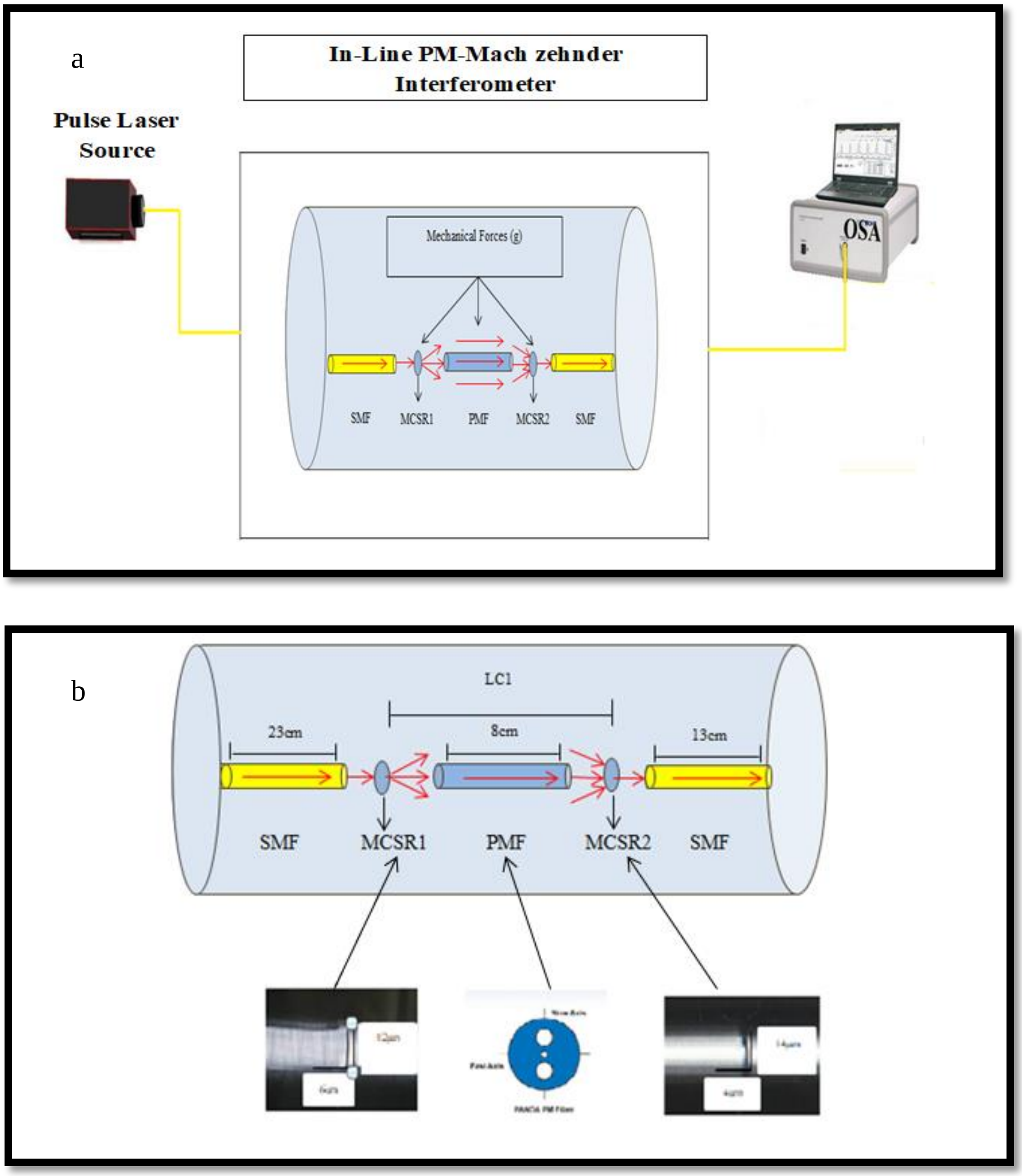

Figure (2.10): schematic diagram of (a) PM-MZI pulse compressor, (b) Single PM-MZI.

The in line single PM-Mach-Zehnder interferometer MZI is made of PMF with three different length 8,16,24 cm sandwiching between two standard single-mode optical fibers SMF with length 23and 13cm. The cladding modes are excited by the first up-taper and then enter the PMF section as the interferometer arm. Finally, both the cladding modes and the core mode are reconnected to the second up-taper, which forms the Mach-Zehnder interferometer. The pictures of these experiments are shown in figure (2.11).

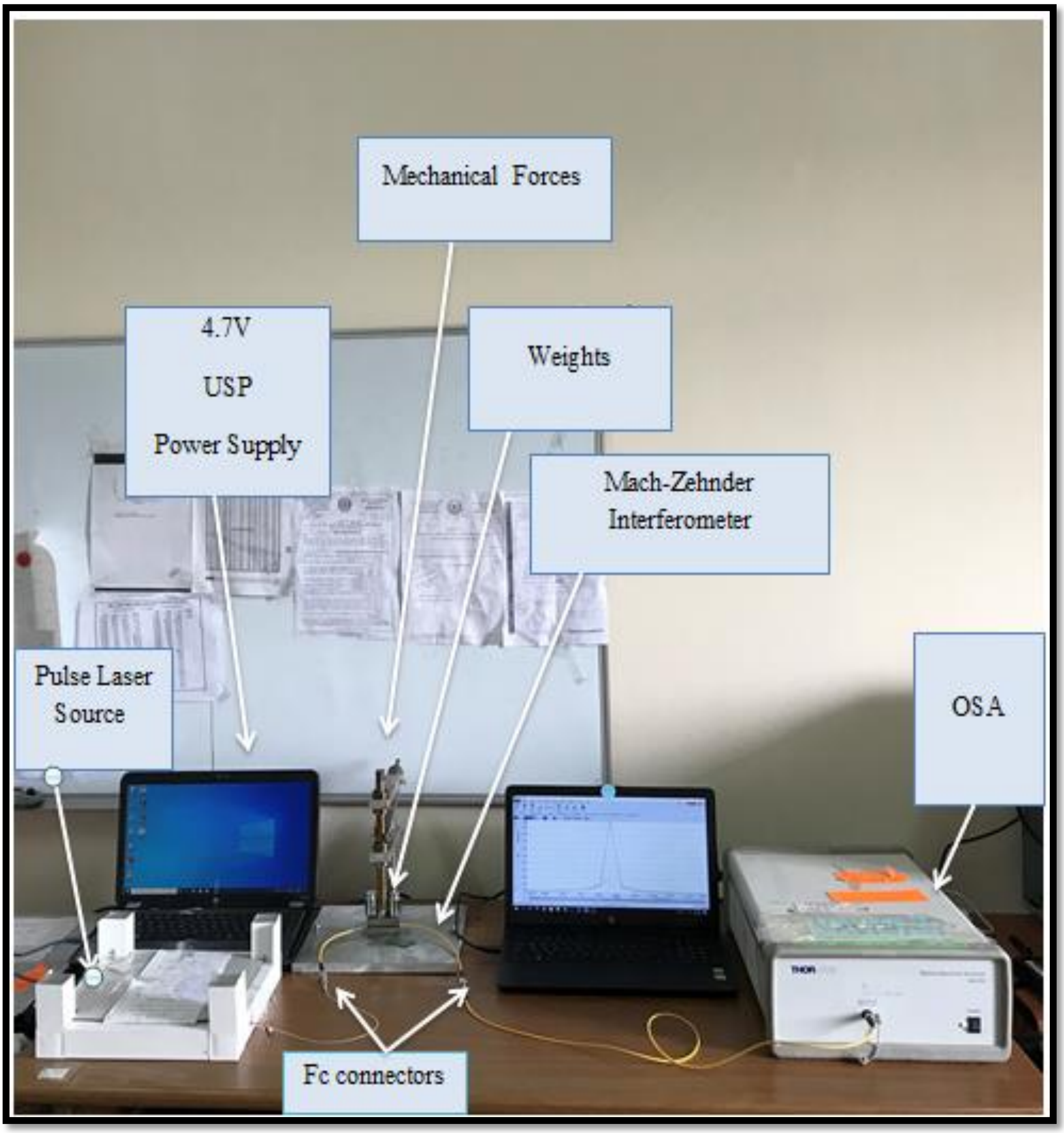

Figure (2.11): The experimental setup for In-line Single PM-MZI.

2.5. 1.2 Cascaded PM-Mach-Zehnder Interferometer (PM-MZI)

The cascaded PM-MZI consists of 2 PM-MZI which mean four micro cavity splicing regions MCSRs ,three cavity length Lc ,the mechanical force in g was varied from (5-100) g applied on the interferometer splicing regions and also will be applied on the PM fiber cross sectional areas.

Figure (2.12) shows the schematic diagram for experimental setup for the tunable cascaded PM-Mach Zehnder interferometer.

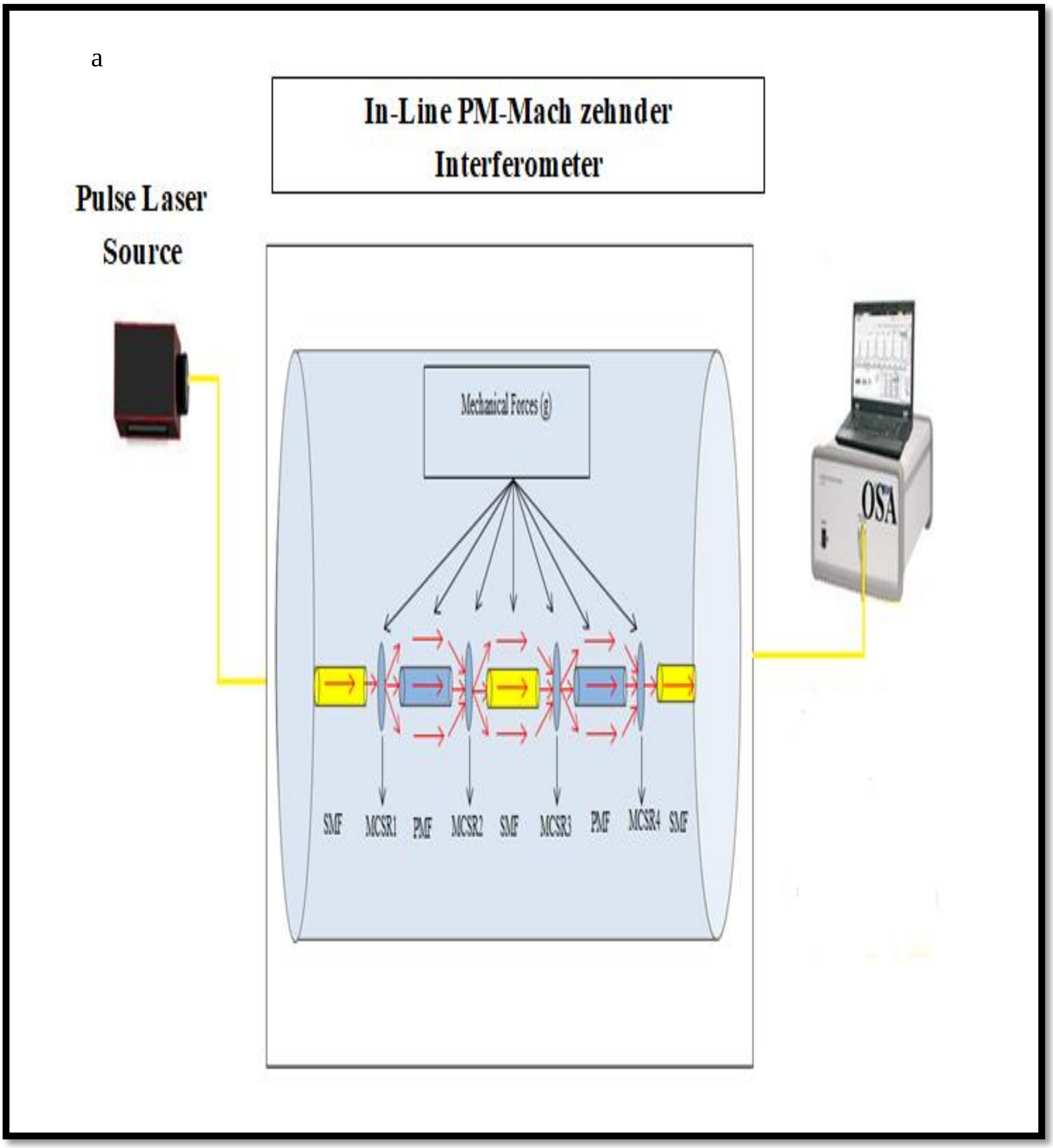

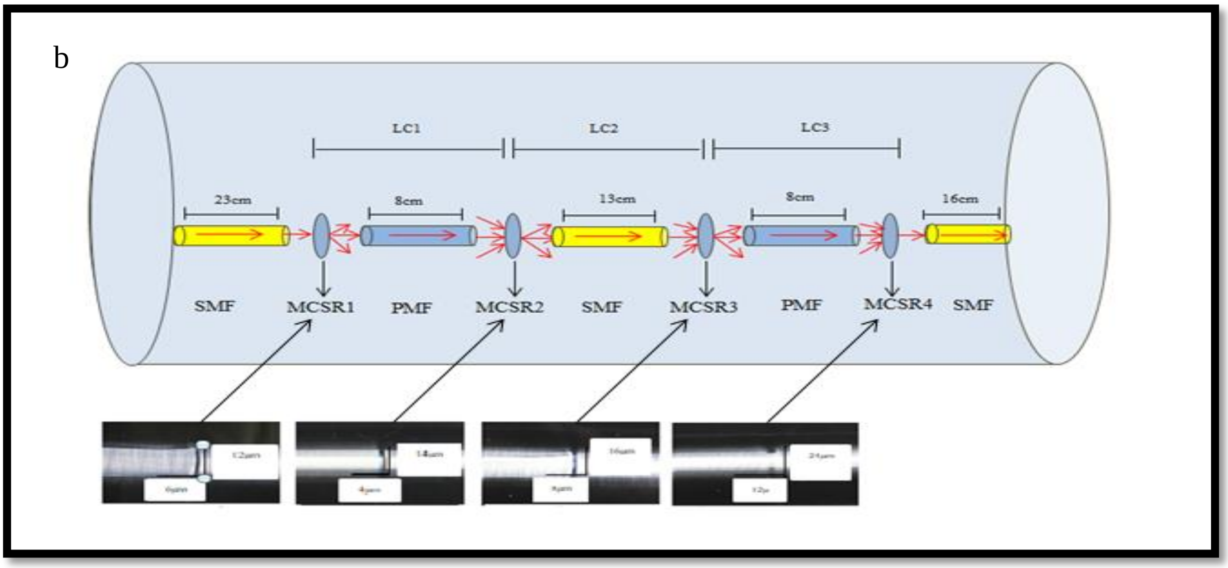

Figure (2.12): Schematic diagram of (a) PM-MZI pulse compressor, (b) cascaded PM-MZI.

The in line cascaded PM-Mach-Zehnder interferometer MZI is made of two PMF with length 8 cm sandwiching between three standard single-mode optical fibers SMFs with lengths 23,13 and16cm .

In each splicing region the cladding modes are excited by the first up-taper and then enter the PMF section as the interferometer arm. Finally, both the cladding modes and the core mode are reconnected to the second up-taper, which forms the Mach-Zehnder interferometer. The pictures of these experiments are shown in figure (2.13).

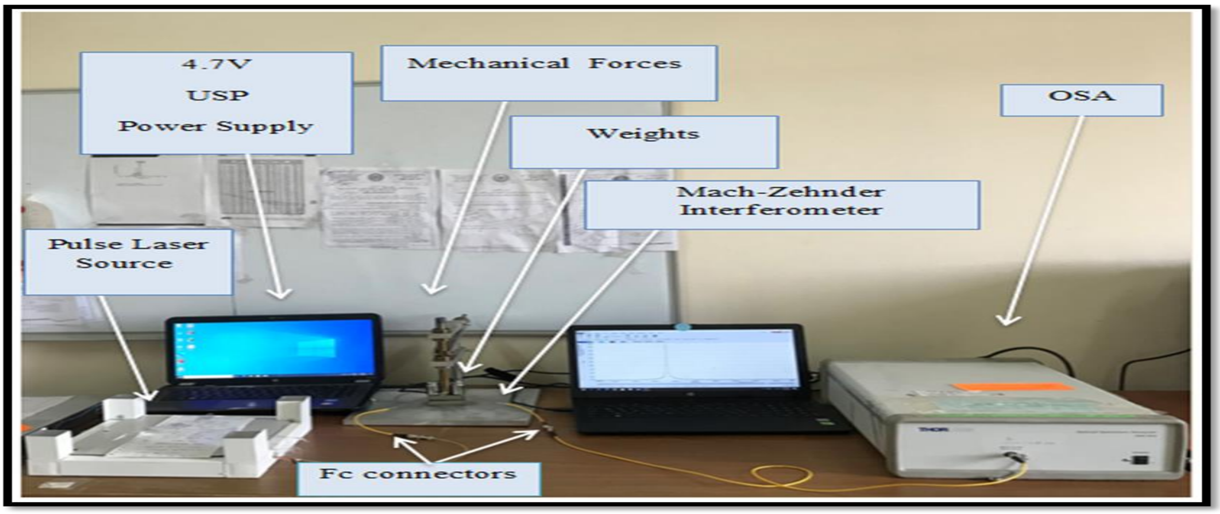

Figure (2.13): The experimental setup for In-line Cascaded PM-MZI.

Chapter Three

Results, Discussion and Future Works

CHAPTER THREE

Results, Dissection, and Conclusions.

3.1 Introduction

In this chapter, simulation and experimental results for tunable laser pulse compression using single and cascaded PM-Mach Zehnder Interferometers will be presented and discussed.

Many affected parameters on the shape and pulse width and peak power after using PM-MZI are studied. These parameters are number of micro cavity splicing regions , the changed in the length of PMF's and mechanical force that applied on the PMF cross section and micro cavity splicing regions.

This chapter can be divided into: simulation and experimental results introduced in section 3.2. Section 3.3 summarizes the main point concluded from this work followed by some suggestions for future work in section 3.4.

3.2 Simulation and Experimental Results

In the following sections the simulation and experimental results are illustrated for single and cascaded PM-Mach-Zender interferometers .

.

3.2.1 Single PM-Mach Zehnder Interferomter

Different mechanical forces are used to make the tunability in the designed fiber Interferomter after applying them on the Polarization maintaining fiber cross sectional area and PM-SMF micro cavity splicing regions. Subsections below shows the simulation and experimental results for single PM-Mach Zehnder interferometers.

3.2.1.1 Simulation Results

Three different lengths of polarization maintaining fibers with (8,16,24) cm have been studied after splicing them between two single mode fibers SMF with lengths 23and 13cm. And the influence of different mechanical forces applied on both cross sectional area and the micro cavity splicing regions of PM fiber had been recorded.

The mechanical force in this work was made by applying different weights (0, 5, 10, 20, 50, 100) g on the PMF.

The elongation for the cross section of PMF will be reducing of the geometric parameters of PMF, this change of parameters caused decreased the group velocity for all modes which propagated through the core and cladding for the fiber and the reducing in parameters of fiber will be changed on the parameters of pulse that propagated through the fiber .Table (3.1) shows the elongation of PMF length after applying different weights and the resulting fiber elongation is characterized in the in the figures (3.1).

Table(3.1):the elongation of PMF after applied different weights on it.

Weights g	**ΔL (cm)**		
	L=8cm	L=16cm	L=24cm
0	0	0	0
5	0.0046568	0.00931	0.01397
10	0.009312	0.01862	0.027936
20	0.01864	0.03728	0.05592
50	0.046568	0.09314	0.139704
100	0.093	0.1862256	0.2794

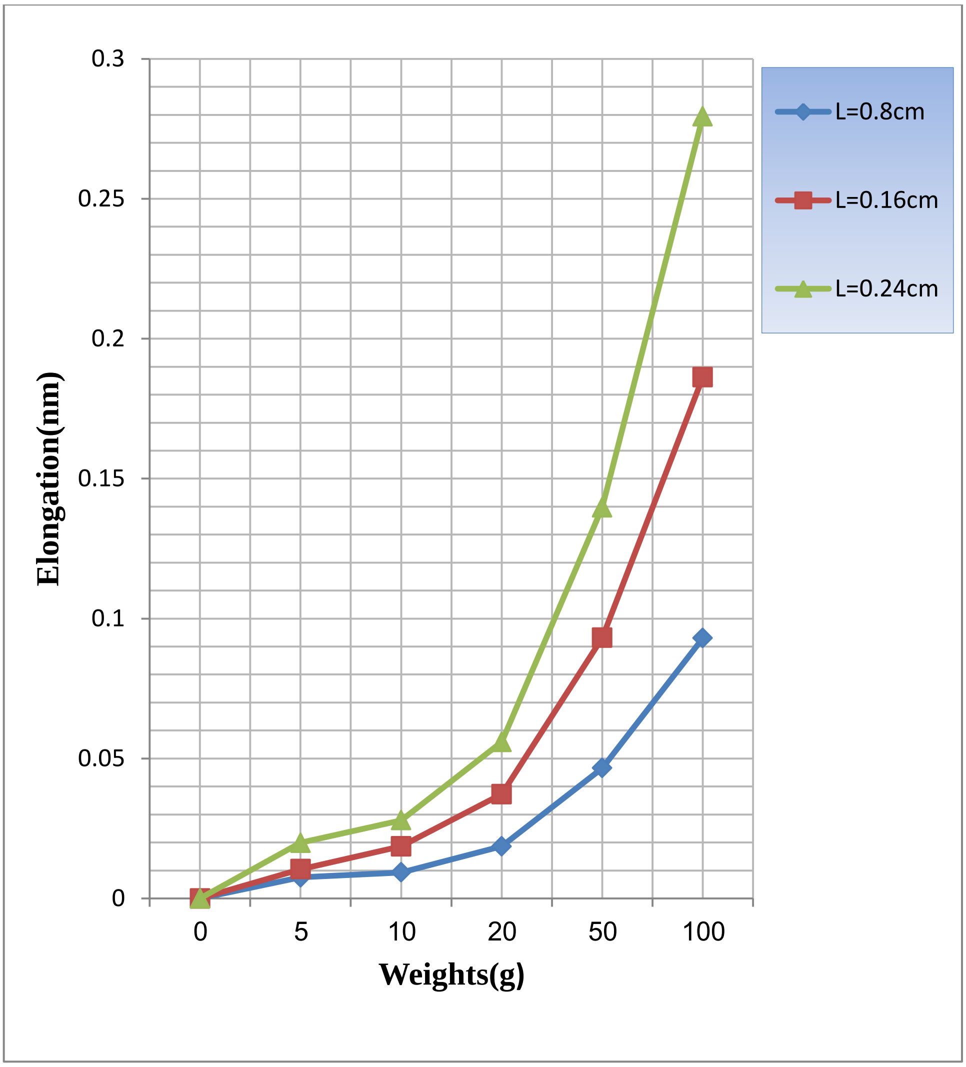

Figure (3.1): PM-Fiber Elongation as a Result of Applied Force Variation.

The boundary mode analysis results of single PM-Mach Zehnder interferometer variation with force are shown in figures (3.2), (3.3) and (3.4) respectively. Since The narrower pulse in time domain can be gained from the wider pulse in spectral domain then the best compressed pulse in this study is a gained from the highest propagation order mode. By observing following figure can see that the higher excitation of higher order modes came from the 8cm PMF after applying 5 g on the cross sectional areas of the fiber and in case of 16 cm PMF after applying two equally 10,20 g on the micro cavity splicing regions .

weights	Forces applied on PMF	Forces applied on splicing region
0	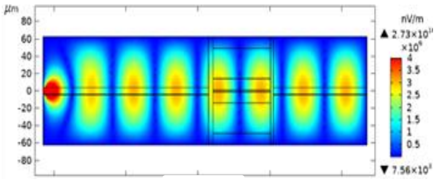 a	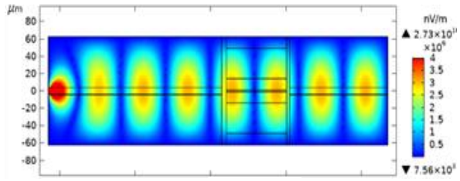 b
5	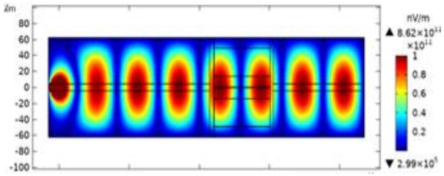 c	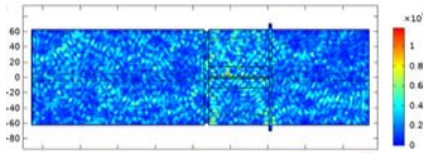 d
10	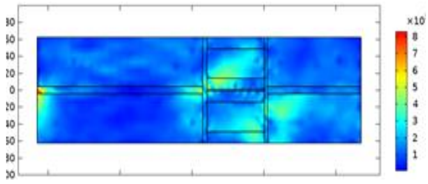 e	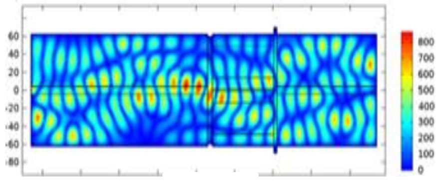 f
20	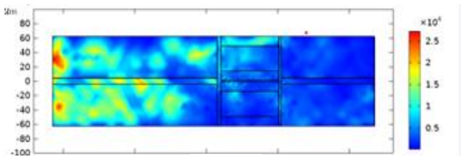 g	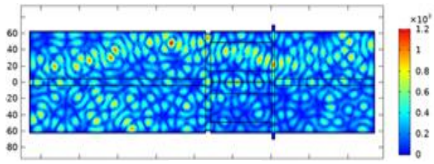 h
50	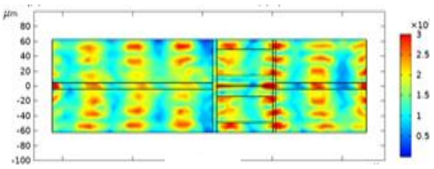 i	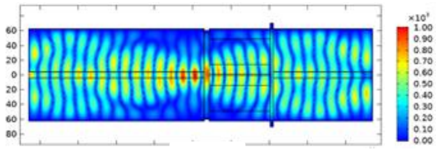 j
100	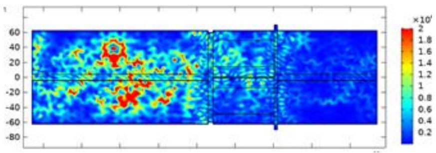 k	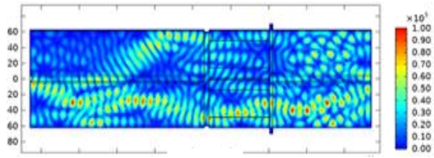 l

Figure (3.2 a-l): The simulation results of boundary mode analysis that demonstrate the mode distribution in single PMF-MZI with 8 cm PM fiber length when different weight are applied PM fiber cross sectional area and also SMF-PMF micro cavity splicing regions.

weights	Forces applied on PMF	Forces applied on splicing region
0	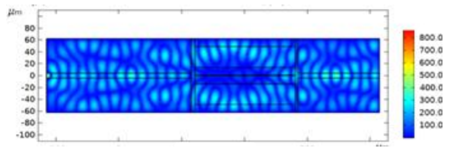 a	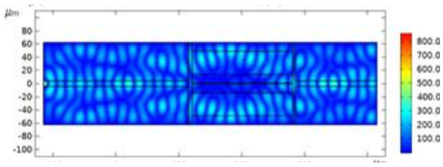 b
5	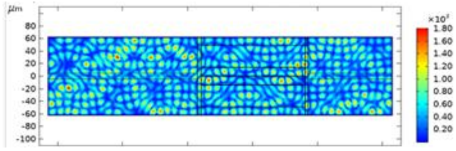 c	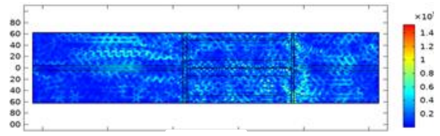 d
10	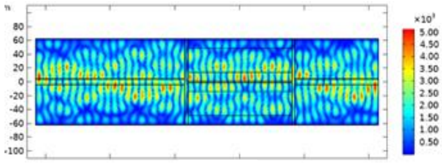 e	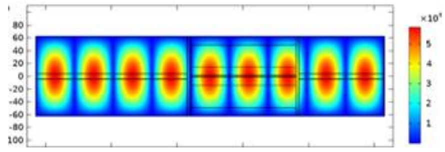 f
20	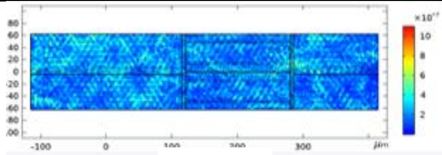 g	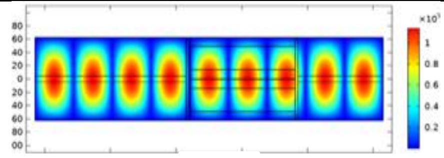 h
50	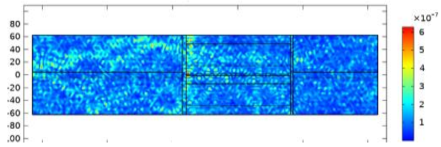 i	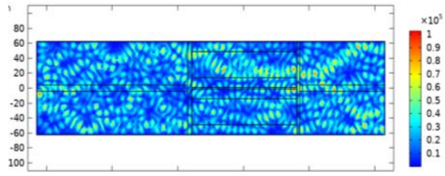 j
100	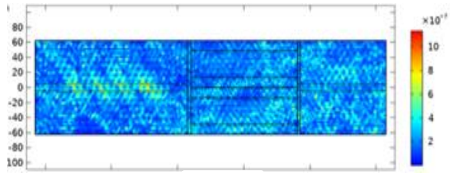 k	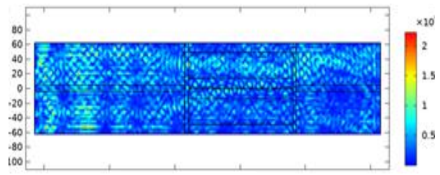 l

Figure (3.3 a-l): The simulation results of boundary mode analysis that demonstrate the mode distribution in single PMF-MZI with 16 cm PM fiber length when different weight are applied PM fiber cross sectional area and also SMF-PMF micro cavity splicing regions.

weights	Forces applied on PMF	Forces applied on splicing region
0	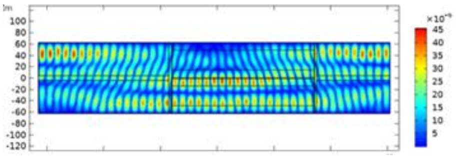 a	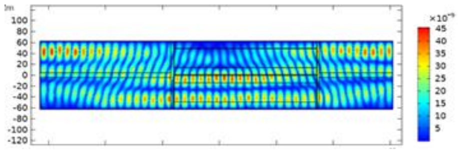 b
5	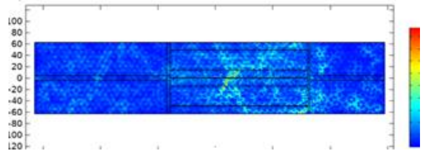 c	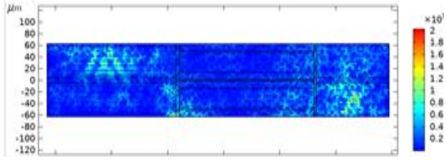 d
10	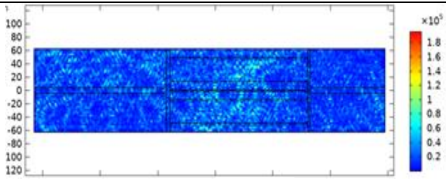 e	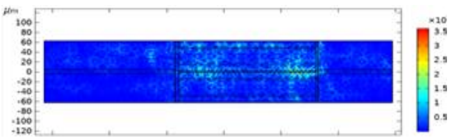 f
20	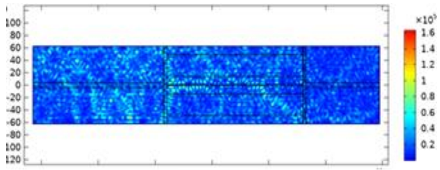 g	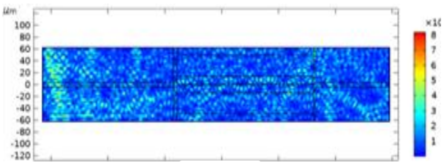 h
50	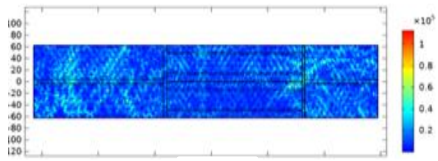 i	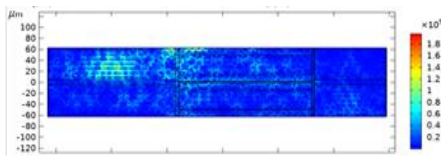 j
100	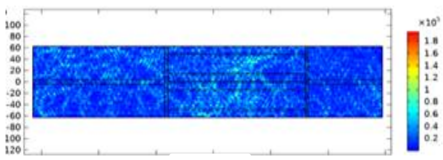 k	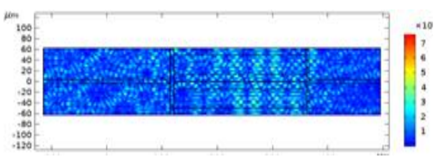 l

Figure (3.4 a-l): The simulation results of boundary mode analysis that demonstrate the mode distribution in single PMF-MZI with 24 cm PM fiber length when different weight are applied PM fiber cross sectional area and also SMF-PMF micro cavity splicing regions.

3.2.1.2 Experimental Results

❖ **Single PM-Mach Zehnder interferomter with length (8cm)**

The output spectrum for the single PM-Mach-Zehnder interferometer was visualized by using optical spectrum analyzer, after applying different mechanical forces, weights in g , on the PM fiber cross sectional areas and PM fiber splicing regions as shown in figure(3.5).

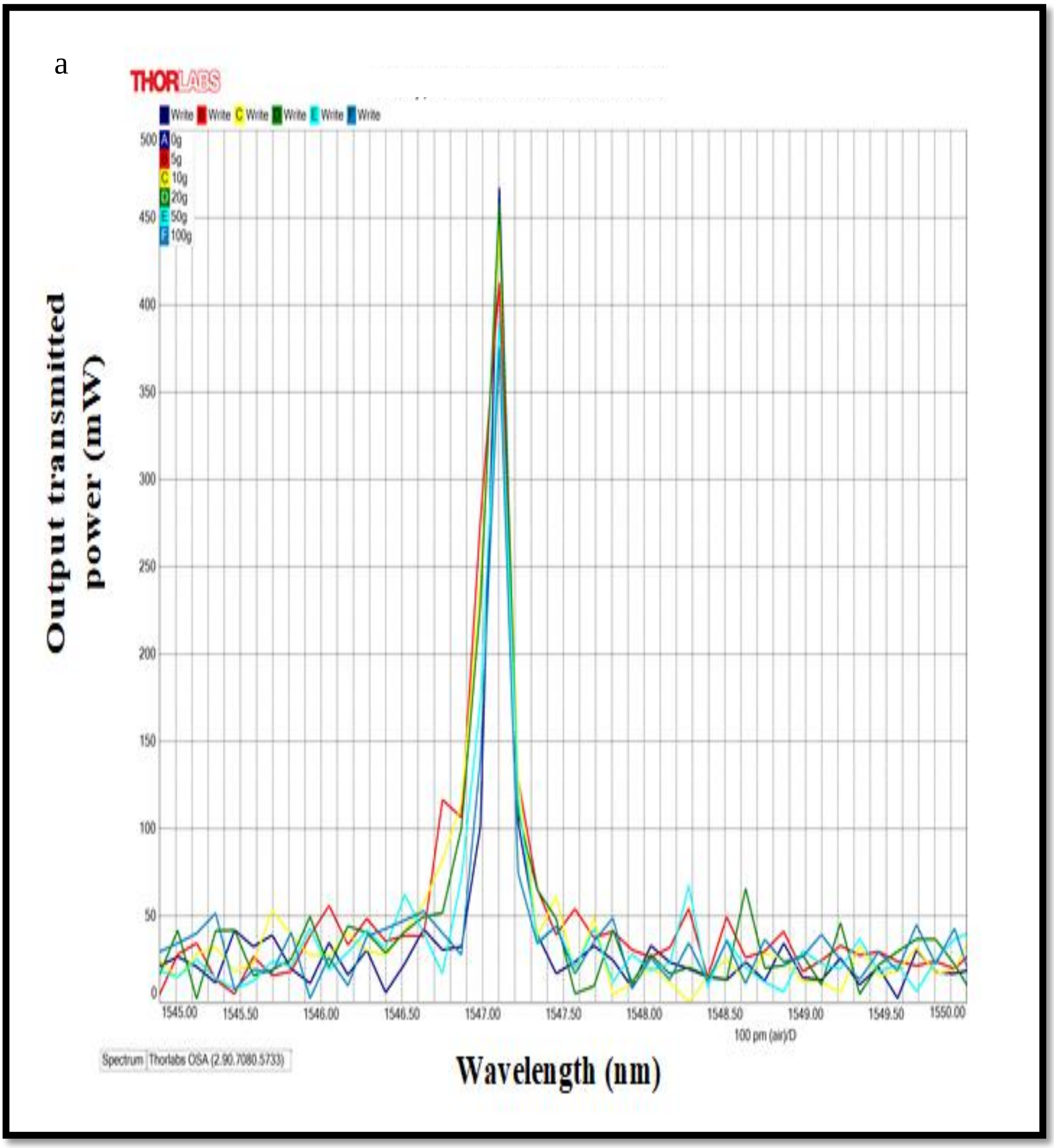

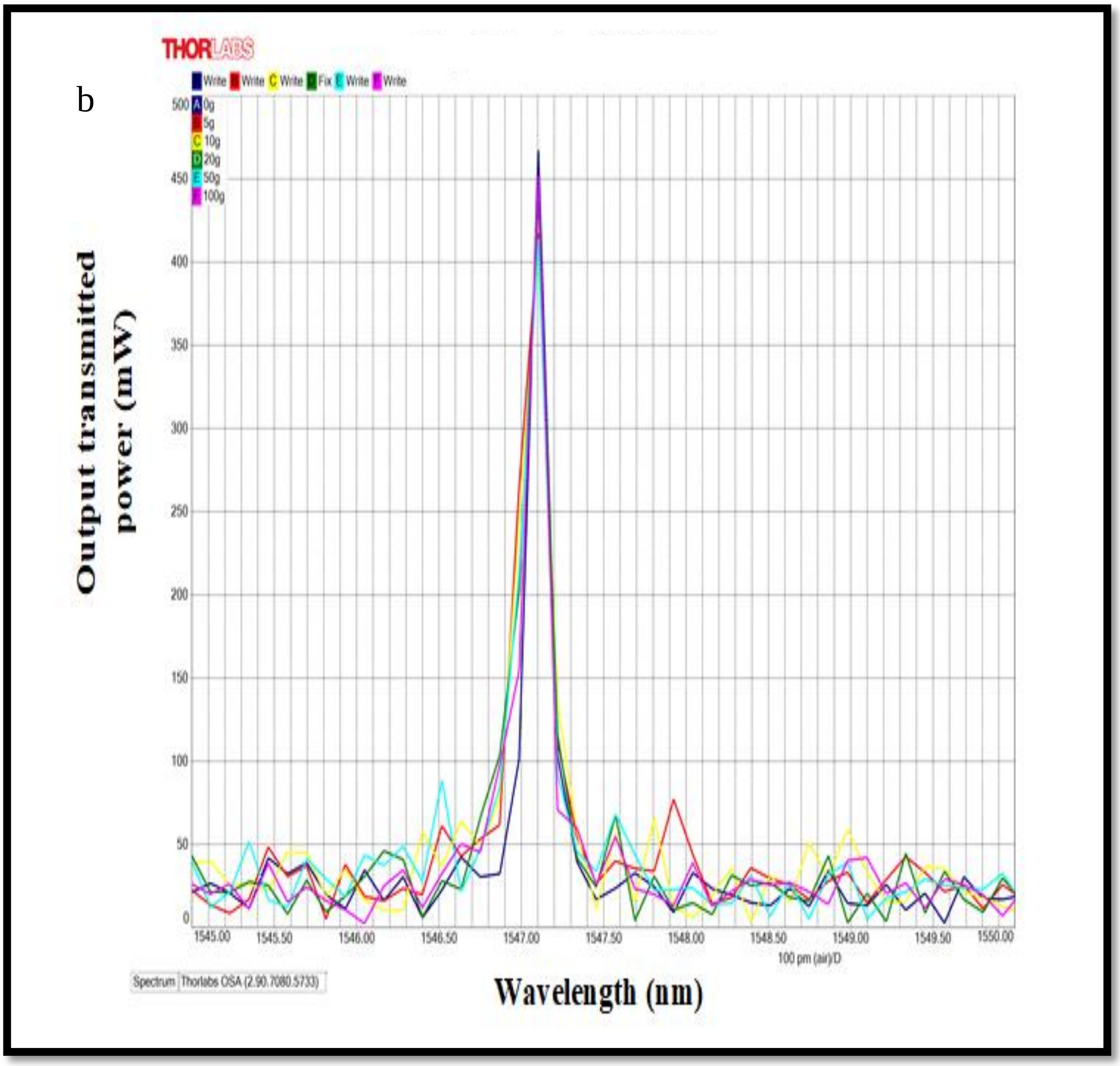

Figure (3.5) : The spectrum of the single PM-Mach Zehnder Interferomter after applying different weights on the PMF in case of single PM-MZI with PM length 8cm (a)cross sectional areas (b)micro cavity splicing regions.

Table (3.2) lists the values of the shift in the central wavelength, the $FWHM_{(Spatially)}$, $FWHM_{(Temporally)}$,output optical power and compression factor for single PM-Mach-Zehnder interferometer after applying different weights on the cross sectional areas of PM fiber and micro cavity splicing regions. The values of the central wavelength , $FWHM_{(Spatially)}$ and the peak power were visualized by using optical spectrum analyzer and the values of, $FWHM_{(Temporally)}$ was calculated according to equations(1.4).

Table(3.2):The effect of different weights on the central wavelength, FWHM$_{(Spatially)}$, FWHM $_{(Temporally)}$,output optical power and compression factor for Single PM-MZI cross sectional areas and micro cavity splicing regions with PMF length (8cm).

Weights (g)	**λc (nm)**		**FWHM$_{(spatiall)}$**		**FWHM (temperoal)**		**Peak power (pW)**		**Compression Factors**	
	Cross section	Splicing regions	Cross section	Splicing regions	Cross section	Splicing regions	Cross section	Splicing regions	Cross section	Splicing regions
0	1547.103	1547.103	130.866	130.866	0.060966	0.060966	467.288	467.288	2.18	2.18
5	1547.076	1547.078	206.046	198.610	0.038720	0.040170	412.719	417.170	1.38	1.44
10	1547.089	1547.085	171.161	192.092	0.046612	0.041533	444.438	405.451	1.67	1.48
20	1547.090	1547.094	161.271	153.635	0.046582	0.051930	458.273	437.320	1.77	1.86
50	1547.096	1547.089	153.484	164.923	0.051981	0.048375	390.686	414.069	1.86	1.73
100	1547.096	1547.097	147.731	141.666	0.054005	0.056318	375.367	451.692	1.93	2.01

From tables (3.2), we can see the spatial FWHM for the pulses after propagated via (PMF with length 8cm) changed in different values after applying different weights, fig (3.6a) shows these changed in the FWHM for the pulses. The applying force on the PMF to achieve the exponentially decreasing dispersion and exponentially increasing nonlinearity profiles

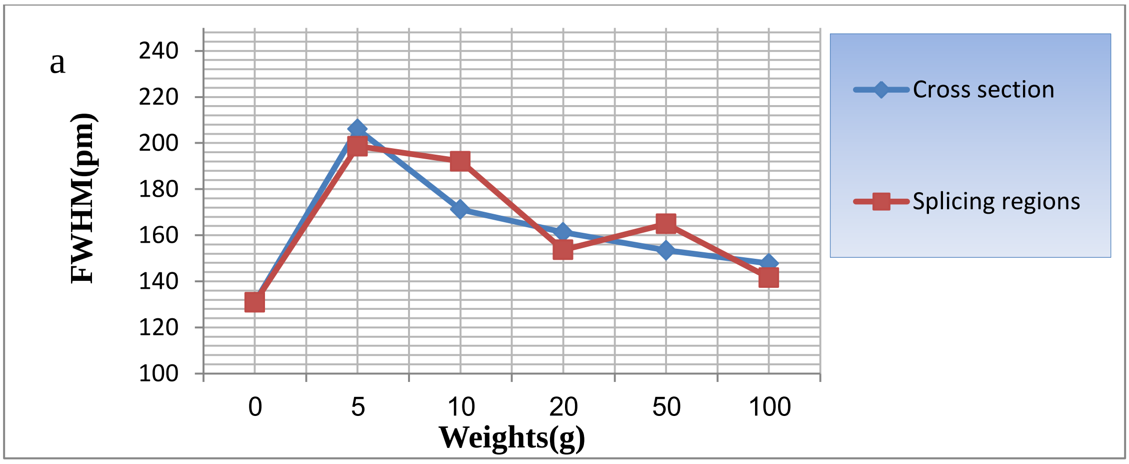

The compression factor is a good indication for obtaining a compressed pulse of the laser source. By using equation (1.3) the best compression factor obtained were (1.38,1.44) for PMF with length 8cm after applying (5) g on the cross sectional area and micro cavity splicing regions respectively. Fig (3.6b) shows the relation between compression factor and the weights which applying on the cross section area and micro cavity splicing regions.

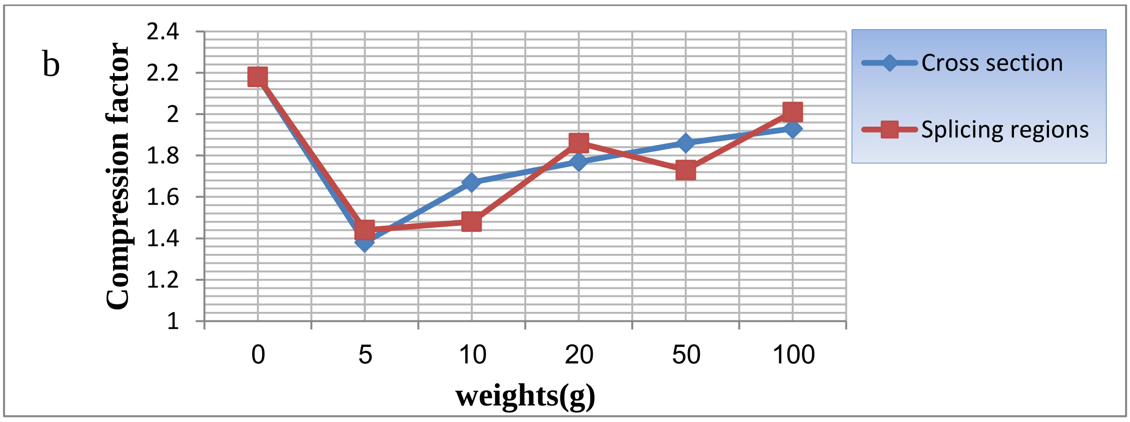

Figure (3.6): The relation between the different weights applying on the cross section area and micro cavity splicing regions of PM fibers (a)FWHM and (b)Compression factor.

❖ Single PM-Mach Zehnder Interferomter With Length (16cm)

The output spectrum for the single PM-Mach-Zehnder Interferometer was visualized by using optical spectrum analyzer after applying different mechanical forces, weights in (g) , on the PM fiber cross sectional area and PM fiber splicing regions as shown in figure(3.7).

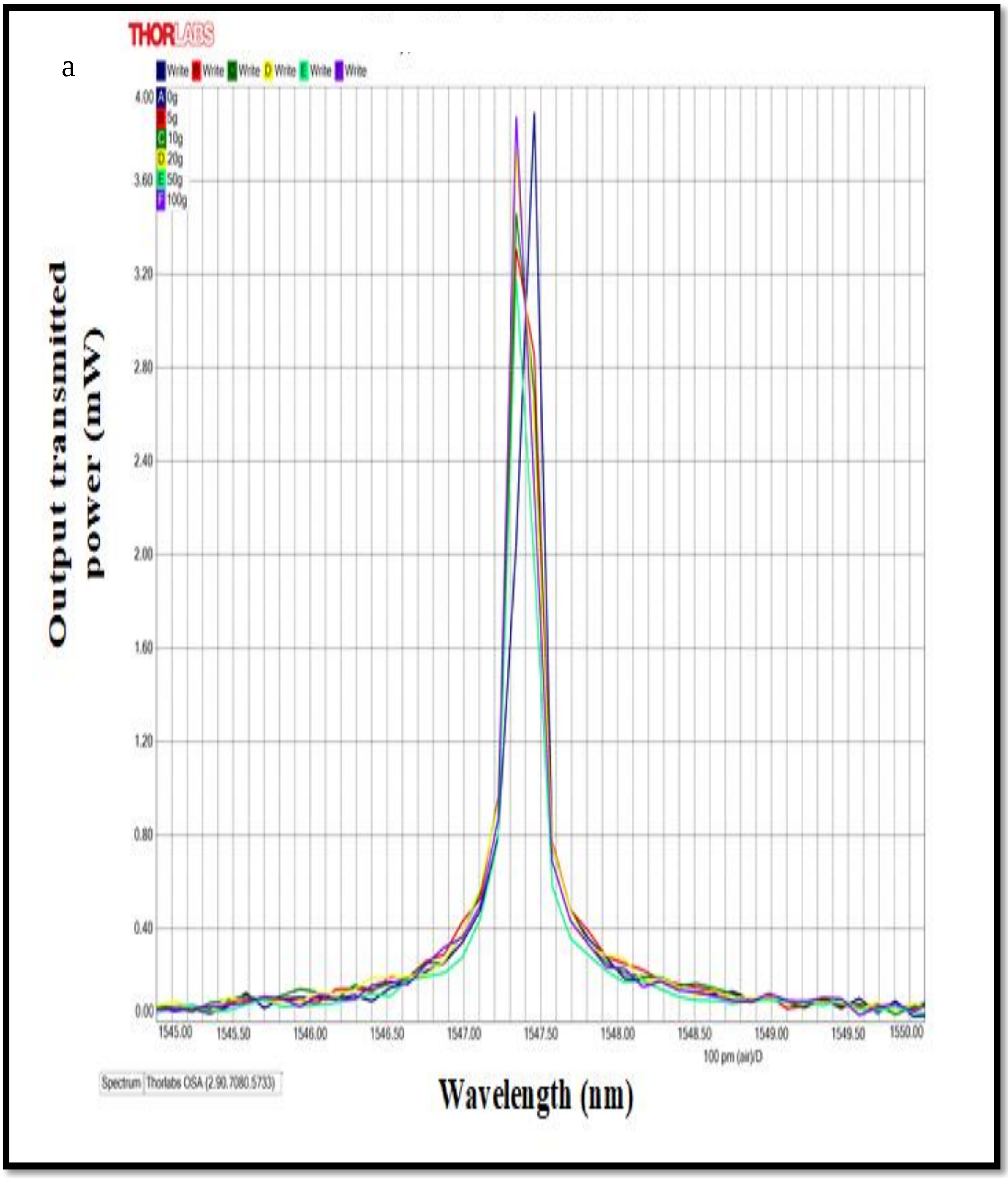

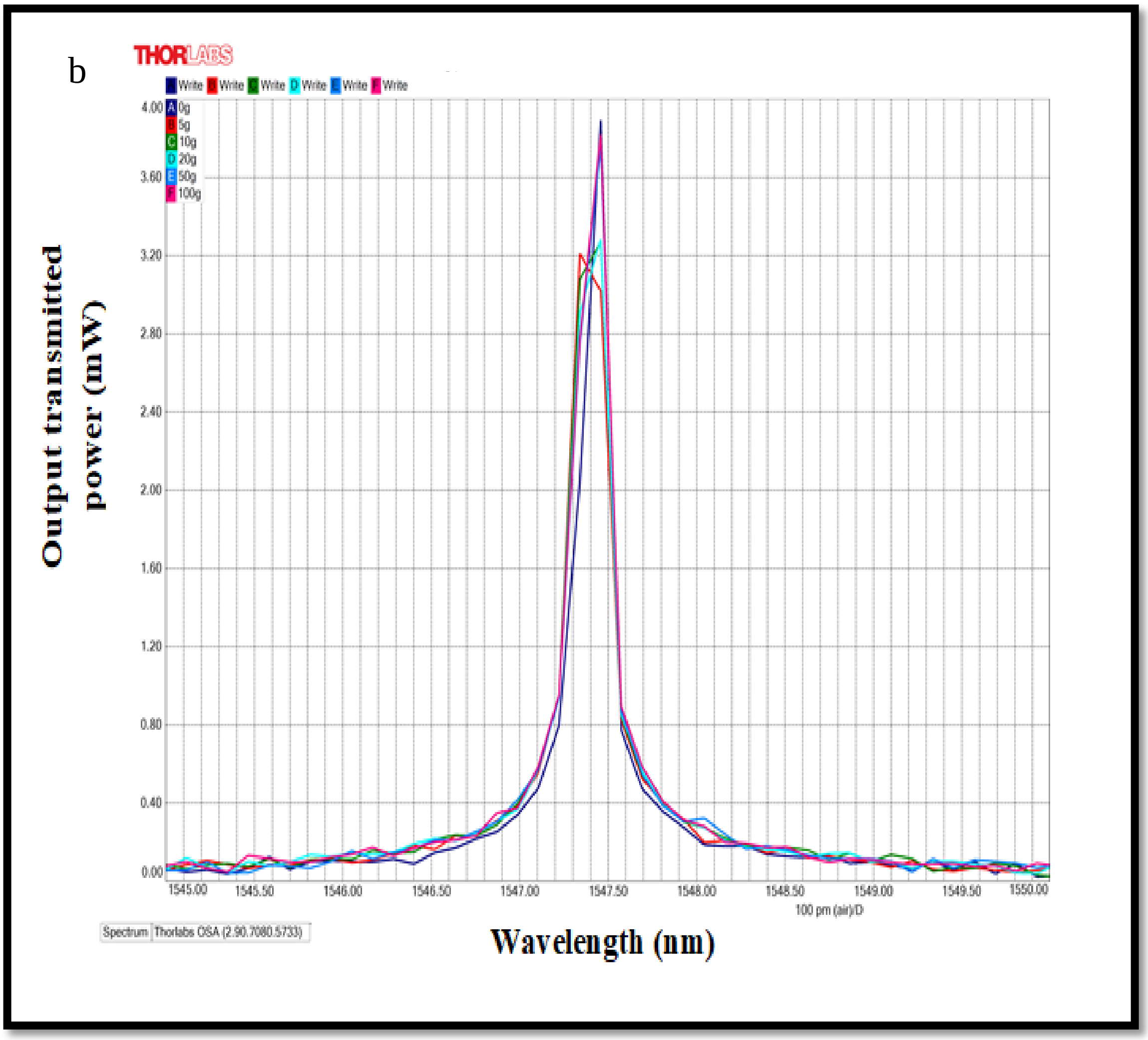

Figure (3.7): The spectrum of the single PM-Mach Zehnder Interferomter after applying different weights on the PMF in case of single PM-MZI with PM length 16cm (a)cross sectional areas (b) micro cavity splicing regions.

Table (3.3) lists the values of the shift in the central wavelength, the $FWHM_{(Spatially)}$, $FWHM_{(Temporally)}$,output optical power and compression factor for single PM-Mach-Zehnder interferometer after applying different weights on the cross sectional areas of PM fiber and PM fiber splicing regions**.** In this table the values of the central wavelength , $FWHM_{(Spatially)}$ and the peak power were visualized by using optical spectrum analyzer and the values of, $FWHM_{(Temporally)}$ was calculated according to equations(1.4) .

Table (3.3): The effect of different weights on the central wavelength, FWHM$_{(Spatially)}$,FWHM $_{(Temporally)}$,output optical power and compression factor for Single PM-MZI cross sectional areas and micro cavity splicing regions with PMF length (16cm).

weights (g)	**λc (nm)**		**FWHM$_{(spatiall)}$**		**FWHM $_{(temperoal)}$**		**Peak power (pW)**		**Compression Factors**	
	Cross section	Splicing regions	Cross section	Splicing regions	Cross section	Splicing regions	Cross section	Splicing regions	Cross section	Splicing regions
0	1547.441	1547.441	174.139	174.139	0.045836	0.045836	3891.02	3891.02	1.64	1.64
5	1547.387	1547.394	243.265	251.584	0.032809	0.031724	3307.67	3209.28	1.17	1.13
10	1547.380	1547.401	233.523	250.175	0.034177	0.031903	3458.99	3267.24	1.22	1.14
20	1547.371	1547.406	216.396	245.861	0.036882	0.032463	3726.88	3282.32	1.32	1.16
50	1547.365	1547.419	204.568	244.538	0.039014	0.032639	3178.20	3754.77	1.39	1.16
100	1547.362	1547.420	195.317	221.709	0.040651	0.036000	3874.71	3818.16	1.46	1.2

From tables (3.3), we can see the spatial FWHM for the pulses after propagated via (PMF with length 16cm) changed in different values after applying different weights, fig (3.8a) shows these changed in the FWHM for the pulses. The applying force on the PMF to achieve the exponentially decreasing dispersion and exponentially increasing nonlinearity profiles.

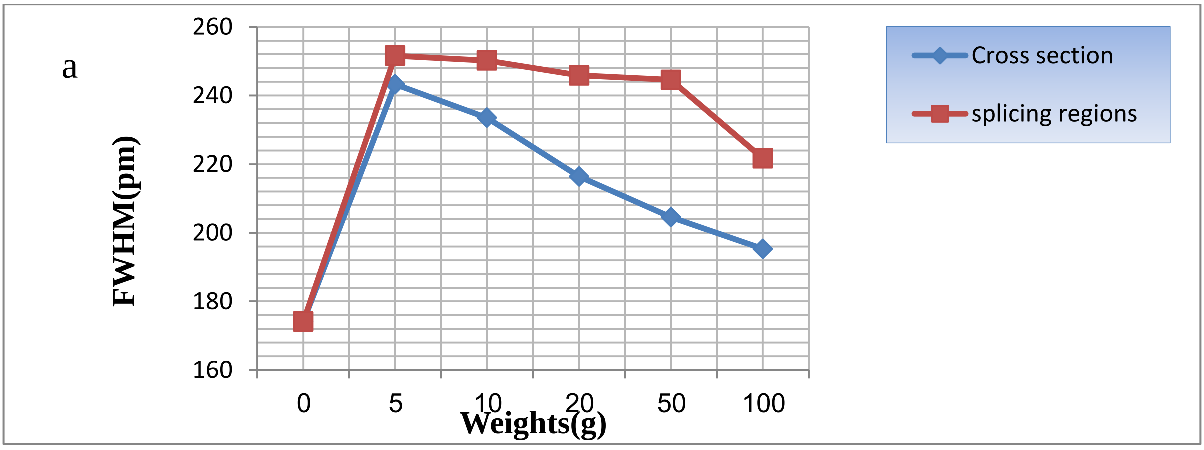

The compression factor is a good indication for obtaining a compressed pulse of the laser source. By using equation (1.3) the best compression factor obtained were (1.13,1.14) for PMF with length 8cm after applying (5,10) g on the micro cavity splicing regions and cross sectional respectively. Fig (3.8b) shows the relation between compression factor and the weights which applying on the cross section area and micro cavity splicing regions.

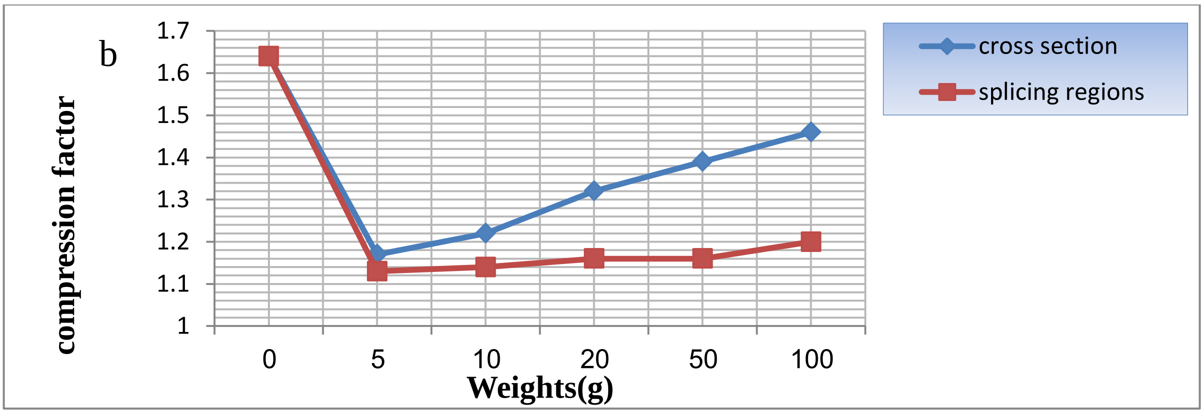

Figure (3.8): The relation between the different weights applying on the cross section area and micro cavity splicing regions of PM fibers and(a)FWHM and (b)Compression factor.

❖ Single PM-Mach Zehnder Interferomter With length (24cm)

The output spectrum for the single PM-Mach-Zehnder Interferometer was visualized by using optical spectrum analyzer , after applying different mechanical forces, weights in (g) , on the PM fiber cross sectional area and PM fiber splicing regions as shown in figure(3.9).

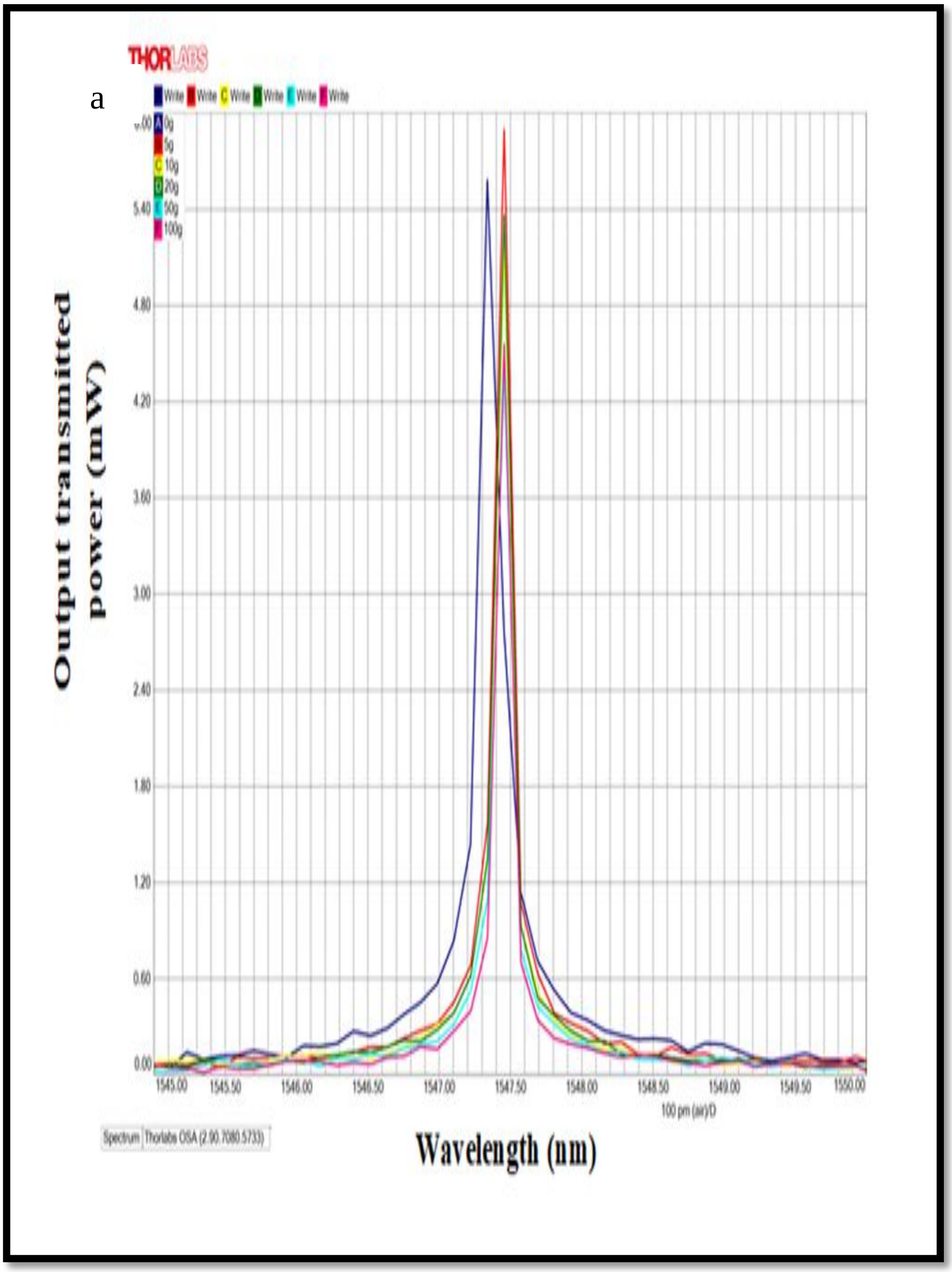

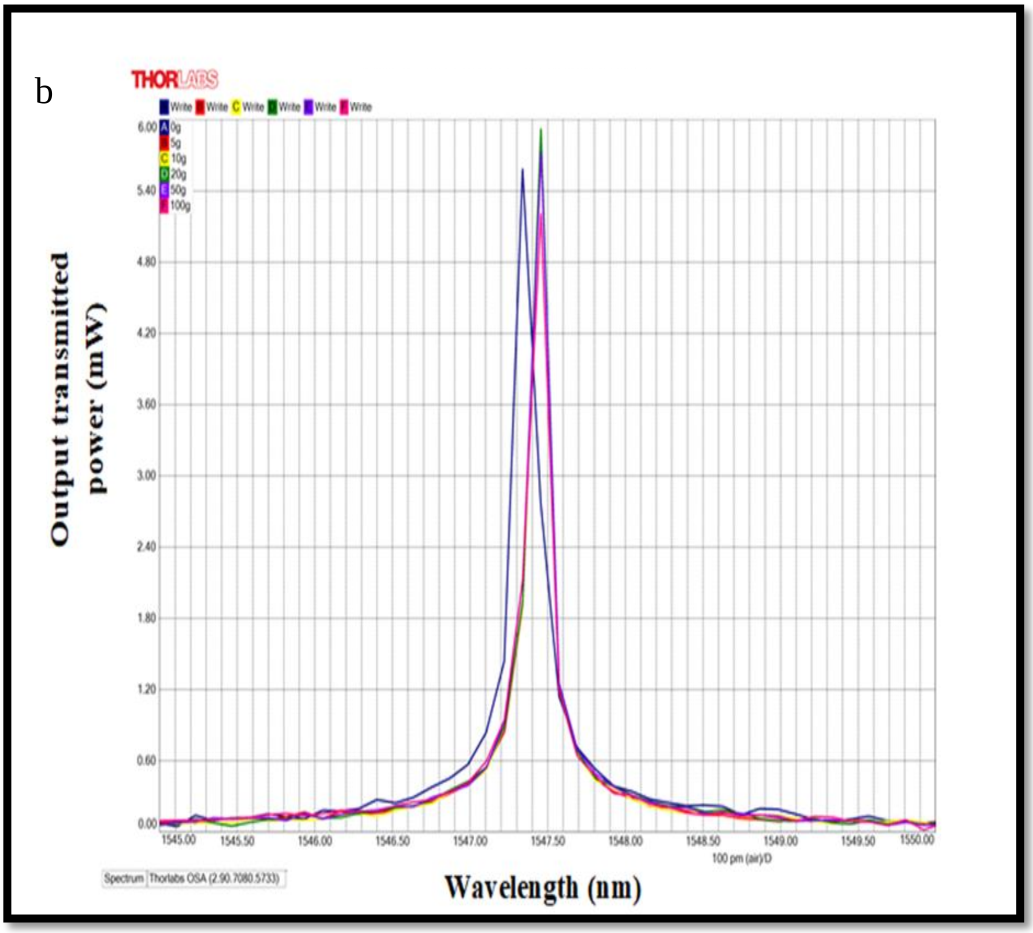

Figure (3.9) : The spectrum of the single PM-Mach Zehnder Interferomter applying different weights on the PMF in case of single PM-MZI with PM length 24cm (a)cross sectional areas (b) micro cavity splicing regions.

Table (3.4) lists the values of the shift in the central wavelength, the $FWHM_{(Spatially)}$, $FWHM_{(Temporally)}$, output optical power and compression factor for single PM-Mach-Zehnder interferometer after applying different weights on the cross sectional areas of PM fiber and the PM fiber splicing regions**.** In this table the values of the central wavelength , $FWHM_{(Spatially)}$ and the peak power were visualized by using Optical Spectrum Analyzer and the values of, $FWHM_{(Temporally)}$ was calculated according to equations(1.4).

Table (3.4):The effect of different weights on the central wavelength, $FWHM_{(Spatially)}$, $FWHM_{(Temporally)}$,output optical power and compression factor for Single PM-MZI cross sectional areas and micro cavity splicing regions with PMF length (24cm).

weights (g)	**λc (nm)**		**FWHM(spatiall)**		**FWHM (temperoal)**		**Peak power (pW)**		**Compression Factors**	
	Cross section	Splicing regions	Cross section	Splicing regions	Cross section	Splicing regions	Cross section	Splicing regions	Cross section	Splicing regions
0	1547.349	1547.349	143.774	143.774	0.055510	0.055510	5585.64	5585.64	1.98	1.98
5	1547.454	1547.453	136.341	142.339	0.048867	0.056077	5902.33	5795.18	2.09	2
10	1547.454	1547.453	134.598	142.917	0.059302	0.055850	5177.40	5846.97	2.12	2
20	1547.454	1547.452	134.847	143.152	0.059193	0.055759	5368.98	5923.90	2.12	1.99
50	1547.454	1547.451	135.114	147.653	0.059076	0.054044	4403.00	5730.68	2.11	1.93
100	1547.456	1547.448	129.289	151.884	0.061738	0.052553	4562.69	5210.50	2.21	1.88

From tables (3.4), we can see the spatial FWHM for the pulses after propagated via (PMF with length 24cm) changed in different values after applying different weights, fig (3.10a) shows these changed in the FWHM for the pulses. The applying force on the PMF to achieve the exponentially decreasing dispersion and exponentially increasing nonlinearity profiles.

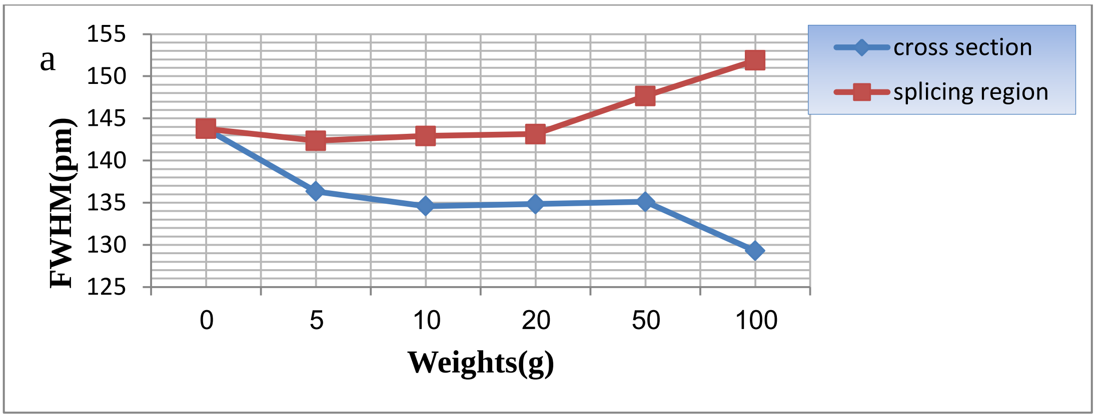

The compression factor is a good indication for obtaining a compressed pulse of the laser source. By using equation (1.3) the best compression factor obtained were (1.88,1.98) for PMF with length 8cm after applying (100, 0) g on the micro cavity splicing regions and cross sectional respectively. Fig (3.10b) shows the relation between compression factor and the weights which applying on the cross section area and micro cavity splicing regions.

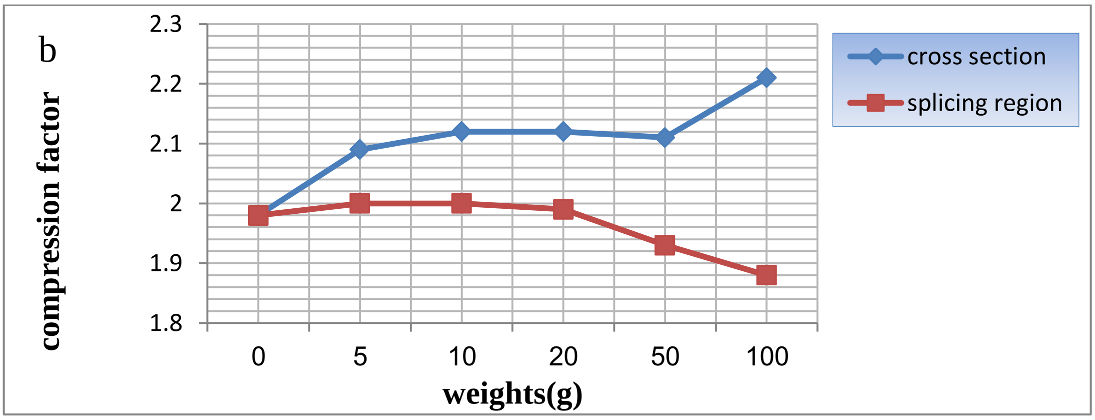

Figure (3.10): The relation between the different weights applying on the cross section area and micro cavity splicing regions of PM fibers and(a)FWHM and (b)Compression factor.

3.2.2 Cascaded PM-Mach Zehnder Interferometers

Different mechanical forces are used to make the tunability in the designed fiber interferomter after applying them on the PM fiber cross sectional area and at the micro cavity splicing regions.

The output spectrum for the cascaded PM-Mach-Zehnder interferometer was visualized by using optical spectrum analyzer, after applying different mechanical forces, weights in (g) , on the PM fiber cross sectional areas and PM fiber splicing regions as shown in figure(3.11).

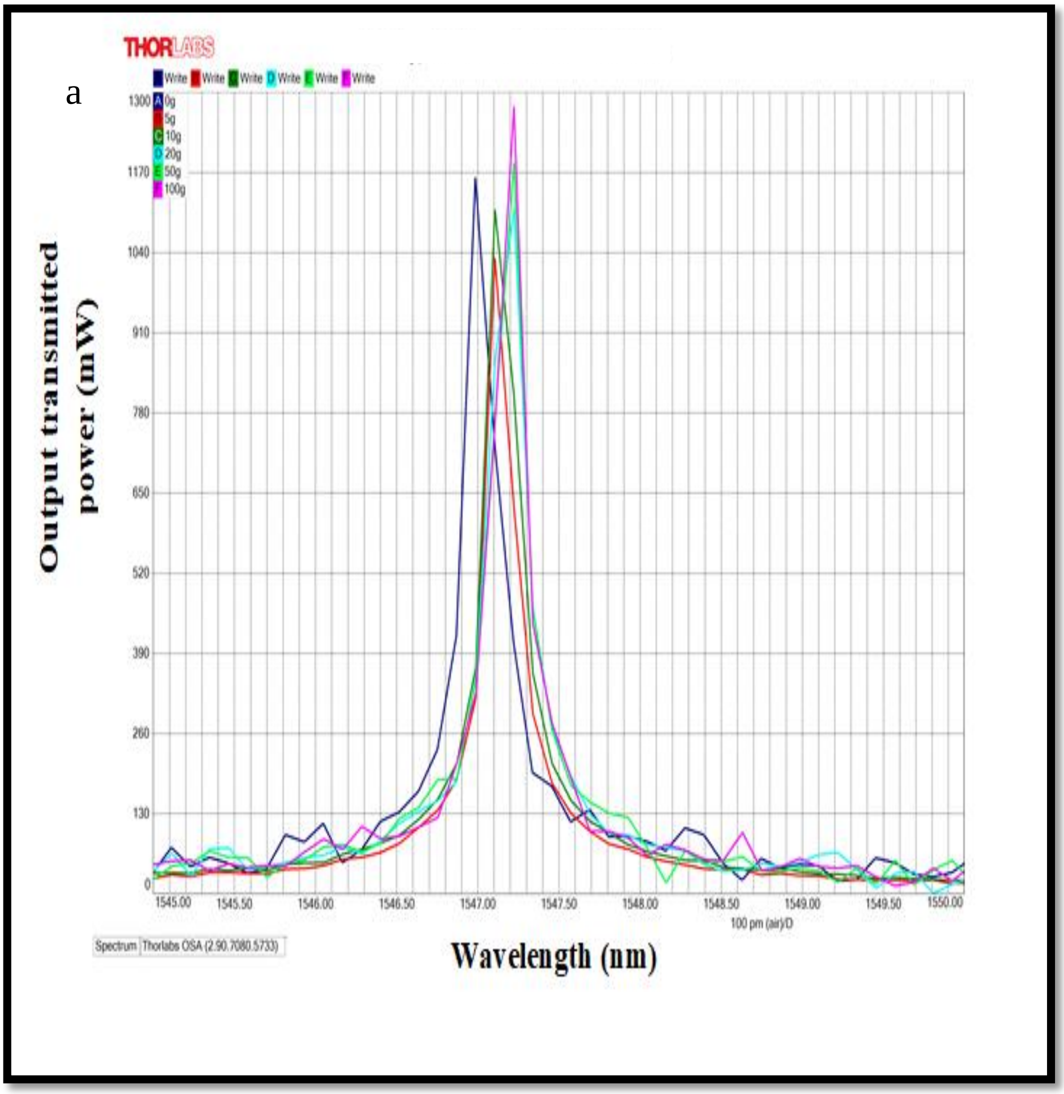

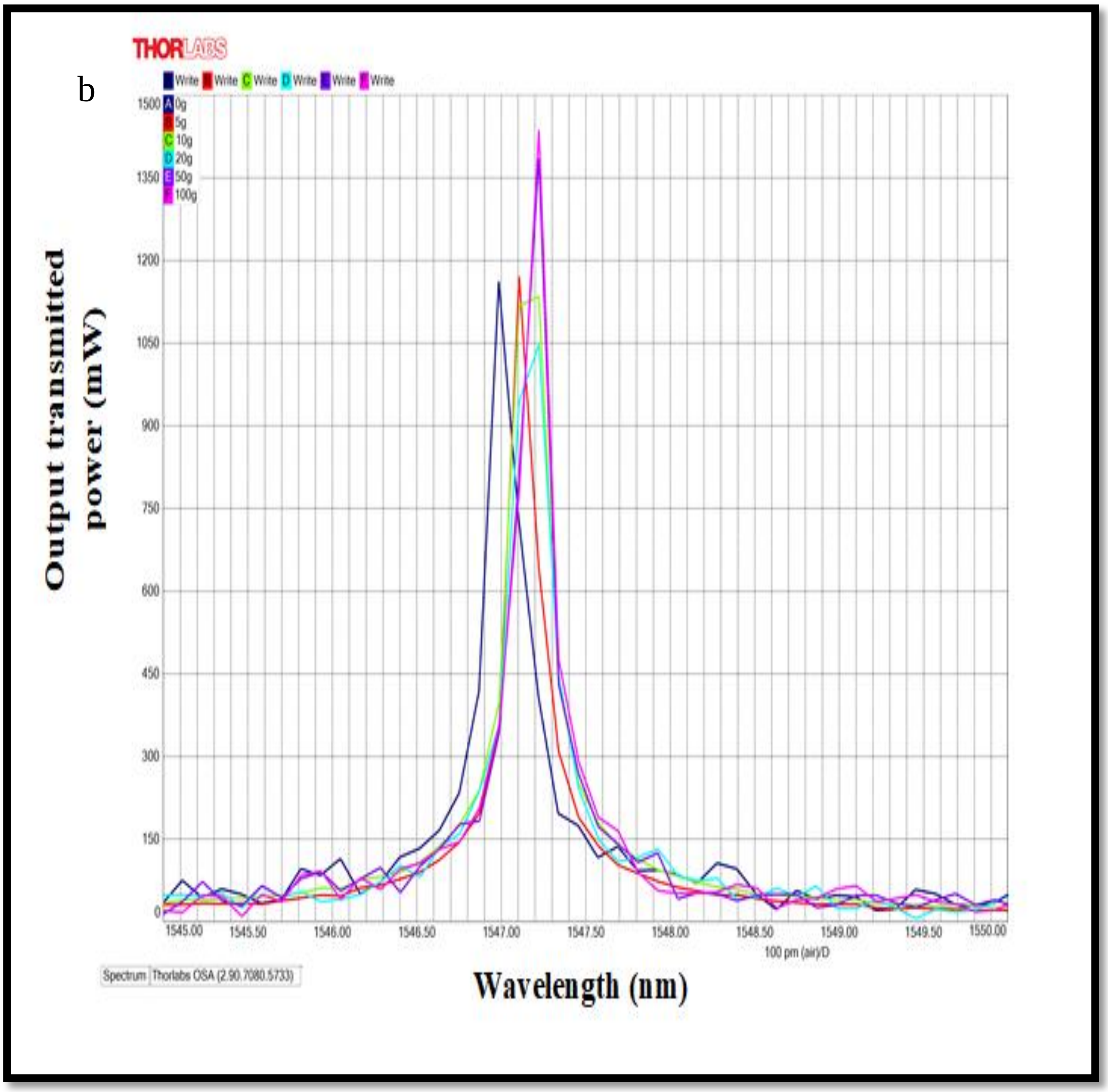

Figure (3.11): The spectrum of the cascaded PM-Mach Zehnder Interferomter after applying different weights on the cross sectional areas of the PMF in case of cascaded PM-MZI.(a) region1 and (b) region2.

Table (3.5) lists the values of the shift in the central wavelength, the $FWHM_{(Spatially)}$, $FWHM_{(Temporally)}$, output optical power and compression factor for single PM-Mach-Zehnder interferometer after applying different weights on the cross sectional areas of PM fiber**.** In this table the values of the central wavelength , $FWHM_{(Spatially)}$ and the peak power were visualized by using Optical Spectrum Analyzer and the values of, $FWHM_{(Temporally)}$ was calculated according to equation (1.4).

Table (3.5): The effect of different weights on the central wavelength, FWHM$_{(\text{Spatially})}$, FWHM$_{(\text{Temporally})}$, output optical power and pulse compression for Cascaded PM-MZI cross sectional areas.

weights (g)		**0**	**5**	**10**	**20**	**50**	**100**
Central wavelength shift (nm)	Region1	1547.217	1547.126	1547.140	1547.187	1547.201	1547.205
	Region2	1547.217	1547.120	1547.166	1547.175	1547.205	1547.210
FWHM $_{(\text{spatially})}$	Region1	141.047	196.272	226.816	232.950	202.264	187.302
	Region2	141.047	179.804	259.730	254.543	185.531	174.181
FWHM ($_{\text{temporally}}$)	Region1	0.056574	0.040651	0.035177	0.034253	0.039450	0.042602
	Region2	0.056574	0.044373	0.030738	0.031347	0.043008	0.045811
Peak power (pW)	Region1	102615.5	1030.981	1109.790	1110.948	1186.184	1277.197
	Region2	102615.5	1170.258	1134.625	1047.965	1385.274	1436.773
Compression Factor (Fc)	Region1	2.02	1.45	1.26	1.22	1.41	1.52
	Region2	2.02	1.59	1.10	1.12	1.54	1.64

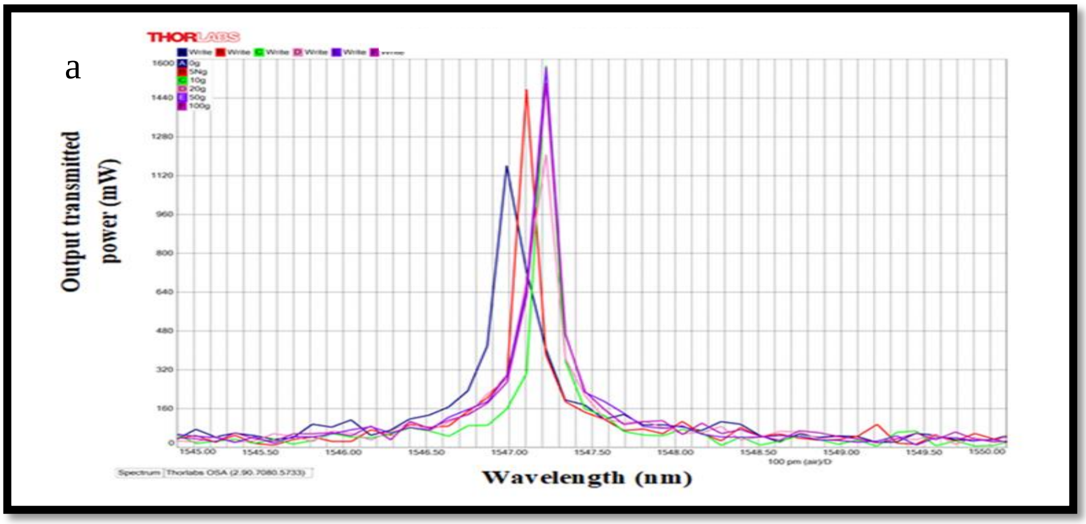
a
THORLABS
Output transmitted power (mW)
Wavelength (nm)

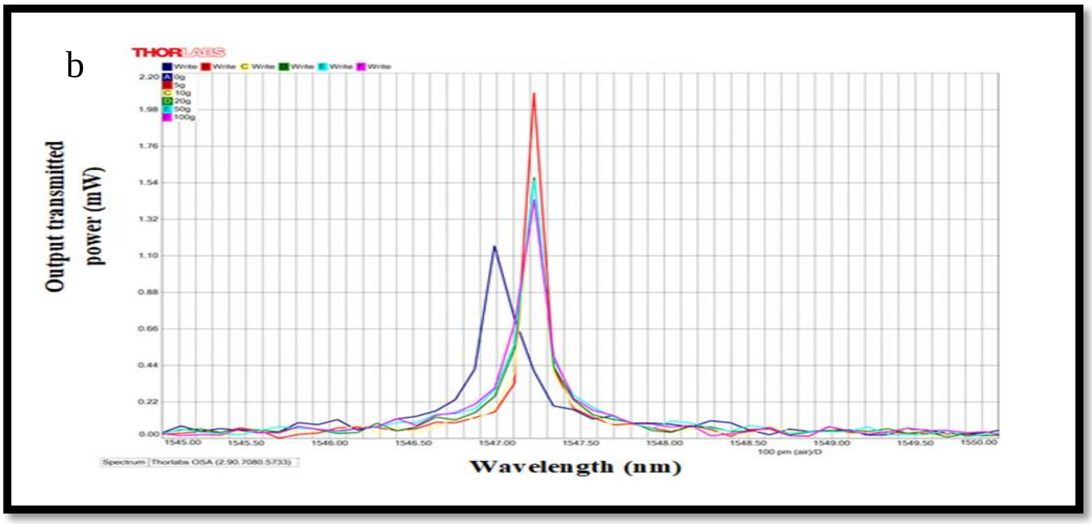
b
THORLABS
Output transmitted power (mW)
Wavelength (nm)

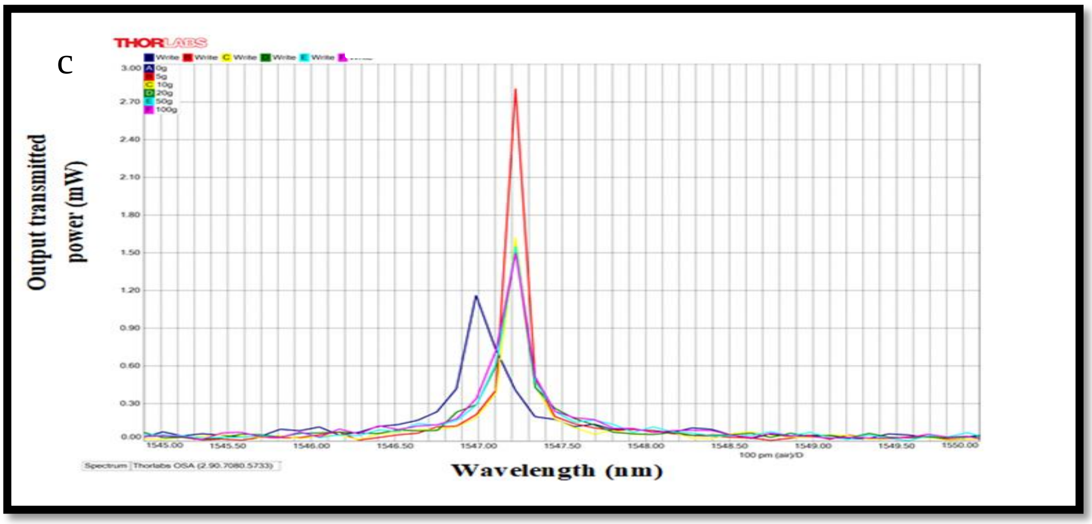
c
THORLABS
Output transmitted power (mW)
Wavelength (nm)

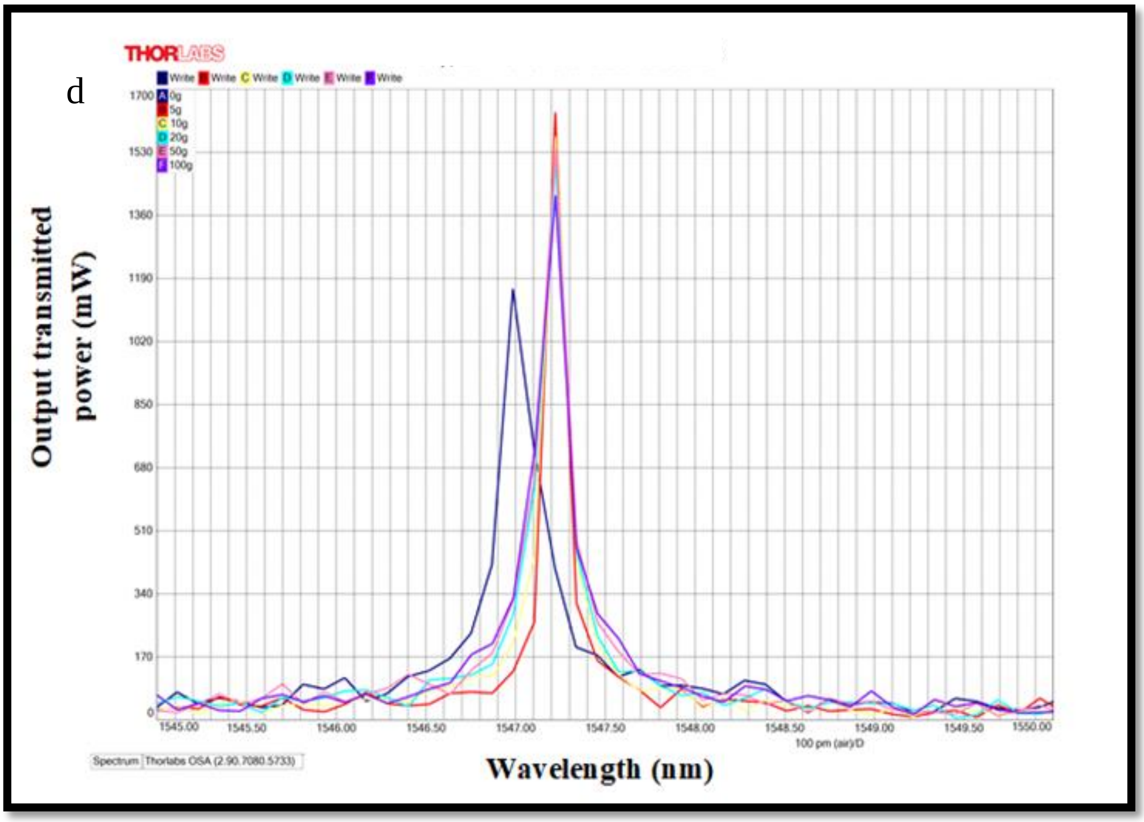

Figure (3.12): shows the spectrum of the cascaded PM-Mach Zehnder Interferomter after applying different weights on the PM fibers splicing regions.

Table (3.6) lists the values of the shift in the central wavelength, the $FWHM_{(Spatially)}$, $FWHM_{(Temporally)}$, output optical power and compression factor for cascaded PM-Mach-Zehnder interferometer after applying different weights on the PM fiber splicing regions**.** In this table the values of the central wavelength , $FWHM_{(Spatially)}$ and the peak power were visualized by using Optical Spectrum Analyzer and the values of, $FWHM_{(Temporally)}$ was calculated according to mathematical equations.

Table (3.6): The effect of different weights on the central wavelength, $FWHM_{(Spatially)}$, $FWHM_{(Temporally)}$, output optical power and pulse compression for Cascaded PM-MZI micro cavity splicing regions .

weights (g)		0	5	10	20	50	100
Central wavelength shift (nm)	Cavity1,2	1547.217	1547.106	1547.223	1547.206	1547.217	1547.217
	Cavity2,3	1547.217	1547.223	1547.222	1547.219	1547.220	1547.215
	Cavity3,4	1547.217	1547.222	1547.223	1547.217	1547.218	1547.215
	Cavity1,4	1547.217	1547.223	1547.222	1547.217	1547.217	1547.212
$FWHM_{(Spatially)}$	Cavity1,2	141.047	129.052	129.850	184.223	151.289	151.261
	Cavity2,3	141.047	126.399	132.729	144.714	146.358	162.805
	Cavity3,4	141.047	125.618	133.663	148.847	151.157	161.274
	Cavity1,4	141.047	125.534	136.875	151.443	153.513	168.483
$FWHM_{(Temporally)}$	Cavity1,2	0.056574	0.061823	0.061452	0.043314	0.052744	0.05275
	Cavity2,3	0.056574	0.063130	0.060119	0.055140	0.054521	0.049013
	Cavity3,4	0.056574	0.063523	0.059699	0.053609	0.052790	0.049478
	Cavity1,4	0.056574	0.063565	0.058298	0.052690	0.051979	0.047361
Peak power (pW)	Cavity1,2	102615.5	1475.520	1573.068	1207.950	1566.239	1501.050
	Cavity2,3	102615.5	2083.485	1565.066	1573.553	1553.639	1439.843
	Cavity3,4	102615.5	2806.43	1620.402	1525.910	1552.625	1496.763
	Cavity1,4	102615.5	1637.286	1572.348	1502.287	1537.434	1414.033
Compression Factor(Fc)	Cavity1,2	2.02	2.21	2.20	1.55	1.89	1.89
	Cavity2,3	2.02	2.26	2.15	1.97	1.95	1.75
	Cavity3,4	2.02	2.27	2.13	1.92	1.89	1.77
	Cavity1,4	2.02	2.27	2.08	1.88	1.86	1.69

3.3 Conclusions

In this work, compression factor is a figure of merit which indicates the performance of the system designed using in-line single and cascaded PM-Mach Zehnder interferometers with PMF made from SMF after stress deformation on its core to made fiber that called panda fiber.

During the experimental and simulation works, several points were concluded which are:

1. Maximum excitation to the higher order modes were obtained when the mechanical force were applied to the PMF's cross sectional area because this fiber has two stress members which make it highly sensitive to any physical effect that cause stress deformation optimum compression factor that are 1.13 after two equally 5g weights are applied on the PM- micro cavity splicing regions when PM fiber length of 16 cm and in the case of cascaded PM-Mach Zehnder interferometer compression factor equal to 1.10 after applied 10g weight on the second PM-cross sectional area with PM fiber length 8 cm.
2. When higher order mode was excited this leads maximum electric field distribution in the cladding region.
3. Producing uniform temperature distribution that can be called temporal interference and in this case PM fiber it look like PM-FBG.
4. Due to the presence of many splicing regions that act as a double convex lens which were excited to the higher order modes in the cladding regions and then causes broadening FWHM spatially and compressed pulse temporally.

3.4 Future works

1. Build Panda-Photonic crystal fiber interferometer for pulse compression.
2. Etching the micro-cavity splicing region to minimize the diffraction region minimizing R_1&R_2 .
3. Using opti-wave system to design and construct PM-MZI.
4. Using double clad fiber to construct Mach-Zehnder interferometer pulse compression.
5. Using Comsol multi-physics to design cascaded PM-MZI.
6. Using intense laser with photosensitivity material for producing Fiber Bragg Grating in the core of SM-PMF or PCF-PMF.

References

References

[1] G.P. Agrawal, "Fiber-Optic Communication Systems", 3rd edition , Jhon Wiley & Sons Inc., (2002).

[2] J. M. Senior, "Optical Fiber Communications principles and practice",3rd edition, Prentice Hall, pp. 26-28, (2009).

[3] G. Keisr, "Optical Fiber Communications," 3rd edition ,(2000).

[4] J. N. Damask, "Polarization Optics in Telecommunications",1st edition ,Springer, (2004).

[5] J. Noda, K. Okamoto and Y. Sasaki, "Polarization-maintaining fibers and their applications ", in Journal of Light wave Technology , Vol. 4, No. 8, pp. 1071-1089, (1986),

[6] R. Zhao, T. Lang, J. Chen and J. Hu, "Polarization-maintaining fiber sensor for simultaneous measurement of the temperature and refractive index ," Optical Engineering, Vol. 56, pp. 057113,(2017).

[7] D. Dobrakowski, A. Rampur, G. Stępniewski, A. Anuszkiewicz, J. Lisowska, D. Pysz, R. Kasztelanic and M. Klimczak, "Development of highly nonlinear polarization maintaining fibers with normal dispersion across entire transmission window ," J. Op, Vol.21, No.1, pp. 015504, (2018).

[8] S. Rashleigh, "Origins and control of polarization effects in single-mode fibers, " J. Light wave Technol., Vol. LT-1, No. 2, pp. 312-331, (1983).

[9] J. Cubik , S. Kepak, J. Doricak, V. Vasinek, A. Liner and M. Papes, "Interferometric sensor based on the polarization-maintaining fibers," Proceedings of SPIE-The International Society for Optical Engineering, Vol.8697, pp.869710,(2012).

[10] H. Wang, F. Tu, J. Li, H. Wei and S. Wang, "Effect of Temperature and Bending on PANDA Polarization-maintaining Fibers Fabricated by PCVD Method, " IEEE Photonics Global @Singapore, pp.1-4, (2008).

[11] M. Ming and K. Liu, "Principles and Applications of Optical Communication", McGraw –Hill, (1996).

[12] T. Zhu, D. Wu, M. Liu and D. Duan, “In-Line Fiber Optic Interferometric Sensors in Single-Mode Fibers”, Sensors, Vol.12, pp.10430-49 (2012).

[13] M. Bass. and E .Van Stryland, “Fiber Optics Handbook, Fiber, Devices, and Systems for Optical Communications”, optical society of America, McGraw –Hill, (2002).

[14] B. H. Lee, Y. H. Kim , K. S. Park, J. B. Eom, M. J. Kim , B. S. Rho, and H. Y. Choi, "Interferometric Fiber Optic Sensors", Sensors, review, 12,pp. 2467-86, (2012).

[15] R. Mehra, H. Shahani, and A. Khan, "Mach-Zehnder Interferometer and it's Applications", International Journal of Computer Applications, JCA Proceedings on National Seminar on Recent Advances in Wireless Networks and Communications, pp.31-36, (2014).

[16] Y. Wang, S. Wang, L. Jiang, H. Huang, L. Zhang, P. Wang, L. Lv, and Z. Cao, “Temperature-insensitive refractive index sensor based on Mach-Zehnder interferometer with two micro cavities,” Chin. Opt. Lett., Vol.15, pp.020603, (2017).

[17] H. Y. Choi, M. J. Kim, and B. H. Lee, “All-fiber Mach-Zehnder type interferometers formed in photonic crystal fiber,” Optics express, Vol. 15, No. 9, pp. 5711–5720, (2007).

[18] Q. Wang, L. Kong, Y. Dang, F. Xia, Y. Zhang, Y. Zhao, H. Hu, J. Li, “High sensitivity refractive index sensor based on splicing points tapered SMF-PCF-SMF structure Mach-Zehnder mode interferometer,” Sensors Actuators, B Chem., vol. 225, pp. 213–220, (2016).

[19] I.P. Kaminow,“Polarization-maintaining fibers,” Appl. Sci. Res. 41, pp. 257-270, (1986).

[20] Z.L. Duan, L.Y. Ren, Y. Zhang, H.Y. Wang, B.L. Yao, and W. Zhao, “Theoretical and experimental study of polarization characteristics of polarization maintaining fiber based on wavelength-sweeping modulation,”. Microw. Opt. Technol. Lett.,Vol. 52, No.7, pp.1466-1469,(2010).

[21] R. Guan, F. Zhu, Z. Gan, D. Huang and Sh.Liu, “Stress birefringence analysis of polarization maintaining optical fibers”, Optical Fiber Technology, Vol.11, pp.240-254 ,(2004).

[22] L. M. Leochun, “Bending loss of Polarization Maintaining Optical Fiber ,” Ms.c thesis ,(1996).

[23] F. Zhang and J.W. Lit, “Temperature and strain sensitivity measurements of high-birefringent polarization-maintaining fibers, ” Applied Optics, Vol. 32, pp.2213-2218, (1993).

[24] S. Rashleigh and M. Marrone, “Temperature dependence of stress birefringence in an elliptically clad fiber, ” Optical Letters, Vol.8, pp.127-129 (1983).

[25] B. Stádník, L. Berka , J. Kratěna , J. Náprstek and J. Doupovec , “Investigation into the birefringence and mechanical stresses in bow-tie fibers ”, Optical and Quantum Electronics Vol.22,pp.279-284 (1990)

[26] V.A. Aksyonov, Yu. K.Chamorovsky, ,G.A. Ivanov, V.A. Isaev, E.D. Isaikina, N.A. Koreneva, K.M. Nametov and A.N. Shvaryov, “Bow-Tie Birefringent Single-Mode Fibers”, Institute of Radio-engineering and Electronics, (1992).

[27] Y. Liu, B. M. A. Rahman and K. T. V. Grattan, “Analysis of the birefringence properties of optical fibers made by a preform deformation technique, ” Journal of Light-wave Technology, Vol. 13, No. 2, pp. 142-147, (1995).

[28] M. E. Froggatt, D. K. Gifford, S. Kreger, M. Wolfe and B. J. Soller, “Characterization of Polarization-Maintaining Fiber Using High-Sensitivity Optical-Frequency-Domain Reflectometry, ” Journal of Light-wave Technology, Vol. 24, No. 11, pp. 4149-4154,(2006).

[29] H. Cherin, “Introduction to optical fibers”, McGraw-Hill, 2nd Edition (1985).

[30] T. Okoshi, “Optical Fibers”, Elsevier, (2012).

[31] D. Marcuse, “Light Transmission Optics” , 2nd edition, (1982).

[32] M. Ohashi, K. Shiraki and K. Tajima, “Optical loss property of silica-based single-mode fibers”, Journal of Light-wave Technology, Vol. 10, No. 5, pp. 539-543, (1992).

[33] M. Arumugam , “Optical Fiber Communication-An Overview”, pramana - journal of physics, Vol. 57, No. 5, pp. 849–869, (2001).

[34] S. Kwan, “Principles Of Optical Fibers”, In partial fulfillment of course requirement for MatE, San Jose State University, (2002).

[35] K. Okamoto, “Fundaments of optical waveguides” ,academic press,(2000).

[36] A.E. Willner, Y.W. Song ,J. Mcgeehan and Z.Pan, “Dispersion Management”, Elsevier, Vol., pp. 353-365,(2005).

[37] N. R. Teja, M.A. Babu, T.R.S. Prasad and T.Ravi, “different types of dispersions in an optical fiber”, International Journal of Scientific and Research Publications, Vol. 2, (2012).

[38] M.H. Aly , S.H. Abouelwafa and A.M.wahba,“Chromatic Dispersion Characteristics of Single-Mode Optical Fibers with Kerr Nonlinearity”, Journal of Optical Communications,Vol.17, No.67-73, (1999).

[39] K.S. Shuraavi and A. Fairooz ,“Optical Fiber - Dispersion, Construction, Application, Technology, Future”,(2016).

[40] P. Shanmugapriya and R. Raveena, “Analysis of Various Types of Fiber Dispersion for Fiber Optical Communication”, International Conference on Smart Structures and Systems,pp.1-5,(2020).

[41] R. Iyer and A. Javed, “Representation of Intermodal Dispersion in Multimode Fiber Links”, in *IEEE* Transactions on Communications, Vol. 31, No. 4, pp. 528-531,(1983).

[42] A. Galtarossa and C. R. Menyuk, “Polarization Mode Dispersion”,1st edition Springer,(2005).

[43] M. Kyselák, P. Dorociak and M. Filka, “The Optical Modulation Format Impact on Polarization Mode Dispersion”, Journal of Computer Science and Network Security, VOL.8 No.5, (2008).

[44] J. P. Gordon, H. Kogelnik, “PMD fundamentals: Polarization mode dispersion in optical fibers”, Proceedings of the National Academy of Sciences, Vol. 97, No.9, pp. 4541-4550,(2000).

[45] C. Xie, L. F. Mollenauer and L. Moller, “Pulse distortion induced by polarization-mode dispersion and polarization-dependent loss in light-wave transmission systems”, IEEE Photonics Technology Letters, Vol. 15, No. 8, pp. 1073-1075, (2003).

[46] Y. J. Rao and D. A. Jackson, “Principles of Fiber-Optic Interferometry”, Springer, pp.167-191,(2000).

[47]A. R. Bahrampour, S. Tofighi, M. Bathaee and F. Farman “Optical Fiber Interferometers and Their Applications”, Optics Communications, Vol.41, No.22, pp.4460-4483, (2012).

[48] P. Hariharan, “Optical Interferometry”, 2nd edition, Elsevier, Academic Press, (2003).

[49] T. Zhu , D. Wu, M. Liu and D. Duan, “In-Line Fiber Optic Interferometric Sensors in Single-Mode Fibers”, sensors Vol.12,pp.10430-10449,(2012).

[50] J. Villatoro, V. Finazzi, G. Badenes, and V. Pruneri, "Highly sensitive sensors based on photonic crystal fiber modal interferometers" Journal of Sensors, Vol. 2009,pp. 747803:1-747803:11, (2009).

[51] C.E. Lee, W.N Gibler, ,R.A. Atkins and H.F. Taylor, “In-line fiber Fabry-Perot interferometer with high-reflectance internal mirrors,”. Journal of Light-wave Technology , Vol.10, pp.1376–1379.(1992).

[52] T. Wei, Y. Han, H.-L. Tsai, and H. Xiao, “Miniaturized fiber inline Fabry-Perot interferometer fabricated with a femtosecond laser,” Optics Letters , vol. 33, no. 6, pp. 536–538, (2008).

[53] K. Murphy, M. Gunther, A. Wang, R. Claus, and A. Vengsarkar, "Extrinsic Fabry-Perot Optical Fiber Sensor," Optical Fiber Sensors,(1992).

[54] D. Hunger, T. Steinmetz, Y. Colombe , C. Deutsch, T. W. Hänsch, and J. Reichel, "A fiber Fabry-Perot cavity with high finesse," New J. Phys., vol. 12, (2010).

[55] Y. J. Rao, "Recent progress in fiber-optic extrinsic Fabry-Perot Interferometric Sensors," Optical Fiber Technology, Vol. 12, No. 3, pp.227-237, (2006).

[56] W. H. Tsai and C. J. Lin, "A novel structure for the intrinsic Fabry-Perot fiber-optic temperature sensor," Journal of Light Technology , Vol. 19, No. 5, pp. 682–686, (2001).

[57]V. R. Machavaram, R. A. Badcock, and G. F. Fernando, "Fabrication of intrinsic fiber Fabry-Perot sensors in silica fibers using hydrofluoric acid etching," Sensors Actuators, A Phys., Vol. 138, No. 1, pp. 248–260, (2007).

[58] X. Wan and H. F. Taylor, "Intrinsic fiber Fabry–Perot temperature sensor with fiber Bragg grating mirrors," Optics Letters , Vol. 27, No. 16, p. 1388, (2002).

[59] B. Culshaw, " The Optical fiber Sagnac Interferometer : an overview of its principle and application," Measurement Science and Technology ,Vol. 17, No.1, (2005).

[60] Y. Yang, L. Lu, F. Yang, Y. Chen and W. Jin, "The fiber optic Sagnac interferometer and its sensing application ," 2015 Optoelectronics Global Conference, pp. 1-6, (2015).

[61] L. Jaroszewicz, Z. Krajewski and P. Marc, "Fiber optic Sagnac interferometer as a sensor of physical quantities ," Proceedings of SPIE - The International Society for Optical Engineering, Vol. 5502, pp. 390-393,(2004).

[62] P. Giacomo, "The Michelson interferometer," Mikrochimica Acta , Vol.93, pp. 19-31 (1987).

[63] R. Kashyap and B. Nayar, “An all single-mode fiber Michelson interferometer sensor,” Journal of Light Technology , vol. 1, No. 4, (1983).

[64] R. Mehra, H. Shahani, and A. Khan, “Mach-Zehnder Interferometer and it's Applications ,” International Journal of Computer Applications ,pp.31-36, (2014).

[65] H. A. Razak, H. Haroon, P. S. Menon, S. Shaari and N. Arsad, “Design and optimization of a Mach-Zehnder Interferometer (MZI) for optical modulators,” IEEE International Conference on Semiconductor Electronics (ICSE2014), pp.301-304,(2014).

[66] Q. Wang, W. Wei, M. Guo and Y. Zhao, “Optimization of cascaded fiber tapered Mach–Zehnder interferometer and refractive index sensing technology”, Sensors and Actuators B: Chemical, Vol. 222, pp.159-165, (2016).

[67] W.W. Li , D.N. Wang , Z.K. Wang and B. Xu, “Fiber inline Mach–Zehnder interferometer based on femtosecond laser inscribed waveguides”, Optics Express, Vol. 26, pp. 11469-11502,(2018).

[68] X. Dong, X. Sun, D. Chu, K. Yin, Z. Luo, C. Zhou, C. Wang, Y. Hu, and J. Duan, “Micro-cavity Mach–Zehnder Interferometer Sensors for Refractive Index Sensing,” IEEE Photonics Technology Letters ,Vol. 28, No. 20, pp.2285-2288,(2016).

[69] L. Jiang, J. Yang, S. Wang, B. Li, and M. Wang, “Fiber Mach-Zehnder interferometer based on micro cavities for high-temperature sensing with high sensitivity,” Optics Letters , Vol.36, pp.3753–3755,(2011).

[70] F. C. Favero, L. Araujo, G. Bouwmans, V. Finazzi, J. Villatoro, and V. Pruneri, “Spheroidal Fabry-Perot microcavities in optical fibers for high-sensitivity sensing,” Optic Express, vol. 20, No. 7, pp. 7112, (2012).

[71] S. Zuoming, S. Ningfang, J. Jing, S. Jingming, and M. Pan, “Low loss fusion splicing polarization-maintaining photonic crystal fiber and conventional polarization-maintaining fiber,” Optical Fiber Technology, Vol. 18, No. 6, pp. 452–456, (2012).

[72] T. Wang and M. Wang , " Micro- Fabry–Perot Interferometer with High Contrast Based on an In-Fiber Ellipsoidal Cavity, " IEEE Photonics Technology Letters, Vol.12, pp.896-996, (2012).

[73] Y. Wang, S. Wang, L. Jiang, H. Huang, L. Zhang, P. Wang, L. Lv, and Z. Cao, "Temperature-insensitive Refractive Index Sensor based on Mach - Zehnder Interferometer with Two Micro-cavities," Chinese Optics Letters, Vol. 15, No. 2, pp. 1–5, (2017).

[74] Z. Chen, X. Xi, W. Zhang, J. Hou, and Z. Jiang, "Low-loss fusion splicing photonic crystal fibers and double cladding fibers by controlled hole collapse and tapering," Journal of Light-wave Technology, Vol. 29, No. 24, pp. 3744-3747, (2011).

[75] G. Agrawal, "Applications of Nonlinear Fiber Optics ," Academic Press, ch.2, pp.160, (2001).

[76] J. Hu, B. Marks, C. Menyuk, J. Kim, Carruthers, T. Thomas , B. Wright, T. Taunay, and E. Friebele, "Pulse compression using a tapered microstructure optical fiber," Optics express. Vol. 14,(2006).

[77] M. Shinriki, H. Takase and H. Susaki, "Pulse compression for a simple pulse ," Aerospace and Electronic Systems IEEE Transactions on, Vol. 44, pp.1623 - 1629,(2008).

[78] F. Yin-juan and P. Ruo-yu, "Research on Pulse Compression Technology of Linear Frequency Modulation Signal," International Conference on Industrial Control and Electronics Engineering, pp. 1131-1133, (2012).

[79] J. Schulte, T. Sartorius, J. Weitenberg, A. Vernaleken, and P. Russbüldt, "Nonlinear pulse compression in a multi-pass cell," Optics Letters. Vol. 41, pp.4511–4514 (2016).

[80] T. S. Rappaport, "Wireless Communication: Principals and Practice," Prentice Hall , (1996).

[81] A. Mushtaque, A. Waqas, Z. Mustaq, A.A. Memon and B.S. Chowdhry, “Loss analysis in optical fiber transmission,”. Journal Engineering Technology , Vol. **5**,pp. 5–10, (2015)

[82] A. Kumar, “ Power Budget for Single Mode Optical Fiber ,” International Journal of Soft Computing and Engineering (IJSCE),Vol. 3, (2014).

[83] M. Kihara, S. Nagasawa and T. Tanifuji, “Return loss characteristics of optical fiber connectors ,” Journal of Light-wave Technology, Vol. 14, No. 9, pp. 1986-1991,(1996).

[84]A. D. Yablon, “Optical fiber fusion splicing,” Springer series,(2005).

[85] A. Al-Azzawi, “Photonics Principles and Practices”, 1st edition,(2007).

[86] T.Adiono, S. Fuada, and S. Harimurti, “Bandwidth Budget Analysis for Visible Light Communication Systems utilizing Commercially Available Components ,” International Conference on Electrical and Electronics Engineering (ELECO),Vol.10, pp.1375-1380,(2017).

[87] A. Nkansah and N. J. Gomes, “Characterization of radio over multimode fiber links using coherence bandwidth”, IEEE Photonics Technology Letters, Vol. 17, No. 12, pp. 2694-2696, (2005).

[88] I.P. Kaminow, T. Li and A. E. Willner, “Optical Fiber Telecommunications V A, Components and Subsystems”, Academic Press (2008).

[89] P. G Agrawal, “Nonlinear Fiber Optics,” Third Edition, (2001).

[90] P. Colman, C. Husko, S. Combrie , I. Sagnes, C. W. Wong and A. D. Rossi, “Temporal solitons and pulse compression in photonic crystal waveguides”, Nature Photonic ,Vol.4,(2010).

[91] M. Y. Chen, H. Subbaraman and R. T. Chen, “One stage pulse compression at 1554nm through highly anomalous dispersive photonic crystal fiber”, Optics Express, Vol.19,(2011).

[92] N. Baquedano, N. Arzate, I. Torres, A. Ferrando, D.E. Herrera, C. Milian "Femtosecond pulse compression in a hollow-core photonic band gap fiber by tuning its cross section", Photonics nanostructure, Vol.10, pp. 594-601,(2012).

[93] S. Olupitan , K. Senthilnathan , P. Babu , R. Raja , S.S. Aphale and K. Nakkeeran "Realizing a robust optical pulse compressor operating at 850 nm using a photonic crystal fiber", Journal of Modern Optics, Vol.60, pp. 368-377,(2013).

[94] L. Cherbia, N. Lamhenea, F. Boukhelkhala and A, Biswasb, "Ultra-short pulse compression at 1065 nm in nonlinear photonic crystal fiber", Vol.125, pp.133-136,(2013).

[95] S. V. Smirnov, S. M. Kobtsev and S. V. Kukarin, "Linear compression of chirped pulses in optical fiber with large step-index mode area", Optics Express ,Vol.23, pp.3914-3919, (2015).

[96] S. O. Atuba, K. Nakkeeran, K. W. Chow, P. Ramesh Babu, A. Manimegalai and K. Senthilnathan "Generation of a train of ultrashort pulses using periodic waves in tapered photonic crystal fibers ", Vol.63, pp. 2246-2258,(2016).

[97] X. Feng, Y. Jin-hui, Member, C. Mei, F. Li, Z. Kang, B. Yan, X. Zhou, Q. Wu, K. Wang, X. Sang, C. Yu, and G. Farrell "Mid-infrared Self-Similar Pulse Compression in a Tapered Tellurite Photonic Crystal Fiber and Its Application in Supercontinuum Generation", Journal of light wave technology ,Vol. pp, pp.1-1, (2018).

[98] Y. Jeong, R. Piccoli, D. Ferachou,V. Cardin, M. Chini, S. Hädrich, J. Limpert, R.Morandotti1, F. Légaré, B. E. Schmidt and L. Razzari "33- Fold pulse compression down to 1.5 cycles in a 6m long hollo-core fiber", Conference on Lasers and Electro-Optics (CLEO),pp.1-2, (2019).

[99] M. Rehan ,G. Kumar , V. Rastogi , D. A. Korobko, and A. A. Sysolyatin, "Compression of Femtosecond Pulses in a wide Wavelength Range Using a Large Mode Area Tapered Fiber", Laser Physics , Vol. 29 ,pp.025104 ,(2019).

[100] A. A. Dawood, T. S. Mansour and Y. I. Hammadi "Demonstration of All-Fiber Pulse Compression Using Hollow Core Photonic Crystal Fibers," Cont.& Math. Sci., Vol.-14, No.-5,pp.158-169,(2019).

[101] E.Vicentini, Y. Wang, D. Gatti, A. Gambetta, P. Laporta, G. Galzerano, K. Curtis, K. Mcewan, C. R. Howle, and N.Coluccelli "Nonlinear pulse compression to 22 fs at 15.6 μJ by an all-solid-state multi-pass approach", Vol.28, No.4, pp.4541-4549,(2020).

[102] W.A. Ramadan, H.H. Wahba, M.A. Shams El-Din and I.G. Abd El-Sadek, "Refractive index retrieving of polarization maintaining optical fibers", Optical Fiber Technology , Vol. 40, pp.69-75,(2017).

[103] W. Inart, and W. Asawamethapant, "The analysis of parameters related to fusion splicing loss of SMF-28 and MP980", pp.1-4. (2012).

[104] J. Rheims, J. Köser and T. Wriedt, " Refractive-index measurements in the near-IR using an Abbe refractometer , " Measurement Science and Technology, Vol.8 , No.6 , (1997).

[105] R.Puzko and A. Merzlikin, "Analytical properties of the effective refractive index , " Optics Communications, Vol. 383, pp. 323-329,(2017).

[106] J. Arriaga, " Effective index model and guided modes in a photonic crystal fiber " ,Physica Status Solidi B-basic Solid State Physics, Vol. 242, No. 9,pp. 1868-1871,(2005).

[107] J.M. Gere and B.J. Goodno , "Mechanics of Materials" , 7th edition, Elsevier,(2009).

[108]W. Young, R. Budynas and A. Sadegh, "Roark's Formulas for Stress and Strain, " 7th edition, McGraw- Hill, (2002).

[109] M. Krzysztof and G. Glinka, "A method of elastic-plastic stress and strain calculation at a notch root , " Materials Science and Engineering, Vol. 50, pp. 93-100,(1981).

[110] J. Lei, Z. Liu, J. Yeo, and T. Yong Ng "Determination of the Young's modulus of silica aerogels - An analytical numerical approach, " Soft Matter, Vol. 9, No. 11367-11373, (2013).

[111] E. Labasova, "Determination of Modulus of Elasticity and Shear Modulus by the Measurement of Relative Strains ," Research Papers Faculty of Materials Science and Technology Slovak University of Technology, Vol.24, (2016).

Appendices

Appendix A

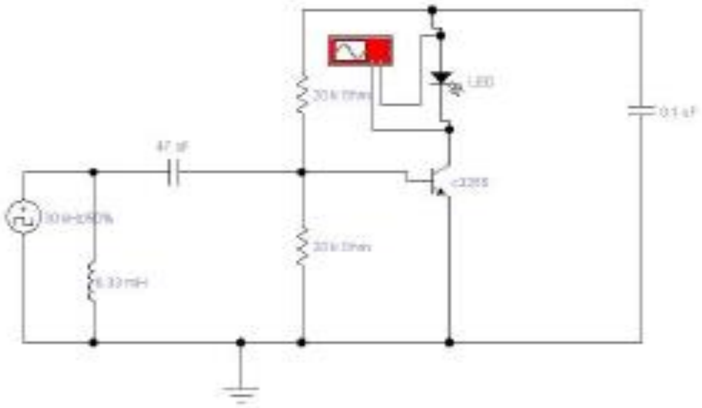

Schematic Diagram of Electronic Chopping circuit

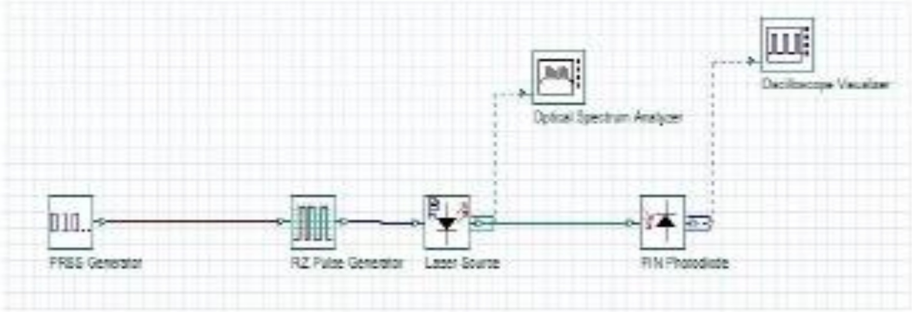

simulation by Opti-system of Electronic Chopping circuit

Specifications

Parameter	Value	Unit
Central wavelength	1546.74	nm
Pulse duration	10	ns
FWHM	286	pm
Pulse repetition rate	30	kHz
Duty-cycle	90%	——
Energy	0.0123	nJ
Power	1229.271	μw
Voltage	2	mV
Frequency	30	kHz

Appendix B

Corning® SMF-28™ Optical Fiber
Product Information

PI1036
Issued: April 2002
Supersedes: December 2001
ISO 9001 Registered

Corning® Single-Mode Optical Fiber

The Standard For Performance

Corning® SMF-28™ single-mode optical fiber has set the standard for value and performance for telephony, cable television, submarine, and utility network applications. Widely used in the transmission of voice, data, and/or video services, SMF-28 fiber is manufactured to the most demanding specifications in the industry. SMF-28 fiber meets or exceeds ITU-T Recommendation G.652, TIA/EIA-492CAAA, IEC Publication 60793-2 and GR-20-CORE requirements.

Taking advantage of today's high-capacity, low-cost transmission components developed for the 1310 nm window, SMF-28 fiber features low dispersion and is optimized for use in the 1310 nm wavelength region. SMF-28 fiber also can be used effectively with TDM and WDM systems operating in the 1550 nm wavelength region.

Features And Benefits

- Versatility in 1310 nm and 1550 nm applications
- Enhanced optical properties that optimize transmission performance
- Outstanding geometrical properties for low splice loss and high splice yield
- OVD manufacturing reliability and product consistency
- Optimized for use in loose tube, ribbon, and other common cable design

The Sales Leader

Corning SMF-28 fiber is the world's best selling fiber. In 2001, SMF-28 fiber was deployed in over 45 countries around the world. All types of network providers count on this fiber to support network expansion into the 21st Century.

Protection And Versatility

SMF-28 fiber is protected for long-term performance and reliability by the CPC® coating system. Corning's enhanced, dual acrylate CPC coatings provide excellent fiber protection and are easy to work with. CPC coatings are designed to be mechanically stripped and have an outside diameter of 245 µm. They are optimized for use in many single- and multi-fiber cable designs including loose tube, ribbon, slotted core, and tight buffer cables.

Patented Quality Process

SMF-28 fiber is manufactured using the Outside Vapor Deposition (OVD) process, which produces a totally synthetic ultra-pure fiber. As a result, Corning SMF-28 fiber has consistent geometric properties, high strength, and low attenuation. Corning SMF-28 fiber can be counted on to deliver excellent performance and high reliability, reel after reel. Measurement methods comply with ITU recommendations G.650, IEC 60793-1, and Bellcore GR-20-CORE.

Optical Specifications

Attenuation

Wavelength (nm)	Attenuation* (dB/km) Premium	Standard
1310	≤0.34	≤0.35
1550	≤0.20	≤0.22

*Alternate attenuation values available upon request.

Point Discontinuity

No point discontinuity greater than 0.10 dB at either 1310 nm or 1550 nm.

Attenuation at the Water Peak

The attenuation at 1383 ± 3 nm shall not exceed 2.1 dB/km.

Attenuation vs. Wavelength

Range (nm)	Ref. λ (nm)	Max. α Difference (dB/km)
1285 - 1330	1310	0.05
1525 - 1575	1550	0.05

The attenuation in a given wavelength range does not exceed the attenuation of the reference wavelength (λ) by more than the value α.

Attenuation with Bending

Mandrel Diameter (mm)	Number of Turns	Wavelength (nm)	Induced Attenuation* (dB)
32	1	1550	≤0.50
50	100	1310	≤0.05
50	100	1550	≤0.10
60	100	1550	≤0.05

*The induced attenuation due to fiber wrapped around a mandrel of a specified diameter.

Cable Cutoff Wavelength (λ_{ccf})

$\lambda_{ccf} \le 1260$ nm

Mode-Field Diameter

9.2 ± 0.4 µm at 1310 nm
10.4 ± 0.8 µm at 1550 nm

Dispersion

Zero Dispersion Wavelength (λ_0):
1302 nm $\le \lambda_0 \le$ 1322 nm

Zero Dispersion Slope (S_0):
≤ 0.092 ps/(nm²·km)

$$\text{Dispersion} = D(\lambda) := \frac{S_0}{4}\left[\lambda - \frac{\lambda_0^4}{\lambda^3}\right] \text{ps/(nm·km)},$$

for 1200 nm ≤ λ ≤ 1600 nm

λ = Operating Wavelength

Polarization Mode Dispersion

Fiber Polarization Mode Dispersion (PMD)

	Value (ps/√km)
PMD Link Value	≤ 0.1*
Maximum Individual Fiber	≤ 0.2

* Complies with IEC 60794-3:2001, section 5.5, Method 1, September 2001.

The PMD link value is a term used to describe the PMD of concatenated lengths of fiber (also known as the link quadrature average). This value is used to determine a statistical upper limit for system PMD performance.

Individual PMD values may change when cabled. Corning's fiber specification supports network design requirements for a 0.5 ps/√km maximum PMD.

Environmental Specifications

Environmental Test Condition	Induced Attenuation 1310 nm/1550 nm (dB/km)
Temperature Dependence -60°C to +85°C*	≤0.05
Temperature-Humidity Cycling -10°C to +85°C*, up to 98% RH	≤0.05
Water Immersion, 23° ± 2°C*	≤0.05
Heat Aging, 85° ± 2°C*	≤0.05

*Reference temperature = +23°C

Operating Temperature Range

-60°C to +85°C

Dimensional Specifications

Length (km/reel): fiber lengths available up to 50.4*

* Longer spliced lengths available at a premium.

Glass Geometry

Fiber Curl: ≥ 4.0 m radius of curvature
Cladding Diameter: 125.0 ± 0.7 μm
Core-Clad Concentricity: ≤ 0.5 μm
Cladding Non-Circularity: ≤ 1.0%

Defined as: $\left[1 - \frac{\text{Min. Cladding Diameter}}{\text{Max. Cladding Diameter}}\right] \times 100$

Coating Geometry

Coating Diameter: 245 ± 5 μm
Coating-Cladding Concentricity: <12 μm

Mechanical Specifications

Proof Test

The entire fiber length is subjected to a tensile proof stress ≥ 100 kpsi (0.7 GN/m²)*.

* Higher proof test levels available at a premium.

Performance Characterizations

Characterized parameters are typical values.

Core Diameter: 8.2 μm

Numerical Aperture: 0.14

NA is measured at the one percent power level of a one-dimensional far-field scan at 1310 nm.

Zero Dispersion Wavelength (λ_0): 1313 nm

Zero Dispersion Slope (S_0): 0.086 ps /(nm²·km)

Refractive Index Difference: 0.36%

Effective Group Index of Refraction, **(N_{eff} @ nominal MFD):**

1.4677 at 1310 nm
1.4682 at 1550 nm

Fatigue Resistance Parameter **(n_d):** 20

Coating Strip Force:

Dry: 0.6 lbs. (3N)
Wet, 14-day room temperature: 0.6 lbs. (3N)

Rayleigh Backscatter Coefficient **(for 1 ns pulse width):**

1310 nm: -77 dB
1550 nm: -82 dB

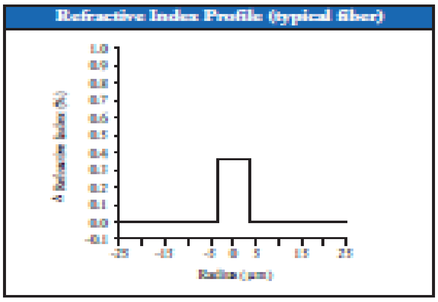

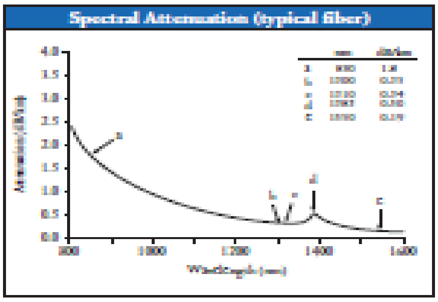

Appendix C

THORLABS

Polarization-Maintaining Fiber: Panda Style

PM1550-XP

Description

Thorlabs' polarization-maintaining fibers, designed for use from 1440 to 1625 nm, are optimized for data and telecom applications where ultra-low attenuation over long distances and resistance to radiation-induced damage are critical.

Specifications

Geometrical & Mechanical	
Core Diameter	8.5 µm
Cladding Diameter	125 ± 2 µm
Coating Diameter	245 ± 15 µm
Core-Clad Offset	≤0.5 µm
Coating Concentricity	≤5 µm
Coating Material	UV Cured, Dual Acrylate
Operating Temperature	-40 to 85 °C
Proof Test Level	≥ 200 kpsi (1.4 GN/m²)

Optical	
Numerical Aperture	0.125
Attenuation	<1.0 dB/km @ 1550 nm
Operating Wavelength	1440 - 1625 nm
Second Mode Cut-off	1380 ± 60 nm
Mode Field Diameter (1/e² fit - near field)	10.1 ± 0.4 µm @ 1550 nm
Beat Length	≤5.0 mm @ 1550 nm
Normalized Cross Talk	≤-40 dB @ 4 m @ 1550 nm

Specifications Subject to Change without Notice

June 10, 2017
TTN019885-S01, Rev C
www.thorlabs.com/contact

Appendix D

THORLABS

Optical Spectrum Analyzers

User Guide

6501 cm-1. To distinguish between these signals in the interferogram, we would need to move away 1 cm from the point of zero path difference (ZPD). The OSA can move ±4 cm in OPD, and so it can resolve spectral features 0.25 cm-1 apart. The resolution of the instrument can be calculated as follows:

$$\Delta\lambda = \Delta k \times 100 \times \lambda^2$$

Here, $\Delta\lambda$ is the resolution in pm, Δk is the OPD in cm-1 (maximum of 0.25 cm-1 for this instrument) and λ is the wavelength in µm.

The resolution of the OSA can be set to High or Low in the main window of the software. In high resolution mode, the retroreflectors translate by the maximum of ±1 cm (±4 cm in OPD), while in low resolution mode, the retroreflectors translate by ±0.25 cm (±1 cm in OPD). In the Setup section of the OSA software (Chapter 7), the length of the interferogram that is used in the calculation of the spectrum can be cut to remove spectral contributions from high-frequency components.

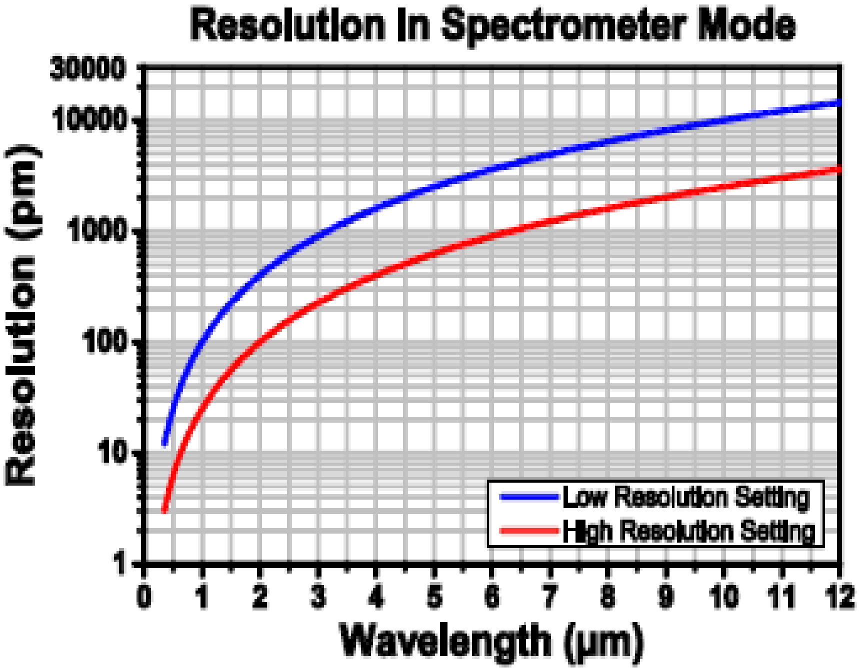

Figure 3 Resolution as a Function of Wavelength

The sensitivity of the instrument depends on the electronic gain used in the sensor electronics. Since an increased gain setting reduces the bandwidth of the detectors, the instrument will run slower when higher gain settings are used. Figure 4 and Figure 5 on the following page show the dependence of the noise floor on the wavelength and OSA model.

Chapter 13 Technical Data

13.1. Common Specifications

Specification	Notes	Value
Spectral Resolution	-	7.5 GHz (0.25 cm^{-1})
Spectral Accuracy[a]		±2 ppm[b]
Spectral Precision[c]		1 ppm
Wavelength Meter Resolution	Wavelength Meter Mode (Linewidth <10 GHz) See Section 4.6	0.1 ppm
Wavelength Meter Display Resolution[d]		9 Decimals
Wavelength Meter Accuracy[e]		±1 ppm
Wavelength Meter Precision[e]		0.2 ppm
Input Power (Max)	CW Source	10 mW (10 dBm)
Input Damage Threshold[f]	-	20 mW (13 dBm)
Power Level Accuracy[g]	-	±1 dB
Optical Rejection Ratio	See Section 4.13	30 dB
Input Fiber Compatibility	-	FC/PC Connectors[h] All Single Mode Patch Cables, Including Fluoride SM Patch Cables Silica Multimode Patch Cables with ≤Ø50 µm Core and NA ≤ 0.22 Fluoride Multimode Patch Cables with ≤Ø100 µm Core and NA ≤ 0.26
Free-Space Input	-	Accepts Collimated Beams up to Ø6 mm Red Alignment Laser Beam Four 4-40 Taps for 30 mm Cage Systems
Dimensions	-	320 mm x 149 mm x 475 mm (12.6" x 5.9" x 18.7")

a. After a 45-minute warm-up, for a single mode FC/PC-terminated patch cable at an operating temperature of 20 - 30 °C.
b. Specified in parts per million. For instance, if the wavelength being measured is 1 µm, the spectral accuracy will be ±2 pm. (±2 pm of accuracy for every 1,000,000 pm, or 1 µm, of wavelength.)
c. Spectral Precision is the repeatability with which a spectral feature can be measured using the peak search tool.
d. Can be set from 0-9 decimals and have an auto option that estimates the relevant number of decimals.
e. Using the same input single mode fiber for all measurements.
f. Limited by the damage threshold of the internal components
g. Specified using Absolute Power Mode, Zero Fill = 2, and Hann apodization, after a 45-minute warm-up, for an operating temperature of 20 - 30 °C. (The different apodization modes available in the OSA software are described in Section 16.2.) The specified wavelength range is 400 - 1000 nm for OSA201C, 600 - 1600 nm for OSA202C, 1.0 - 2.4 µm for OSA203C, 1.3 - 5.0 µm for OSA205C, and 2.0 - 11.0 µm for OSA207C. Each specification is valid for a single mode FC/PC-terminated patch cable, as well as for a collimated free-space beam with diameter < 3 mm and divergence < 3 mrad, assuming the included protective window is installed in the free-space aperture.
h. Connectors for other fiber input receptacles are available upon request. Contact techsupport@thorlabs.com for details.

الخلاصة

يعد ضغط النبض بالليزر تقنية مهمة في منظومات الاتصالات البصرية المتقدمة ذات معدل نقل البيانات العالي خاصة في تطبيق استشعار الشبكة الضوئية.

في هذه الرسالة , تم تصميم متداخل الليف البصري المفرد المحافظ على الاستقطاب لضغط الاشارة البصرية من نوع Mach Zehnder Interferomter باستخدام Comsol multi-physics الإصدار 5.5، وباستخدام ثلاثة أطوال متغيرة من الألياف المحافظة على الاستقطاب 8،16،24 cm مقسمة بين جزأين من SMF-28 بطول 13،23 cm على التوالي لتمييز توزيع الانماط داخل Mach zehnder Interferomter. كما تم بناء مقاييس التداخل المفردة والمتتالية من نوع PM-Mach-Zehnder باستخدام ألياف المحافظة للاستقطاب ، حيث كانت الطاقة الداخلة إلى مقاييس التداخل ناتجه من خلال انتشار مصدر الليزر النبضي , علما ان الشعاع الصادر من هذا المصدر له عرض نبضه $\tau = 10$ ns و FWHM = 286 pm وطاقة مقدارها $P_p = 1.227$ mW متمركزة عند الطول الموجي $\lambda =$ 1546.7 n. تم الحصول على أقصى إثارة لأنماط الترتيب في منطقة الكسوة بواسطة Comsol والتي أشارت إلى القيم المثلى لعوامل الضغط التي تبلغ 1.1103 في حالة تسليط 5 g على منطقة المقطع العرضي للألياف المستقطبة عندما كان طول الفايبر 8 cm . عمليا ، تم الحصول على عاملين من عوامل الانضغاط أحدهما بمقدار 1.13 مع مقياس التداخل المفرد من نوع Mach Zehnder interferometer ، بقوة 5 g تم تسليطها على منطقة اللحام الصغيرة والثاني بمقدار 1.10 مع مقياس التداخل المتراصف Mach Zehnder interferometer الذي يتكون من قطعتين من Polarization Maintaining Fiber طول كل منهما 8 سم طول و 10 g وزن تم تسليطها على منطقة المقطع العرضي الثاني للفايبر. يحتوي مقياس التداخل المتراصف المحافظ على الاستقطاب على عامل ضغط أدنى نظرًا لحقيقة أن العديد من مناطق الربط تعمل كعدسة محدبة مزدوجة تسبب الإثارة الأعلى لأنماط الترتيب المساندة في الألياف المتداخل والذي يؤدي في توسع FWHM مكانيًا وضغطً النبضة مكانيا.

وزارة التعليم العالي والبحث العلمي

جامعة بغداد
معهد الليزر للدراسات العليا

ضغط الاشارة البصرية باستعمال متداخل الليف البصري المحافظ على الاستقطاب من نوع ماخ-زيندر

رسالة مقدمة الى

معهد الليزر للدراسات العليا / جامعة بغداد / لاستكمال متطلبات نيل شهادة ماجستير علوم في الليزر/ الهندسة الالكترونية والاتصالات

من قبل

براء حسن مطر

بكالوريوس هندسة الليزر والالكترونيات البصرية

2016

بإشراف

الأستاذ المساعد الدكتورة تحرير صفاء منصور

1442هـ 2021م